

# **Envelope-Assisted RF Digital Predistortion for Broadband Radio-over-Fiber Systems with RF Power Amplifiers**

Weijie Tang

A Thesis

in

The Department

of

Electrical and Computer Engineering

Presented in Partial Fulfillment of the Requirements

For the Degree of Master of Applied Science at

Concordia University

Montreal, Quebec, Canada

March, 2017

© Weijie Tang, 2017

**CONCORDIA UNIVERSITY  
SCHOOL OF GRADUATE STUDIES**

This is to certify that the thesis prepared

By: Weijie Tang

Entitled: Envelope-Assisted RF Digital Predistortion for Broadband Radio-over-Fiber Systems with RF Power Amplifiers

and submitted in partial fulfillment of the requirements for the degree of

**Master of Applied Science (Electrical and Computer Engineering)**

complies with the regulations of this University and meets the accepted standards with respect to originality and quality.

Signed by the final examining committee:

_____	Chair
Dr. R. Raut	
_____	External Examiner
Dr. C. Assi	
_____	Internal Examiner
Dr. W.-P. Zhu	
_____	Supervisor
Dr. J.X. Zhang	

Approved by: \_\_\_\_\_  
Dr. W.E. Lynch, Chair  
Department of Electrical and Computer Engineering

\_\_\_\_\_ 20\_\_\_\_\_

\_\_\_\_\_ Dr. Amir Asif, Dean,  
Faculty of Engineering and Computer  
Science

# ABSTRACT

Envelope-Assisted RF Digital Predistortion for Broadband Radio-over-Fiber Systems with RF  
Power Amplifiers

Weijie Tang

Wireless communications play an extremely important role in our daily life. The ubiquitous cellphones and smartphones can provide not only voice service but also data service when they are connected to cellular network. With the enormous amount of mobile applications available to smartphones, people can listen to music, watch movies, check emails, update and share information on social media anytime and anywhere on their smartphones. All of these activities are possible because of the fast development of the wireless communication technology. Nowadays many people are enjoying the entertainments brought by 4G technology. In the meantime, companies and engineers in telecommunication industry have already been developing the 5G technology.

To support the high data transmission rate of 4G or 5G technology, a complex and robust infrastructure is essential. Radio-over-Fiber (RoF) technology is a good solution to build such an infrastructure. RoF transmission can provide extremely high capacity with very low attenuation. Besides, RoF transmission system is much cheaper compared to the traditional way of transmission such as microwave coaxial cable or digital optical fiber transmission. However, like other analog systems, RoF system suffers from signal distortion induced by nonlinearities.

RF power amplifier is needed to transmit the signal from a base station to the handsets because the attenuation of RF signal in the air is very high. Although many new types of RF power amplifiers have been designed to improve the power efficiency and the linearity, nonlinearity is still a big problem.

To reduce the distortion of an RoF system, as well as that induced by an RF power amplifier, a new digital predistortion (DPD) technique, envelope-assisted RF digital predistortion, is presented in this thesis. This DPD model is evolved from the memory polynomial, and

composed of an RF memory polynomial and a baseband memory polynomial. Therefore, this model takes both the RF signal and the baseband envelope as inputs to realize the digital predistortion. The RF polynomial is aimed to suppress the in-band nonlinearity, out-of-band nonlinearity and short-term memory effect, while the baseband polynomial is aimed to weaken the in-band nonlinearity and long-term memory effect. The indirect learning architecture is adopted and the least squares method is used to calculate the coefficients of the model.

The validity of the proposed DPD has been proved by simulation and experiment. In the simulation system, an RoF model is built which can induce both short-term and long-term memory effects, as well as the in-band and out-of-band nonlinearities. The optimal RF and baseband memory depths of the proposed DPD adopted in the simulation system have been found in terms of error vector magnitude (EVM) improvement and complexity. After the establishment of the memory depths, three simulation cases have been run to evaluate the performance of the proposed DPD. The first case is a normal two-band test, where two 20 MHz LTE signals are located at 800 MHz and 900 MHz. Simulation results show that EVM is improved by 14.6 dB, adjacent channel power ratio (ACPR) is suppressed by 13.5 dB, and third order intermodulation distortion (IMD3) is weakened by 19.5 dB. In the second case, two LTE signals are closely located at 800 MHz and 840 MHz. Simulation results show that EVM is improved by 16.3 dB, ACPR is suppressed by 15.5 dB, and IMD3 is weakened by 27.5 dB. In the third case, three LTE signals are located at 800 MHz, 850 MHz and 900 MHz. EVM is improved by 15.7 dB, ACPR is suppressed by 15.2 dB and IMD3 is weakened by 14.1 dB. The performance of the proposed DPD has also been compared to that of a baseband 2D DPD. Comparison results show that 2D DPD is only better at improving the EVM and ACPR in the first case, and the proposed DPD is superior to the 2D DPD on all the other aspects. Especially, the proposed DPD is not limited by the number of signal bands, while the 2D DPD is limited to two-band scenarios.

Experimentation has been conducted to further prove the effectiveness of the proposed DPD in a real RoF system. A similar test flow is adopted as in the simulation work. Firstly the optimal RF and baseband memory depths have been found. Then three test cases have been done. In the first case, EVM is improved by 6.9 dB, ACPR is suppressed by 14.8 dB, and IMD3 is weakened by 12.2 dB. In the second case, EVM is improved by 4.8 dB, ACPR is suppressed by

8.6 dB, and IMD3 is weakened by 9.5 dB. In the third case, EVM is improved by 8.9 dB, ACPR is suppressed by 16 dB, and IMD3 is weakened by 13.6 dB. Comparison with the 2D DPD shows the same result as in the simulation that the 2D DPD is only better at improving the EVM and ACPR in the first case. Influence of input power on EVM improvement has been studied. Experiment results show that the EVM improvement can be optimized at specific input power level. Sampling bandwidth has been reduced by down-converting the RF signal and sampling it at an intermediate frequency. Therefore, the implementation cost of the proposed DPD could be greatly reduced. In the two-band test, experiment results show that the performance of the proposed DPD with down conversion is even better than that of without down conversion. Influence of sampling bandwidth on EVM improvement has also been studied and the experiment results show that after down conversion, higher sampling bandwidth does not lead to significant EVM improvement.

## **ACKNOWLEDGEMENTS**

I would like to express my sincere gratitude to Professor John Xiupu Zhang for his insightful advice, help and great support for me to finish my thesis.

I would also like to express my appreciation to my colleague Dr. Ran Zhu for his patient help and advice during the experimental verification processes.

I am also deeply indebted to my colleague Lara A. Juras, who has gone through all the pain to help me review my thesis and made countless marks and comments.

I would also like to thank Xiaoran Xie and Hao Sun for their assistance in the lab.

I am very grateful to my parents and parents-in-law for their endless love, understanding and support.

I would like to say a very big thanks to my wife Yi Tang for her unconditional love and support during my study in Concordia University and for encouraging me all the time in my life. I would also express my love to my daughter Xinyue Tang and my son Xinyang Tang.

# Table of Contents

<b>List of Figures</b> .....	<b>x</b>
<b>List of Tables</b> .....	<b>xvi</b>
<b>List of Acronyms</b> .....	<b>xvii</b>
<b>Chapter 1. Introduction</b> .....	<b>1</b>
1.1 Wireless Communications .....	1
1.1.1 A Brief History of Mobile Wireless Communications .....	1
1.1.2 Architecture Evolution .....	2
1.2 Radio-over-Fiber Transmission Systems .....	5
1.3 Motivation and Contribution .....	8
1.4 Thesis Outline .....	9
<b>Chapter 2. Background and Literature Review</b> .....	<b>11</b>
2.1 RoF Technologies .....	11
2.1.1 Optical Fibers .....	11
2.1.2 Lasers .....	12
2.1.3 Optical Modulators .....	14
2.1.4 Optical Receivers .....	16
2.1.5 RF Power Amplifier .....	18
2.2 Distortions in RoF Transmission Systems .....	21
2.2.1 Nonlinearity .....	21
2.2.2 Memory Effect .....	22
2.2.3 Distortions in Electrical Domain .....	22
2.2.4 Distortions in Optical Domain .....	23
2.3 Linearization Techniques for RoF Transmission Systems .....	25
2.3.1 Optical Linearization Techniques .....	26

2.3.2	Analog Predistortion .....	27
2.3.3	Digital Predistortion .....	29
<b>Chapter 3.</b>	<b>Theoretical Analysis of Envelope-Assisted RF DPD .....</b>	<b>34</b>
3.1	Modeling Nonlinearities and Memory Effects of RoF Systems .....	34
3.2	Envelope-Assisted RF DPD .....	35
3.3	Indirect Learning DPD Structure .....	37
3.4	Extraction of Model Coefficients .....	38
<b>Chapter 4.</b>	<b>Simulation with Envelope-Assisted RF DPD .....</b>	<b>41</b>
4.1	Overview of the Simulation System .....	41
4.2	RoF Model.....	43
4.3	Optimal Memory Depth of the RF Polynomial.....	45
4.4	Optimal Memory Depth of the Baseband Polynomial .....	46
4.5	Comparison with Baseband DPD Techniques .....	47
4.5.1	Case 1: Band 1 @800MHz and Band 2 @900MHz.....	48
4.5.2	Case 2: Band 1 @800MHz and Band 2 @840MHz.....	54
4.5.3	Case 3: Band 1 @800MHz, Band 2 @850MHz and Band 3 @900MHz.....	58
4.5.4	Complexity Consideration.....	62
4.6	Simulation Summary.....	63
<b>Chapter 5.</b>	<b>Experiments with Envelope-Assisted RF DPD .....</b>	<b>65</b>
5.1	Experiment Setup Overview .....	65
5.2	RoF Model.....	66
5.3	Optimal Memory Depth of the RF Polynomial.....	66
5.4	Optimal memory Depth of the Baseband Polynomial .....	66

5.5	Comparison with Baseband DPD Techniques .....	67
5.5.1	Case 1: Band 1 @800MHz and Band 2 @900MHz.....	68
5.5.2	Case 2: Band 1 @800MHz and Band 2 @840MHz.....	71
5.5.3	Case 3: Band 1 @800MHz, Band 2 @850MHz and Band 3 @900MHz.....	75
5.6	Influence of Input RF Power on EVM .....	80
5.7	Improvement on Sampling Bandwidth .....	81
5.8	Influence of Sampling Bandwidth on EVM.....	84
5.9	Experiment Summary.....	85
<b>Chapter 6.</b>	<b>Conclusion.....</b>	<b>87</b>
6.1	Thesis Conclusion .....	87
6.2	Future Work .....	89
<b>Reference</b>	<b>.....</b>	<b>90</b>

# List of Figures

Figure 1-1 Traditional macro base station .....	3
Figure 1-2 Distributed architecture .....	4
Figure 1-3 C-RAN architecture .....	4
Figure 1-4 RoF transmission system architecture .....	6
Figure 1-5 Schematic of an RoF link .....	6
Figure 2-1 Structure of Fabry-Perot laser .....	12
Figure 2-2 Output spectrum of a Fabry-Perot laser .....	13
Figure 2-3 Structure of DBR laser .....	13
Figure 2-4 Output spectrum of a DBR laser .....	13
Figure 2-5 Structure of DFB laser .....	14
Figure 2-6 Direct modulation of a laser .....	14
Figure 2-7 Transmission characteristic of a directly modulated laser .....	15
Figure 2-8 Transmitter using an external modulator .....	15
Figure 2-9 Phase modulation in a LiNbO <sub>3</sub> crystal .....	16
Figure 2-10 Structure of an MZM .....	16
Figure 2-11 A simple optical receiver .....	17
Figure 2-12 Optical IQ coherent receiver .....	17
Figure 2-13 A typical IV characteristic curve for NPN transistor .....	19
Figure 2-14 Schematic of Doherty PA .....	20
Figure 2-15 Schematic of envelope tracking power amplifier .....	20
Figure 2-16 Nonlinearity of a power amplifier .....	21
Figure 2-17 Memory effect of the input signal on the output signal .....	22
Figure 2-18 Output spectrum from a power amplifier .....	23
Figure 2-19 Output spectrum around the two signals from a power amplifier .....	23
Figure 2-20 Transmission characteristic of a directly modulated laser .....	24
Figure 2-21 Response characteristics of a typical photodetector .....	24
Figure 2-22 Classification of linearization techniques .....	26
Figure 2-23 Schematic of mixed polarization linearization .....	27

Figure 2-24 Schematic of dual-wavelength linearization .....	27
Figure 2-25 Schematic of analog predistortion circuit reported in [30] .....	28
Figure 2-26 Schematic of analog predistortion circuit reported in [31] .....	28
Figure 2-27 Schematic of analog predistortion circuit reported in [33] .....	29
Figure 2-28 Block diagram of DPD .....	30
Figure 2-29 Block diagram of RF DPD .....	30
Figure 3-1 Correction of nonlinearity .....	34
Figure 3-2 Correction of memory effect .....	35
Figure 3-3 Baseband samples and RF samples .....	36
Figure 3-4 Indirect learning structure for DPD .....	37
Figure 4-1 Indirect learning DPD structure of the proposed DPD in LTE communication .....	41
Figure 4-2 Indirect learning DPD structure of the proposed DPD for two-band test .....	42
Figure 4-3 RoF model for simulation .....	43
Figure 4-4 Input-output curve of the nonlinear model .....	44
Figure 4-5 Mapping function between $x_b$ and $a$ .....	45
Figure 4-6 EVM vs RF memory depth (Left: lower band. Right: upper band.) .....	46
Figure 4-7 EVM vs baseband memory depth (Left: lower band. Right: upper band.) .....	46
Figure 4-8 EVM vs memory depth of the 2D DPD .....	47
Figure 4-9 Output spectrum from 500 MHz to 1200 MHz in simulation (case 1) .....	48
Figure 4-10 Spectrum around the lower band in simulation (case 1) .....	49
Figure 4-11 Spectrum around the upper band in simulation (case 1) .....	49
Figure 4-12 Constellation of signal in lower band without DPD (a) before phase adjustment and (b) after phase adjustment .....	50
Figure 4-13 Constellation of signal in lower band with the proposed DPD (a) before phase adjustment and (b) after phase adjustment .....	50
Figure 4-14 Constellation of signal in lower band with 2D DPD (a) before phase adjustment and (b) after phase adjustment .....	50
Figure 4-15 Constellation of signal in upper band without DPD (a) before phase adjustment and (b) after phase adjustment .....	51
Figure 4-16 Constellation of signal in upper band with the proposed DPD (a) before phase adjustment and (b) after phase adjustment .....	51

Figure 4-17 Constellation of signal in upper band with 2D DPD (a) before phase adjustment and (b) after phase adjustment.....	52
Figure 4-18 AM-AM and AM-PM distortion on lower-band signal with and without proposed DPD .....	52
Figure 4-19 AM-AM and AM-PM distortion on upper-band signal with and without proposed DPD .....	53
Figure 4-20 AM-AM and AM-PM distortion on lower-band signal with and without baseband DPD .....	53
Figure 4-21 AM-AM and AM-PM distortion on upper-band signal with and without baseband DPD .....	54
Figure 4-22 Output spectrum from 500 MHz to 1100 MHz in simulation case 1 .....	55
Figure 4-23 Spectrum around the lower band in simulation case 2.....	55
Figure 4-24 Spectrum around the upper band in simulation case 2.....	56
Figure 4-25 Constellation of signal in lower band without DPD (a) before phase adjustment and (b) after phase adjustment.....	56
Figure 4-26 Constellation of signal in lower band with proposed DPD (a) before phase adjustment and (b) after phase adjustment .....	56
Figure 4-27 Constellation of signal in lower band with 2D DPD (a) before phase adjustment and (b) after phase adjustment.....	57
Figure 4-28 Constellation of signal in upper band without DPD (a) before phase adjustment and (b) after phase adjustment.....	57
Figure 4-29 Constellation of signal in upper band with proposed DPD (a) before phase adjustment and (b) after phase adjustment .....	57
Figure 4-30 Constellation of signal in upper band with 2D DPD (a) before phase adjustment and (b) after phase adjustment.....	58
Figure 4-31 Output spectrum from 500 MHz to 1200 MHz in simulation case 3.....	58
Figure 4-32 Spectrum around the lower band in simulation case 3.....	59
Figure 4-33 Spectrum around the middle band in simulation case 3.....	59
Figure 4-34 Spectrum around the upper band in simulation case 3.....	60
Figure 4-35 Constellation of signal in lower band without DPD (a) before phase adjustment and (b) after phase adjustment.....	60

Figure 4-36 Constellation of signal in lower band with the proposed DPD (a) before phase adjustment and (b) after phase adjustment .....	61
Figure 4-37 Constellation of signal in middle band without DPD (a) before phase adjustment and (b) after phase adjustment.....	61
Figure 4-38 Constellation of signal in middle band with the proposed DPD (a) before phase adjustment and (b) after phase adjustment .....	61
Figure 4-39 Constellation of signal in upper band without DPD (a) before phase adjustment and (b) after phase adjustment.....	62
Figure 4-40 Constellation of signal in upper band with the proposed DPD (a) before phase adjustment and (b) after phase adjustment .....	62
Figure 5-1 Experiment setup of the RoF transmission link .....	65
Figure 5-2 EVM vs RF memory depth (Left: lower band. Right: upper band.).....	66
Figure 5-3 EVM vs baseband memory depth (Left: lower band. Right: upper band.).....	67
Figure 5-4 EVM vs memory depth of the 2D DPD .....	67
Figure 5-5 Output spectrum from 500 MHz to 1200 MHz in experiment case 1.....	68
Figure 5-6 Spectrum around the lower band in experiment case 1.....	68
Figure 5-7 Spectrum around the upper band in experiment case 1.....	69
Figure 5-8 Constellation of signal in lower band without DPD (a) before phase adjustment and (b) after phase adjustment .....	69
Figure 5-9 Constellation of signal in lower band with the proposed DPD (a) before phase adjustment and (b) after phase adjustment .....	70
Figure 5-10 Constellation of signal in lower band with 2D DPD (a) before phase adjustment and (b) after phase adjustment.....	70
Figure 5-11 Constellation of signal in upper band without DPD (a) before phase adjustment and (b) after phase adjustment.....	70
Figure 5-12 Constellation of signal in upper band with the proposed DPD (a) before phase adjustment and (b) after phase adjustment .....	71
Figure 5-13 Constellation of signal in upper band with 2D DPD (a) before phase adjustment and (b) after phase adjustment.....	71
Figure 5-14 Output spectrum from 500 MHz to 1100 MHz in experiment case 2.....	72
Figure 5-15 Spectrum around the lower band in experiment case 2.....	72

Figure 5-16 Spectrum around the upper band in experiment case 2.....	73
Figure 5-17 Constellation of signal in lower band without DPD (a) before phase adjustment and (b) after phase adjustment.....	73
Figure 5-18 Constellation of signal in lower band with the proposed DPD (a) before phase adjustment and (b) after phase adjustment .....	74
Figure 5-19 Constellation of signal in lower band with 2D DPD (a) before phase adjustment and (b) after phase adjustment.....	74
Figure 5-20 Constellation of signal in upper band without DPD (a) before phase adjustment and (b) after phase adjustment.....	74
Figure 5-21 Constellation of signal in upper band with the proposed DPD (a) before phase adjustment and (b) after phase adjustment .....	75
Figure 5-22 Constellation of signal in upper band with 2D DPD (a) before phase adjustment and (b) after phase adjustment.....	75
Figure 5-23 Output spectrum from 500 MHz to 1200 MHz in experiment case 3.....	76
Figure 5-24 Spectrum around the lower band in experiment case 3.....	76
Figure 5-25 Spectrum around the middle band in experiment case 3.....	77
Figure 5-26 Spectrum around the upper band in experiment case 3.....	77
Figure 5-27 Constellation of signal in lower band without DPD (a) before phase adjustment and (b) after phase adjustment.....	78
Figure 5-28 Constellation of signal in lower band with the proposed DPD (a) before phase adjustment and (b) after phase adjustment .....	78
Figure 5-29 Constellation of signal in middle band without DPD (a) before phase adjustment and (b) after phase adjustment.....	78
Figure 5-30 Constellation of signal in middle band with the proposed DPD (a) before phase adjustment and (b) after phase adjustment .....	79
Figure 5-31 Constellation of signal in upper band without DPD (a) before phase adjustment and (b) after phase adjustment.....	79
Figure 5-32 Constellation of signal in upper band with the proposed DPD (a) before phase adjustment and (b) after phase adjustment .....	79
Figure 5-33 Influence of input RF power on EVM .....	80
Figure 5-34 Output spectrum from 550 MHz to 1150 MHz.....	81

Figure 5-35 Spectrum around lower band .....	82
Figure 5-36 Spectrum around upper band .....	83
Figure 5-37 Constellation of lower band .....	83
Figure 5-38 Constellation of upper band .....	84
Figure 5-39 EVM vs sampling bandwidth on lower band.....	84
Figure 5-40 EVM vs sampling bandwidth on upper band.....	85

## List of Tables

Table 1-1 Basic comparison among mobile communication generations .....	2
Table 4-1 Number of coefficients vs memory depth .....	63
Table 4-2 Number of coefficients vs nonlinearity degree .....	63
Table 4-3 Comparison of EVM improvement in simulation .....	64
Table 4-4 Comparison of ACPR improvement in simulation .....	64
Table 4-5 Comparison of IMD3 improvement in simulation .....	64
Table 5-1 Comparison of EVM improvement in experiment .....	85
Table 5-2 Comparison of ACPR improvement in experiment .....	85
Table 5-3 Comparison of IMD3 improvement in experiment .....	86

# List of Acronyms

ACPR	Adjacent Channel Power Ratio
ADC	Analog-to-Digital Converter
AMPS	Advanced Mobile Phone System
APD	Analog Predistortion
ASIC	Application-Specific Integrated Circuit
ASK	Amplitude Shift Keying
AWG	Arbitrary Waveform Generator
BBU	Baseband Unit
CDMA	Code Division Multiple Access
CPU	Central Processing Unit
C-RAN	Cloud Radio Access Network
CWDM	Coarse Wavelength-Division Multiplexing
D-AMPS	Digital AMPS
DBR	Distributed Bragg Reflector
DDR	Dynamic Deviation Reduction
DFB	Distributed-Feedback
DPD	Digital Predistortion
DSP	Digital Signal Processor
DWDM	Dense Wavelength-Division Multiplexing
DWL	Dual-Wavelength Linearization
EAM	Electro-Absorption Modulator
ET	Envelope Tracking

EVM	Error Vector Magnitude
FFT	Fast Fourier Transform
FIR	Finite Impulse Response filter
FPGA	Field-Programmable Gate Array
FSK	Frequency Shift Keying
FWM	Four-Wave Mixing
GaAs	Gallium Arsenide
GaN	Gallium Nitride
GMP	Generalized Memory Polynomial
GMSK	Gaussian Minimum Shift Keying
GSM	Global System for Mobile Communications
iFFT	Inverse Fast Fourier Transform
IFWM	Intra-channel Four-Wave Mixing
IIR	Infinite Impulse Response filter
IMD2	2nd Order Intermodulation Distortion
IMD3	3rd Order Intermodulation Distortion
IMD5	5th Order Intermodulation Distortion
IXPM	Intra-channel Cross-Phase Modulation
LDMOS	Laterally Diffused Metal Oxide Semiconductor
LED	Light-Emitting Diode
LMS	Least Mean Squares
LNA	Low-Noise Amplifier
LS	Least Squares
LTE	Long-Term Evolution
LTE-A	Long-Term Evolution Advanced

MCF	Multi-Core Fiber
MDM	Mode-Division Multiplexing
MIMO	Multiple-Input and Multiple-Output
MMF	Multi-Mode Fiber
MP	Memory Polynomial
MSE	Mean Squared Error
MSTO	Mobile Switching Telephone Office
MZM	Mach-Zehnder Modulator
OFDMA	Orthogonal Frequency-Division Multiple Access
ORx	Optical Receiver
OTN	Optical Transport Network
OTx	Optical Transmitter
PD	Photodetector
PSK	Phase Shift Keying
QAM	Quadrature Amplitude Modulation
QPSK	Quadrature Phase Shift Keying
RAN	Radio Access Network
RF	Radio Frequency
RLS	Recursive Least Squares
RoF	Radio-over-Fiber
RRH	Remote Radio Head
RRU	Remote Radio Unit
SC-FDMA	Single-Carrier Frequency-Division Multiple Access
SFDR	Spur-Free Dynamic Range
SLM	Single-Longitudinal-Mode

SMF	Single Mode Fiber
SOA	Semiconductor Optical Amplifier
SPM	Self-Phase Modulation
TD-CDMA	Time-Division Code-Division Multiple Access
TDMA	Time-Division Multiple Access
TD-SCDMA	Time-Division Synchronous Code-Division Multiple Access
W-CDMA	Wideband Code-Division Multiple Access
XPM	Cross-Phase Modulation

# Chapter 1. Introduction

## 1.1 Wireless Communications

### 1.1.1 A Brief History of Mobile Wireless Communications

Wireless communication technology has gone through four generations and the fifth generation is under development as well [1]. The first generation cellular systems were launched in early 1980s, among which the most famous was Advanced Mobile Phone System (AMPS) developed by Bell Labs. Since AMPS featured analog modulation techniques, therefore the spectral efficiency was quite low.

The second generation cellular systems emerged in the 1990s. Global System for Mobile Communications (GSM), CDMAOne and Digital AMPS (D-AMPS) were the three competitors. All of these 2G standards were developed based on the digital communication technology, which includes digital modulation technique, digital multiple access method, etc. Three most basic digital modulation techniques are amplitude shift keying (ASK), phase shift keying (PSK), and frequency shift keying (FSK). In order to further increase the spectral efficiency, some advanced digital modulation techniques were developed, such as quadrature phase shift keying (QPSK),  $\pi/4$  differential QPSK ( $\pi/4$ -DQPSK), Gaussian minimum shift keying (GMSK) and the most popular n-QAM. For the multiple access method, time division multiple access (TDMA) or code division multiple access (CDMA) were adopted in the second generation standards.

The third generation mobile communication technology heavily relied on the CDMA technique. All the third generation mobile standards, W-CDMA, TD-CDMA, TD-SCDMA and CDMA2000, were developed based on the CDMA technique. The transfer rate was significantly increased in these third generation standards, from 64 Kbps of the 2G standards to 2 Mbps, which made it possible to use mobile phones to surf on internet or to make video calls.

Companies did not stop with 3G, and they moved on to the fourth generation standards or Long-Term Evolution (LTE). To increase the frequency efficiency, Orthogonal Frequency-

Division Multiple Access (OFDMA) for the downlink and Single-Carrier Frequency-Division Multiple Access (SC-FDMA) for the uplink were adopted for the air interface. In fact, LTE does not meet the technical criteria of the 4G standard, but the LTE-Advanced (LTE-A) does. Combined with the advanced modulation techniques and the multiple-input and multiple-output (MIMO) technique, the peak download rate could reach as high as 299.6 Mbps (20 MHz, 64QAM, 4x4 MIMO) in the LTE standard. With the additional carrier aggregation technique, the LTE-A can provide almost 3.3 Gbps peak download rate (100 MHz, 128QAM, 8x8 MIMO).

To improve user experience of mobile internet, engineers are developing the fifth generation mobile standard which aims to provide a 100 Gbps peak download rate.

Below in Table 1-1 is a basic comparison among mobile communication generations. It reveals that both the speed and the working frequency go higher and higher as generations advance. This is a challenge for the upcoming 5G technology to transport the signals inside the radio access network (RAN).

Table 1-1 Basic comparison among mobile communication generations

<b>Feature</b>	<b>1G</b>	<b>2G</b>	<b>3G</b>	<b>4G</b>	<b>5G</b>
<b>Deployment</b>	1980	1990	2001	2010	~2020
<b>Frequency band</b>	800 MHz	900 MHz	2100 MHz	2600 MHz	3-90 GHz
<b>Speed</b>	2 Kbps	64 Kbps	2 Mbps	1 Gbps	100 Gbps
<b>Technology</b>	analog cellular	GSM, CDMAOne	W-CDMA, TD-CDMA, TD-SCDMA and CDMA2000	LTE-A	to be defined

### 1.1.2 Architecture Evolution

In the 1G and 2G mobile cellular network, a traditional RAN consisted of many all-in-one base stations and a backhaul, which connects these base stations to Mobile Switching Telephone Offices (MSTOs), as shown in Figure 1-1. Baseband signals are transmitted through the backhaul network between the base stations and the MSTOs. Each base station integrates

radio frequency (RF), analog, digital, and power functions in a huge cabinet. The base station cabinet is usually placed in a dedicated room, where all necessary supporting facilities are available, such as power, backup battery, air conditioning, backhaul transmission equipment, etc. The antennas can usually be seen on the top of the base station tower. RF signals, generated by the base stations or received by the antennas, propagate through RF cables between the base station and the antenna. In this kind of architecture, it tends to be costly to install and maintain the base stations.

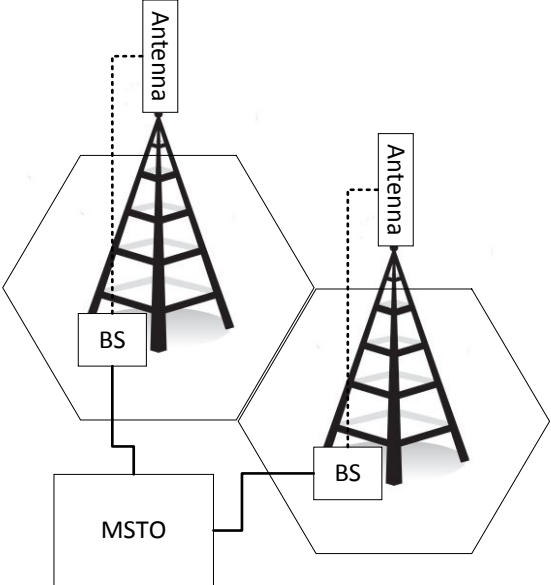


Figure 1-1 Traditional macro base station

In the current 3G and 4G network, distributed base station architecture is introduced, where the traditional all-in-one base station is divided into two parts: remote radio head (RRH) and baseband unit (BBU), as shown in Figure 1-2. The RRH and BBU are connected by optical fiber, through which the digital baseband signals are transmitted. The RRH is usually installed on the top of the tower allowing it to be very close to the antenna and keeping the transmission loss between the antenna and the RRH very low. The BBU can be placed in a more flexible site because the optical fiber induces very low loss.

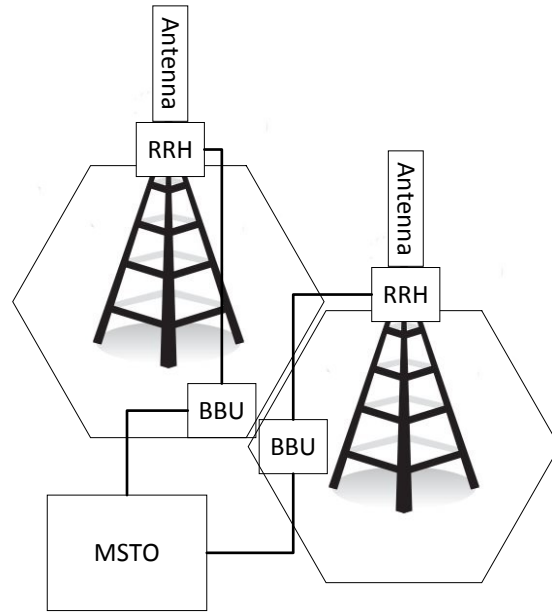


Figure 1-2 Distributed architecture

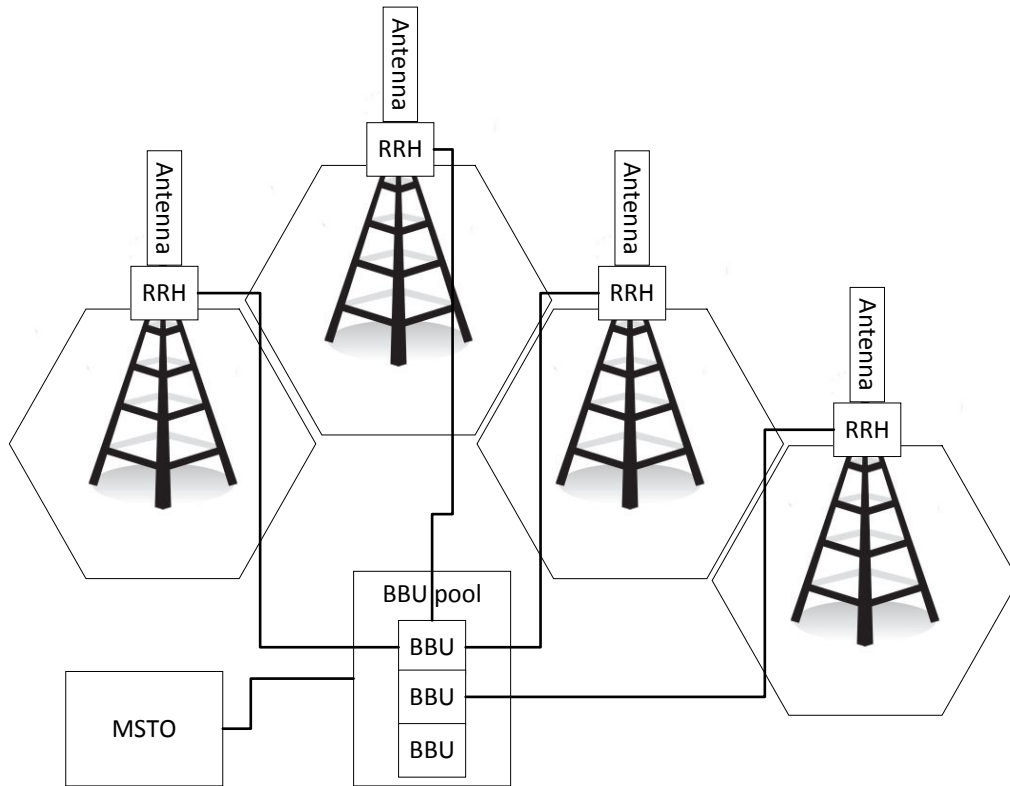


Figure 1-3 C-RAN architecture

The Cloud Radio Access Network (C-RAN), or Centralized Radio Access Network architecture, as shown in Figure 1-3, has been deployed in some countries for the 2G, 3G and 4G systems and is proposed to be adopted into the upcoming 5G system [2]. C-RAN further evolved

from the distributed architecture. All the BBUs are relocated to one of the BBU pools. Each BBU can serve multiple RRHs and all the BBUs in each BBU pool are connected with each other so that they can communicate with each other at very low latency. This makes it possible to allocate the frequency resource dynamically among the RRHs that are connected to the same BBU pool. Besides, a centralized BBU pool also means low installation and maintenance cost. The backhaul connects the BBU pool to the MSTO while the fronthaul connects the RRHs to the BBU pool. The Coarse Wavelength Division Multiplexing (CWDM) or Dense Wavelength Division Multiplexing (DWDM) based optical transport network (OTN) are employed in the fronthaul.

The fronthaul in C-RAN is built based on digital optical fiber transmission. Digital baseband signals are transmitted between the RRH and the BBU. Therefore, the RRH still needs to integrate the complex functions such as analog to digital conversion, digital to analog conversion, modulation, demodulation, up-conversion, down-conversion, etc. Taking into account the coexistence of 2G, 3G, 4G, and the upcoming 5G, the RRH is still a complex and costly system. Especially for the 5G network, small cells, including femtocells, picocells and microcells, will probably be extensively deployed, which could cause the number of RRHs to increase sharply. Therefore, any effort that can simplify the architecture of the RRH and lower the cost of the RRH is worthwhile.

## 1.2 Radio-over-Fiber Transmission Systems

Radio-over-Fiber (RoF) is such a technology that can simplify the architecture of the RRH [3]. The RoF system shares the same architecture as the C-RAN system, except that the fronthaul links are built based on the RoF technology. RoF technology employs the optical fiber to transmit the RF signals between the Central Processing Unit (CPU) and the Remote Radio Unit (RRU). Therefore, functions such as up-conversion, down-conversion, modulation and demodulation can be done in the BBU instead of RRH. The architecture is shown in Figure 1-4.

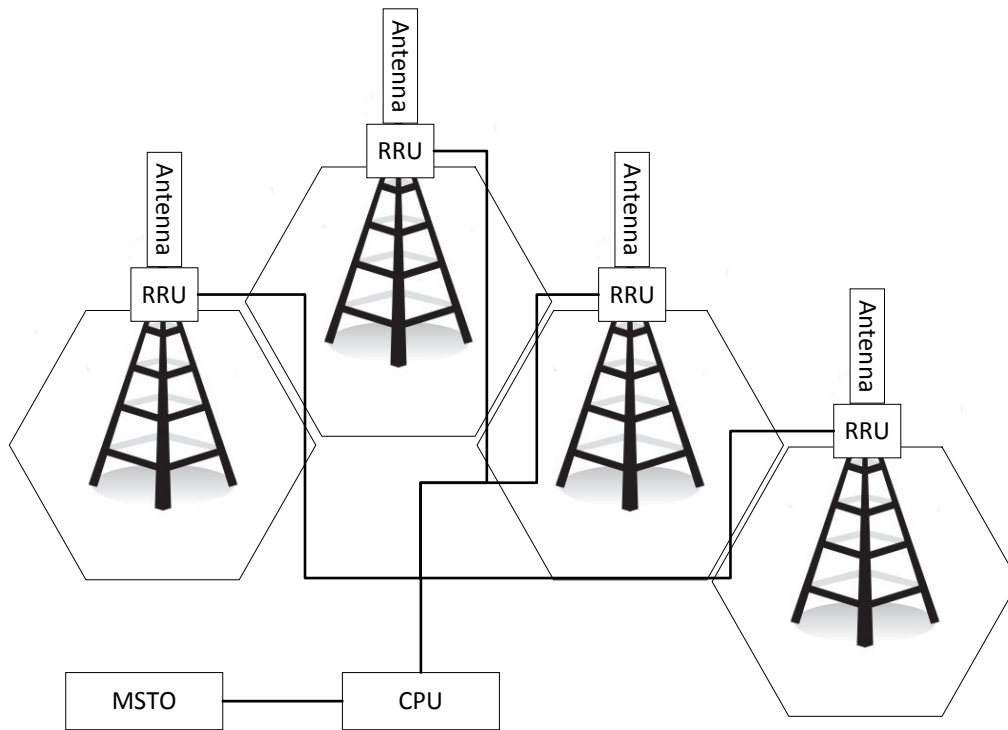


Figure 1-4 RoF transmission system architecture

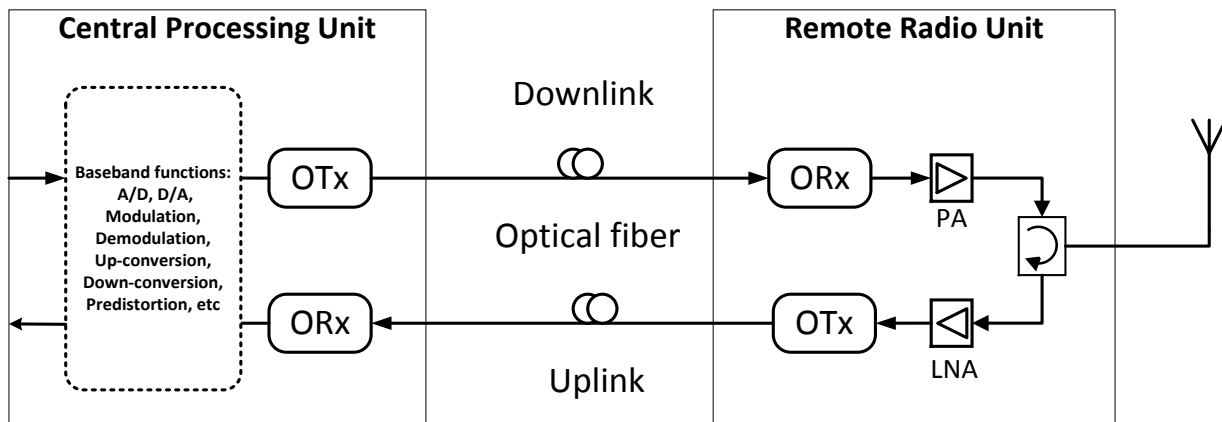


Figure 1-5 Schematic of an RoF link

Figure 1-5 is a more detailed illustration of the optical link between CPU and RRU. In the downlink, referring to the transmission from the CPU to the RRU, RF signals are generated inside the CPU after digital modulation and up-conversion. The RF signals are further modulated onto the optical carrier by the optical modulator inside the optical transmitter (OTx). The optical modulation could be done by direct modulation or external modulation. In the case of direct modulation, the modulation is done directly in the laser by changing the driving current. External modulation could be done by an electro-absorption modulator (EAM) or Mach-Zehnder

modulator (MZM). After the optical modulation, the modulated optical signals are transmitted through optical fiber. An optical receiver (ORx) like a photodiode, detects the optical signals and extracts the RF signals in the form of electrical signal. The RF signals are amplified in the power amplifier (PA) before they are fed into the antenna. A similar process exists in the uplink, only in a reverse sequence.

RoF technology has many obvious advantages and benefits compared with the other transmission ways. Firstly, the attenuation loss is very low because of the transmission through optical fiber. A standard single mode fiber (SMF) only induces attenuation loss below 0.2dB/km and 0.4 dB/km in the 1550 nm and the 1310 nm window respectively [4]. In traditional transmission lines such as microwave coaxial cables, the impedance increases with frequency, which means it is very hard to transport broadband signals with cables or a lot of repeaters or amplifiers will be needed.

Secondly, the bandwidth of optical fiber is extremely large. Even in the case of a single mode fiber, the bandwidth could be several THz, whereas the maximal bandwidth of the cable is only several GHz [4]. The large bandwidth of optical fiber could easily meet the increasing needs nowadays as well as that of the upcoming 5G technology.

Thirdly, the cost of the whole transmission system can be greatly reduced. As shown in Figure 1-5, the structure of the RRU is quite simple. It consists of an optical receiver, an optical transmitter, a power amplifier in the downlink, a low-noise amplifier (LNA), and a circulator. All the baseband components are relocated into the CPU, where these baseband components can be reused or shared among many CPU-RRU links. Besides, the cost of optical fibers is also much lower than that of cables.

In addition to the advantages mentioned previously, the optical fiber is immune to electromagnetic interference [4], so the noise floor could be much lower. As we know, lower noise level means higher signal bandwidth.

Furthermore, the RRU of the RoF system is transparent to the communication protocols. The RRU can serve any new protocol, as long as the signal band is located within the working frequency band of the RRU. Whereas in current architectures, different protocols need to employ

different modules, and this is one of the reasons that the base station is becoming more and more complex and costly.

However, the RoF transmission system is basically an analog system, so it inevitably suffers from impairments such as nonlinearity and memory effect. Modules or circuitries such as optical modulators, photodiodes, optical fibers, RF power amplifiers, matching networks, etc., can all contribute to the signal distortion. In order to deploy the RoF transmission system, linearization technique must be used to reduce the signal distortion.

### 1.3 Motivation and Contribution

Just like a usual RF transmission system, the RoF transmission system also suffers from signal distortions, such as nonlinearity and memory effect. These signal distortions lead to higher error vector magnitude (EVM) and higher adjacent channel power ratio (ACPR). When there are two or more signals transmitted simultaneously, the third order intermodulation distortion (IMD3) and the fifth order intermodulation distortion (IMD5) may be too powerful that some measures must be taken to suppress them.

So far, many predistortion techniques have been proposed to tackle the issue of signal distortion in the RoF transmission system [5]. Basically they can be divided into two classes: analog predistortion (APD) and digital predistortion (DPD) techniques. Both APD and DPD have their own advantages and disadvantages. APD is usually cost-effective but is mainly targeted on the out-of-band distortion such as IMD3 and IMD5. DPD is usually applied to the baseband signal because of the limited bandwidth of the analog-to-digital converters (ADCs), so it is good at improving the in-band distortion and out-of-band distortion which is close to the signal in frequency domain, such as power leakage in adjacent channels. However, baseband DPD cannot be used for improving the out-of-band IMD3 or IMD5 distortion.

With the commercial availability of the RF sampling ADC, it is possible to implement the DPD on the RF signal. In this thesis, the envelope-assisted RF digital predistortion technique is proposed to linearize the RoF systems with RF power amplifiers. It can simultaneously eliminate the in-band and out-of-band nonlinearity, and short- and long-term memory effect. Two-band and three-band tests have been conducted which show improvement in EVM, ACPR

and IMD3 simultaneously.

## 1.4 Thesis Outline

The rest of the thesis is organized as follows:

Chapter 2 introduces more details of the RoF technology and the sources of signal distortions in the RoF transmission systems. A literature review of the linearization techniques for RoF transmission systems is presented.

Chapter 3 gives the theoretical analysis of the DPD technique and demonstrates how the proposed envelope-assisted RF DPD evolves from the traditional baseband DPD. The indirect learning structure is introduced since it is commonly adopted by the majority of the DPDs to simplify the extraction of the coefficients.

In chapter 4, the simulation system is introduced, which is built with Matlab. Details of the flow of the simulation are given. Optimal parameters of the proposed DPD model are achieved by running simulation. Two-band and three-band tests have been run to evaluate the performance of the proposed DPD. In the first two-band test, two 20 MHz LTE signals are located at 800 MHz and 900 MHz. In the second two-band test, two 20 MHz LTE signals are located at 800 MHz and 840 MHz, very close to each other. In the three-band test case, three 20 MHz LTE signals are located at 800 MHz, 850 MHz and 900 MHz. Comparisons has been made between the proposed DPD model and a conventional baseband DPD model. Complexity has also been compared between these two models. Simulation results show that the proposed DPD is capable of dealing with in-band and out-of-band nonlinearities, short-term and long-term memory effects of RoF transmission system simultaneously. Besides, the performance of the proposed DPD is not limited by the number of bands.

In chapter 5, the experiment setup is introduced. Optimal parameters of the proposed DPD model applied in the real RoF link are have been decided by experiments. Two-band and three-band tests have been conducted to evaluate the performance of the proposed DPD in the real RoF link. In the first two-band test, two 20 MHz LTE signals are located at 800 MHz and 900 MHz. In the second two-band test, two 20 MHz LTE signals are located at 800 MHz and

840 MHz. In the three-band test case, three 20 MHz LTE signals are located at 800 MHz, 850 MHz and 900 MHz. Comparison to a conventional baseband DPD has also been made. Experiment results almost agree with the simulation results. Influence of input power on EVM has been studied. Sampling bandwidth has been decreased to reduce the cost to implement the DPD and the experiment result shows that the performance of the DPD is not degraded.

Chapter 6 concludes the current research and suggests the future work toward a more cost-effective predistortion technique.

## Chapter 2. Background and Literature Review

This chapter introduces the key technologies that make up the whole RoF transmission system. In the RoF transmission system, the most important parts are optical modulator and optical receiver, while the optical fiber is the medium that the optical signals propagate through. Optical modulator modulates the optical carrier signal with the electrical RF signal, whereas optical receiver converts the optical signal to the electrical signal so that the signal can be further processed by the digital signal processor (DSP), field-programmable gate array (FPGA) or application-specific integrated circuit (ASIC). When the signals are transformed between electrical domain and optical domain, signal distortion is created or enhanced. There are several types of signal distortions in the RoF transmission system, which can be induced in the electrical domain or the optical domain. The distortions in both domains will be discussed, as well as the linearization techniques to suppress these distortions.

### 2.1 RoF Technologies

#### 2.1.1 Optical Fibers

The idea that an optical fiber might be used as a means of communication was proposed by Charles Kao and George Hockham in 1966 [6]. Corning Glass Works successfully produced the first single-mode fiber with attenuation below 20 dB/km in 1970, which made the idea of optical fiber transmission technically feasible. In 1977, that idea turned into reality after the first optical telecommunication system was installed in Chicago. In 1979, attenuation loss at 1550 nm of single-mode fibers was reduced to 0.2 dB/km. Since then the optical communication systems have been extensively deployed around the world.

Single-mode fiber (SMF) supports only one guided mode, while multi-mode fiber (MMF) can support more than one guided mode. One guided mode corresponds to an incident ray on the fiber with a specific angle. MMF has much larger core radius (25-35  $\mu\text{m}$ ) compared with single-mode fiber (4-9  $\mu\text{m}$ ). This makes it easier to align the fiber-to-fiber or fiber-to-transceiver connections. Besides, MMF can work with inexpensive optical source, such as light-emitting diode (LED). However, because of intermodal dispersion, MMF cannot be used for long-haul

and/or high-bit-rate applications. Typically, MMF can only be used in the link of a few kilometers at a bit rate of 1 Gb/s. Since SMF does not suffer from intermodal dispersion, it can be used for long-haul (1000 km – 30,000 km) and high-bit-rate (10 Gbps – 100 Gbps) applications.

Mode-division multiplexing (MDM) has attracted intensive research efforts recently since each mode of the MMF could carry independent data. Therefore, the bandwidth of the MMF can be increased by a factor  $M$ , where  $M$  is the number of modes of the MMF. However, the performance of this technique is affected by the intermodal dispersion and cross-talk between the different modes [7].

Multi-core fiber (MCF) is another way to spatially increase the capacity limit of the optical communication system [8]. MCF combines the benefits of low cross-talk and capacity enhancement. In 2011, the length of the MCF transmission reached as long as 76.8 km [9].

### 2.1.2 Lasers

Laser is the optical source which generates the optical signal. A classical Fabry-Perot laser has the simplest structure, as shown in Figure 2-1. The incident optical wave is amplified in the gain medium between the cleaved facets. Figure 2-2 shows the output spectrum of a Fabry-Perot laser [4]. As can be seen, besides the main mode, there are also many side modes which carry a significant fraction of power. Lasers, which have this kind of output spectrum, are called multi-longitudinal-mode laser. These side modes will cause intersymbol interference at the receiver because of dispersion. Therefore, it is desirable to use a single-longitudinal-mode (SLM) laser.

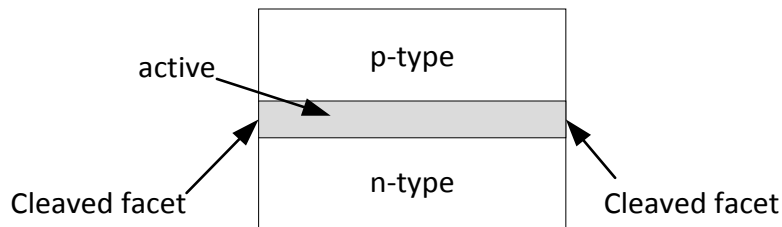


Figure 2-1 Structure of Fabry-Perot laser

To suppress the side modes, the cleaved facets are replaced by Bragg gratings, which are

periodically corrugated reflectors. This new design is called distributed Bragg reflector (DBR) laser, as shown in Figure 2-3. The output spectrum of DBR laser is shown in Figure 2-4.

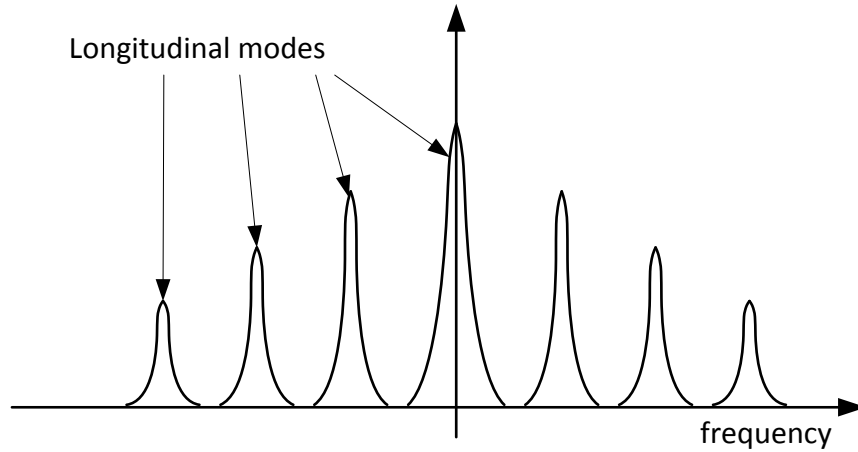


Figure 2-2 Output spectrum of a Fabry-Perot laser

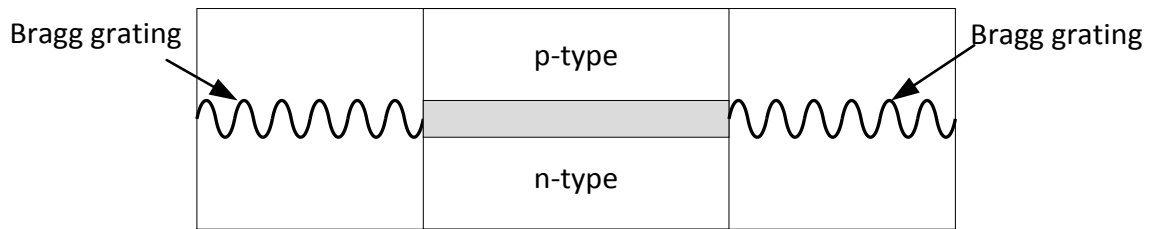


Figure 2-3 Structure of DBR laser

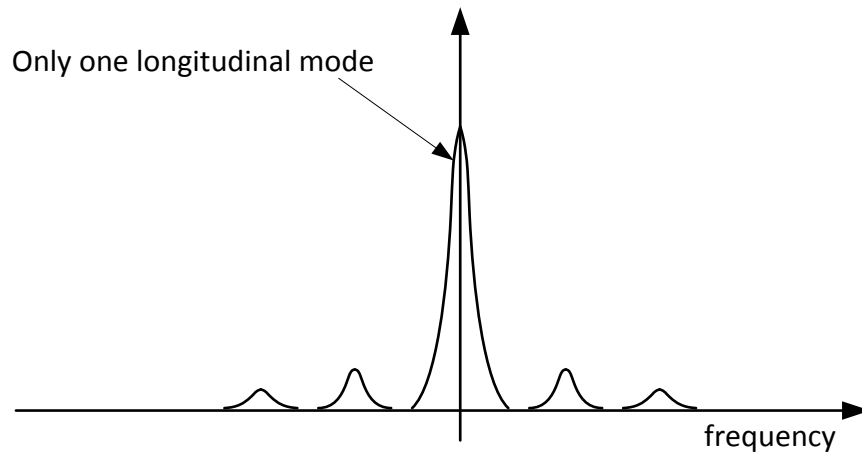


Figure 2-4 Output spectrum of a DBR laser

However, the corrugated region induces too much loss, which decreases the efficiency of the laser. To tackle this issue, the distributed-feedback (DFB) laser was designed, where the

Bragg grating is fabricated above the active region, as shown in Figure 2-5. Nowadays DFB lasers are widely used in the transmitters in optical fiber communications, as well as CD players, computer memory readers, etc.

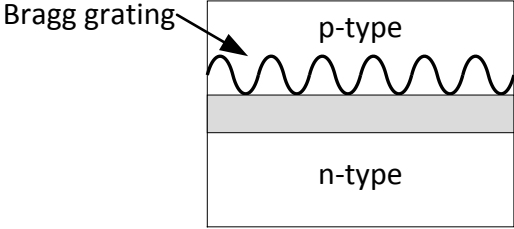


Figure 2-5 Structure of DFB laser

### 2.1.3 Optical Modulators

Optical modulator modulates the optical signal with message signals, either digital signals or analog signals. There are two types of optical modulation techniques: direct modulation and external modulation.

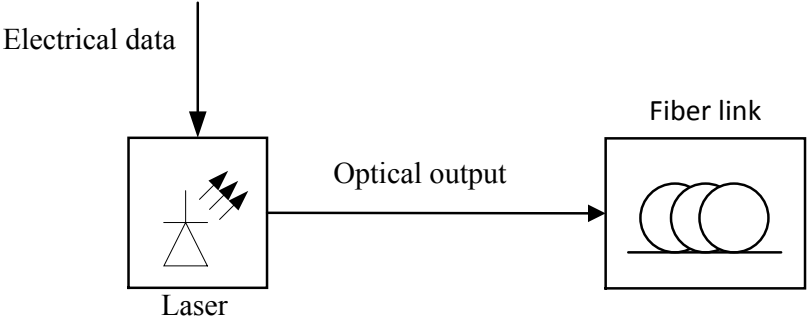


Figure 2-6 Direct modulation of a laser

In direct modulation, the laser’s driving current is modulated by the message signal, as shown in Figure 2-6. The measured transmission characteristic of a directly modulated laser is shown in Figure 2-7. As can be seen, the nonlinearity between the input and output is obvious. Besides, the bandwidth of the directly modulated laser is limited by the frequency chirp of the laser [10]. The advantage of the direct modulation is the simple structure and low cost.

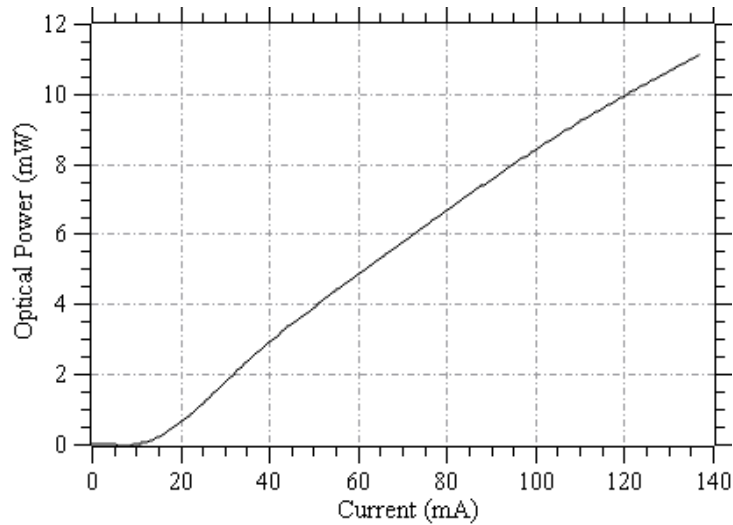


Figure 2-7 Transmission characteristic of a directly modulated laser

For applications, such as backhaul of the RoF transmission system or the current telecommunication system, external modulators are preferred because of the higher bandwidth. There are three widely used external modulators: the phase modulator, the Mach-Zehnder modulator (MZM), and the electro-absorption modulator (EAM). The typical structure of the transmitter using an external modulator is shown in Figure 2-8.

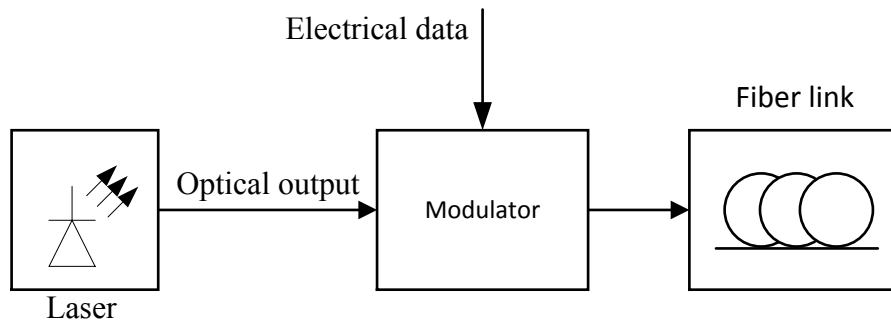


Figure 2-8 Transmitter using an external modulator

Phase modulator is designed based on the principle that the refractive index of an electro-optic crystal changes proportionally to the electric field intensity applied on it. When the refractive index changes the phase of the optical signal also changes [4]. The structure of a phase modulator is shown in Figure 2-9.

The structure of an MZM is shown in Figure 2-10. As can be seen, there are two arms in an MZM, and each works as a phase modulator. These two arms are connected to the input and

output ports with two power dividers. In such a combination, an MZM can be used to realize ASK or PSK in optical domain.

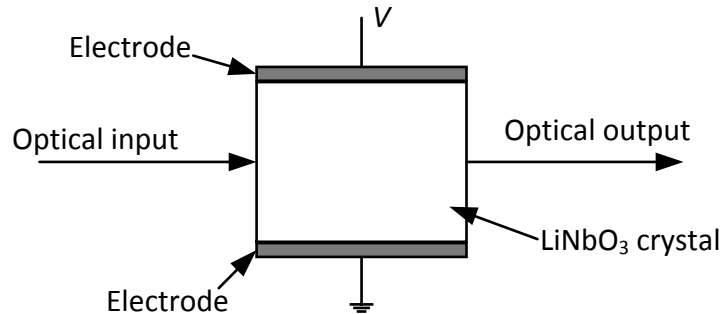


Figure 2-9 Phase modulation in a LiNbO<sub>3</sub> crystal

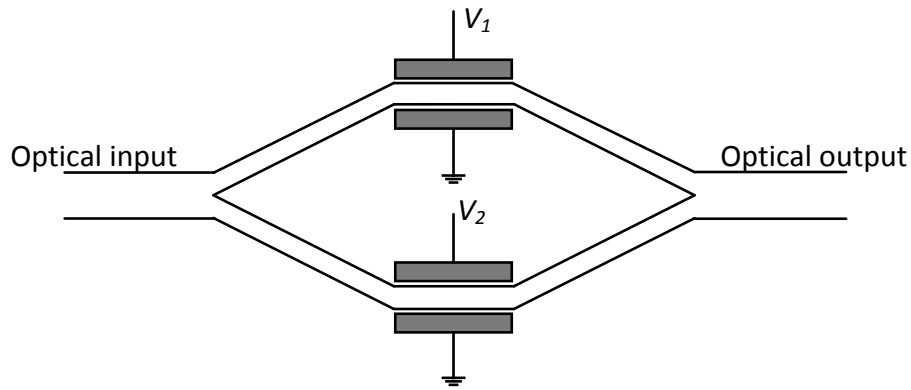


Figure 2-10 Structure of an MZM

EAM is designed based on another characteristic of the semiconductor. When the applied electrical field is increased, the band gap of the semiconductor will decrease. If the band gap changes from a level below the photon energy to a level above the photon energy, the optical output will change accordingly, or vice versa. The EAMs are very effective, usually come in very small sizes, and can easily be integrated with the laser diode in one chip. However they also have the problem of frequency chirps as the directly modulated lasers do.

#### 2.1.4 Optical Receivers

In the simplest form, an optical receiver consists of a photodetector (PD), a preamplifier and the electrical signal processing circuit, as shown in Figure 2-11 [4]. The photodetector converts the received light into electrical current, which is then amplified by the preamplifier. The signal processing circuit could be an analog filter and/or some other electrical components.

There are various types of photodetectors. Some photodetectors have no internal gain, such as PN photodiodes and PIN photodetectors, while some have, such as avalanche photodetectors.

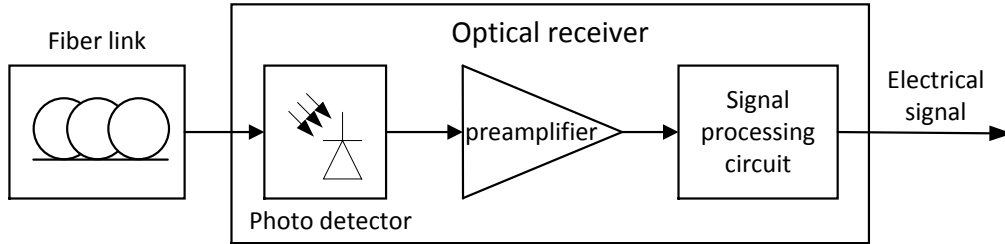


Figure 2-11 A simple optical receiver

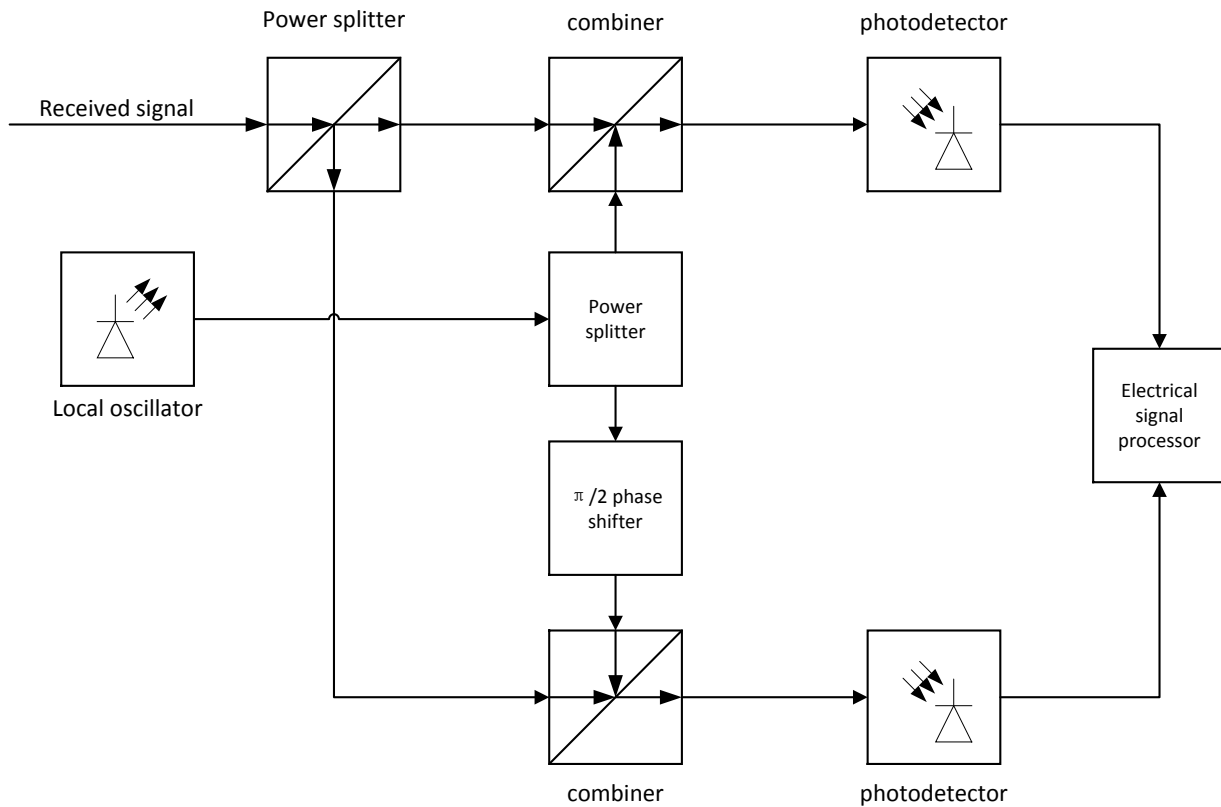


Figure 2-12 Optical IQ coherent receiver

The optical receiver could be designed as a direct (incoherent) receiver, or a coherent receiver. In the direct optical receiver, the power of the incident light is converted into current directly. The phase and frequency information is not taken into consideration. On the contrary, the output of the coherent receiver is related not only to the power of the light, but also to the phase or frequency of the light. The block diagram of IQ coherent receiver is shown in Figure

2-12, which can perform QAM demodulation.

### 2.1.5 RF Power Amplifier

RF power amplifier is not new in RoF technology, but it is still a very important component in the RoF transmission system because wireless signals attenuate very fast in the air, and the higher the frequency, the faster the attenuation. Therefore, if the signals are sent out without amplification, nothing will be received by the users' mobile phones.

When designing or choosing the RF power amplifier, efficiency and linearity are two most important properties that we should pay attention to. The reason why power efficiency is so important is that the RF power amplifier has probably the highest power consumption in the base station. RF power amplifier works in a way that it converts the DC power to RF power in the form of the amplified signal. Therefore, higher power efficiency means lower operating cost for base station.

While the power amplifier boosts the signals' power level, it also induces nonlinearity to the signals. This is determined by the physical characteristics of the power amplifier, no matter it is fabricated by the laterally diffused metal oxide semiconductor (LDMOS) technology, gallium arsenide (GaAs) technology or gallium nitride (GaN) technology, because they share the similar IV characteristic curve. A typical IV characteristic curve for NPN silicon transistor is shown in Figure 2-13 [11].

There are a lot of operation modes and the classical ones are Class A, Class B, Class AB, and Class C [12]. The classification of these modes is based on the location of the bias point of the power amplifiers.

The bias point of Class A is located in the middle of the working range. The output could be very linear when the signal is small. However, the power efficiency is very low. Even the theoretical maximum is only 50%.

The bias point of Class B is located at the threshold voltage, so the power amplifier outputs signal only when the input signal is greater than the threshold. The theoretical power

efficiency could reach 78.6%, which is much higher than that of Class A. However the nonlinearity is also much stronger than that of Class A.

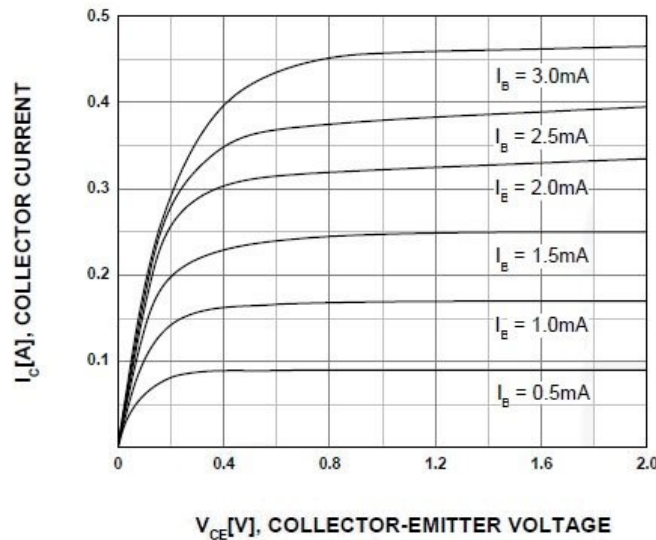


Figure 2-13 A typical IV characteristic curve for NPN transistor

Actually it is very difficult to precisely design a Class B power amplifier because of the variation of the threshold voltage. Therefore, Class AB is a more practical choice. The bias point of Class AB is slightly above the threshold voltage and the power efficiency still can theoretically reach over 70%.

The power transistor of Class C is biased below the threshold voltage. The power efficiency could be as high as 100%, but the linearity is very poor. This type of power amplifier could be used in applications where signal distortion is not a problem, such as the FM transmission.

However, most of the applications have very strict requirement for the linearity of the signals. Therefore, some new techniques have been used to design the more efficient power amplifier while keeping the linearity at acceptable level. The Doherty amplifier and envelope tracking have gained a lot of research interests for a long time.

The Doherty amplifier was proposed by W. Doherty in 1935 [13], this architecture and its several variations dominate the market of RF power amplifier used in the base stations. The schematic of the Doherty amplifier is shown in Figure 2-14 [12]. As can be seen, the

Doherty amplifier is composed of a main amplifier, which works in Class AB mode for all signal levels, and a peaking amplifier, which works in Class C mode and only turns on at high power input. With such an architecture, the linearity of the output signal at the high power-level can be improved when the main amplifier is saturated but the peaking amplifier turns on.

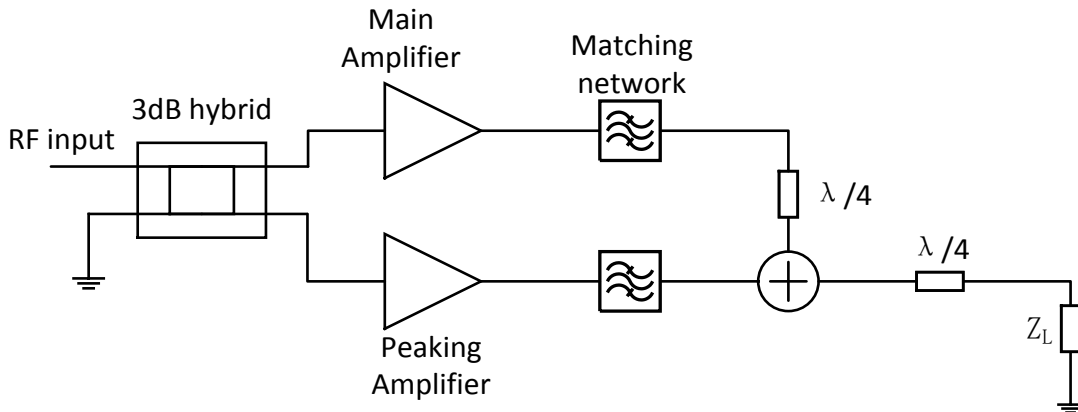


Figure 2-14 Schematic of Doherty PA

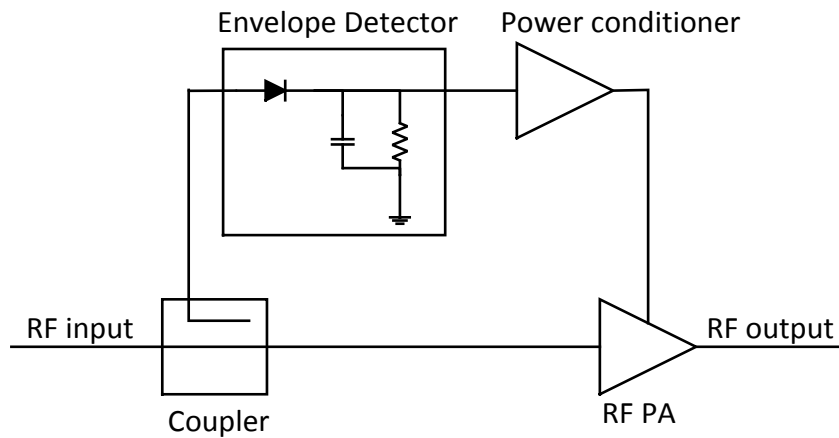


Figure 2-15 Schematic of envelope tracking power amplifier

The envelope tracking (ET) power amplifier adopts the polar modulation technique where the DC bias of the power transistor is modulated according to the magnitude of the modulation signal, thus to make the power amplifier work at maximum efficiency at all time. The structure of the ET power amplifier is shown in Figure 2-15 [12]. ET PA attracted extensive attention because of its high power efficiency and high linearity [14]. Lots of patents have been applied to build the technical barrier by some corporations [15-20].

## 2.2 Distortions in RoF Transmission Systems

Distortion includes nonlinearity and memory effect. Nonlinearity refers to the nonlinear relationship between the input and output signals, in terms of power, voltage or any other characteristic. This is static relationship, while memory effect is a dynamic relationship between the input and output signals. If a device or electrical component has memory effect, the present value of the output signal is influenced by the history of the input signal and/or output signal.

Signal distortions in RoF transmission system includes those in electrical domain and those in optical domain. In the electrical domain, the RF power amplifier contributes the most part of the nonlinearities and memory effects. The signal distortions in optical domain are mainly caused by optical modulators, optical receivers and optical fibers.

### 2.2.1 Nonlinearity

Nonlinearity refers to the nonlinear relationship between the input and output signals and almost all analog devices or circuits have nonlinearity to some extent. A typical nonlinear relationship between the input power and output power of an RF power amplifier is shown in Figure 2-16. In the linear region, the output power increases proportionally to the input power. However, in the saturation region, the output power deviates from linear relationship farther and farther as the input power increases.

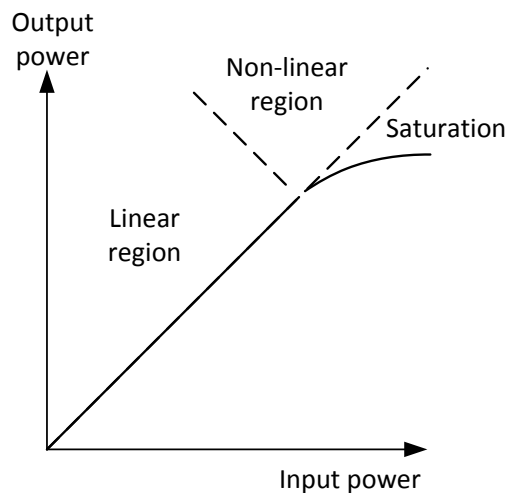


Figure 2-16 Nonlinearity of a power amplifier

## 2.2.2 Memory Effect

As shown in Figure 2-17, memory effect refers to the influence of the history of the input signal and/or the output signal on the current output signal. The number of samples which have significant influence on the current output signal is called the memory depth of a device.

According to the memory depth, memory effects can be divided into short-term and long-term memory effects. For an RF power amplifier, the short-term memory effect lasts in the order of several cycles of the RF signal, while the long-term memory effect occurs on the timescale of the modulation signal or even longer. Matching networks and device capacitances are the main contributors of short-term memory effect, while thermal effects, charge trapping, bias circuit effects, and control circuitry are the main mechanisms for long-term memory effect [12].

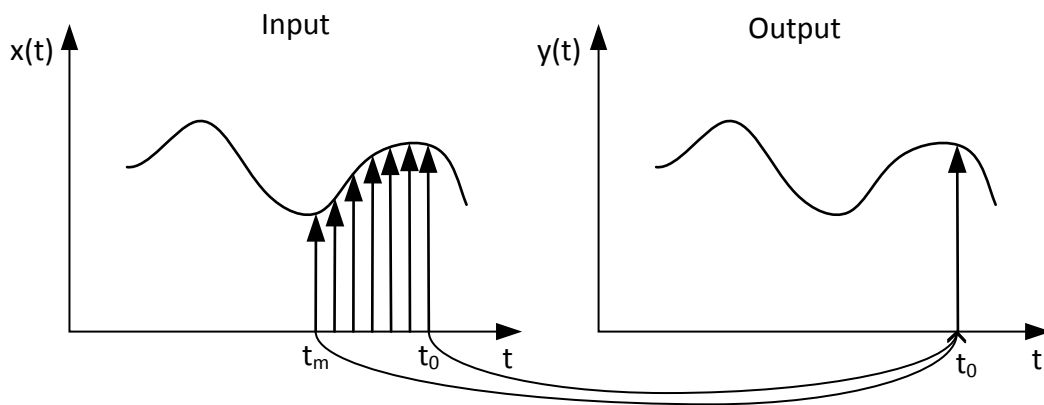


Figure 2-17 Memory effect of the input signal on the output signal

## 2.2.3 Distortions in Electrical Domain

RF power amplifier produces most of the distortion in the electrical domain. In the traditional wireless communication architectures, the nonlinear characteristic of the RF PA has been extensively studied [21]. The distortion is usually examined in frequency domain, as shown in Figure 2-18 and Figure 2-19. Figure 2-18 shows the output spectrum from PA model in a two-tone test. The frequencies of the two input signals are  $f_1$  and  $f_2$ . The distortions include the second-order intermodulation distortion (IMD2) at  $f_2 - f_1$ , harmonic distortion at  $2f_1$ ,  $2f_2$ ,  $3f_1$  and  $3f_2$ , as well as the third-order intermodulation distortion (IMD3) and fifth-order intermodulation distortion (IMD5) residing close to the signals, as shown in Figure 2-19.

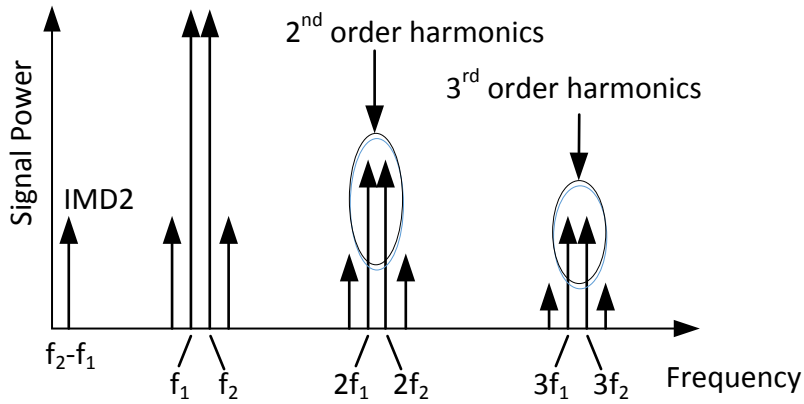


Figure 2-18 Output spectrum from a power amplifier

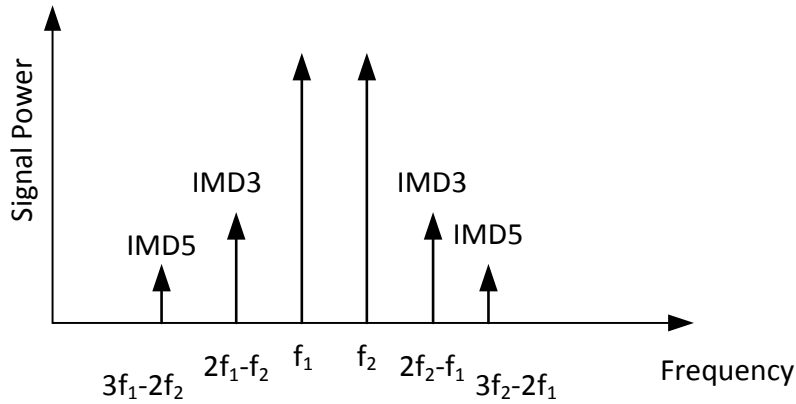


Figure 2-19 Output spectrum around the two signals from a power amplifier

Besides the intermodulation and harmonic distortions, there are also some other types of distortions, such as self-biasing, AM-to-AM and AM-to-PM effects, cross-modulation distortion [12], which are not shown here.

## 2.2.4 Distortions in Optical Domain

In the fronthaul of an RoF transmission system, optical modulators, optical receivers and optical fibers contribute most of the signal distortion.

Optical direct modulator produces the nonlinearity because of the nonlinear relationship between the input driving current and output optical power, as shown in Figure 2-20. The MZM and EAM will have the same issue if the level of the driving current is too high.

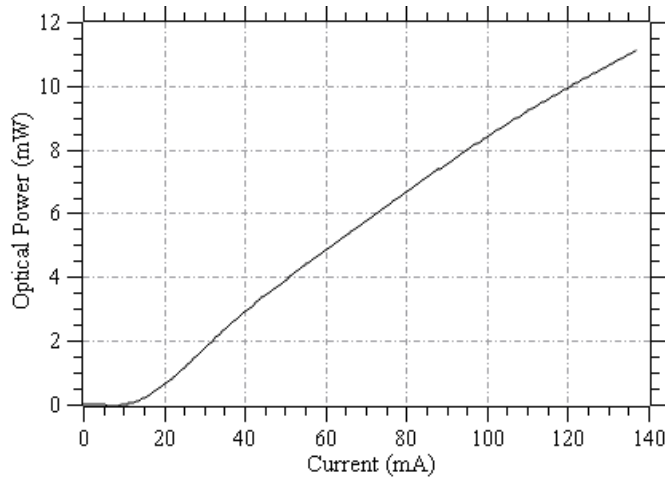


Figure 2-20 Transmission characteristic of a directly modulated laser

Frequency chirping is another source of signal distortion in optical modulators. As the driving current changes, the electrical field changes, then the refractive index of the active layer in the modulator changes. The change of refractive index causes frequency chirping, which leads to pulse broadening [4].

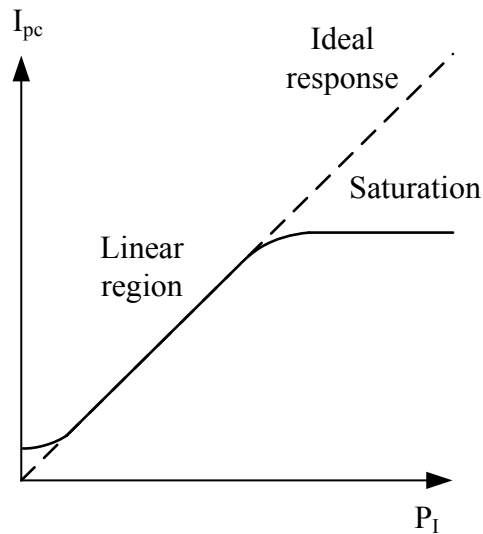


Figure 2-21 Response characteristics of a typical photodetector

An optical receiver produces nonlinearity as well, as shown in Figure 2-21. In the saturation region, even if the input optical power ( $P_I$ ) increases, the photocurrent ( $I_{pc}$ ) no longer increases. However, the optical transmission system usually works at low optical power levels, so the saturation is not a problem in most cases.

When an optical receiver converts optical power into electrical current, it also induces shot noise and thermal noise [4]. The shot noise refers to the fluctuations in photocurrent owing to the quantum nature of photons. The thermal noise is produced by the random movement of electrons related to temperature.

As the optical signal propagates through optical fiber, the optical fiber also induces nonlinearity to the signal. Firstly, different frequency components travel at different speed in the fiber, and this makes a pulse broadened after the optical transmission. This is called fiber dispersion. Secondly, refractive index of the fiber changes proportionally to the optical intensity, which is known as the Kerr effect. Because of the Kerr effect, the optical fiber causes self-phase modulation (SPM), cross-phase modulation (XPM), four-wave mixing (FWM), intra-pulse self-phase modulation, intra-channel four-wave mixing (IFWM) and intra-channel cross-phase modulation (IXPM) [4]. Thirdly, the thermal fluctuation of fiber density due to thermo-elastic motions of the molecules results in modulation of the reflective index of the fiber, which acts as reflective index grating. The scattering of light caused by this kind of grating is called stimulated Brillouin scattering. The scattered light propagates in the backward direction, affects the output of the laser and finally degrades the signal-to-noise ratio (SNR) at the optical receiver. Finally, stimulated Raman scattering is another important kind of nonlinearity that is caused by the interaction between optical field and molecules. Incident light with high power can excites molecular vibrations at the frequency of the incident light and then stimulate the molecules to emit photons.

## 2.3 Linearization Techniques for RoF Transmission Systems

To eliminate the effect of the signal distortion in RoF transmission systems, many linearization techniques have been proposed [5]. The classification of these techniques is shown in Figure 2-22.

As can be seen, the linearization can be performed in optical domain using optical linearization techniques, or in electrical domain using electrical ones. The electrical linearization techniques can be further divided into analog approaches and digital approaches.

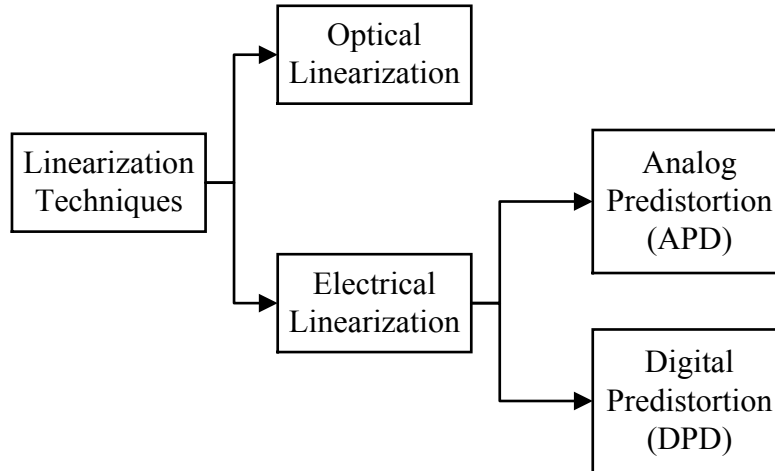


Figure 2-22 Classification of linearization techniques

### 2.3.1 Optical Linearization Techniques

Optical linearization techniques usually feature higher bandwidth compared with electrical counterparts, so they are very suitable for the broadband linearization for RoF transmission systems. However, they are more complex to implement than those in electrical domain. Besides, these techniques usually only deal with out-of-band distortions, such as IMD3, IMD5, harmonics, etc., but they can do little with the in-band distortion or memory effects. It would be better if these techniques could be combined with digital predistortion techniques.

One optical approach is to use mixed polarization to suppress the IMD3 in the RoF link [22-25]. The schematic is shown in Figure 2-23. The optical carrier passes through the first linear polarizer which is set to an angle of  $\alpha$  with respect to the z-axis and placed before the optical modulator. Another linear polarizer is placed after the optical modulator, with an angle of  $\beta$ . By carefully choosing the value of  $\alpha$  and  $\beta$ , the third-order intermodulation distortion can be significantly suppressed, and the spur-free dynamic range (SFDR) can be improved by 12.5 dB in experiment [22]. The mixed polarization technique can be further improved by substituting the second linear polarizer with a semiconductor optical amplifier (SOA) [26].

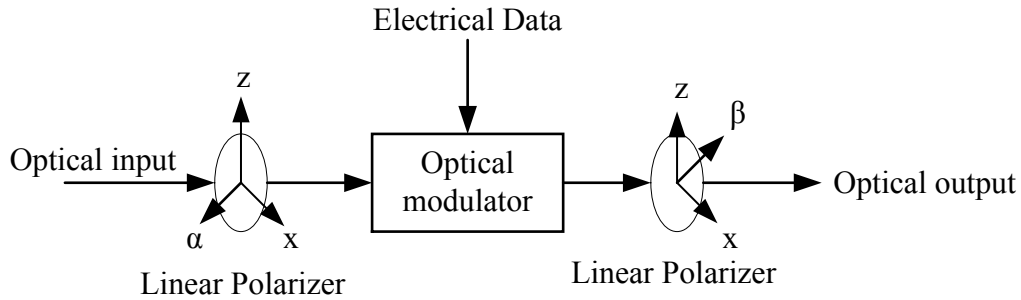


Figure 2-23 Schematic of mixed polarization linearization

Dual-wavelength linearization (DWL) is another optical approach to suppress the nonlinearity [27]-[29]. Figure 2-24 shows the schematic of the DWL. Two lasers with different wavelengths are used to generate two lights, which are coupled together and then modulated in the optical modulator. By changing the power ratio of the two lasers, the distortion can be suppressed. The third-order nonlinearity induced by EAM and MZM was suppressed by 30 dB and 26 dB respectively [27], [28]. The second-order nonlinearity induced by EAM was decreased by 23 dB [29].

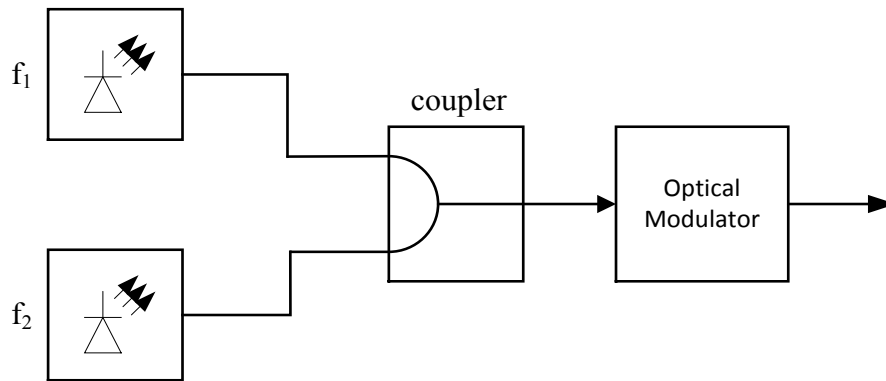


Figure 2-24 Schematic of dual-wavelength linearization

### 2.3.2 Analog Predistortion

Many analog linearization techniques have been proposed. Analog predistortion circuit is also a quite promising way for RoF applications. Analog circuits are very simple, cost-effective, and of low power consumption, and at the meantime, they are broadband [5]. However, just like the optical linearization techniques, most of the analog predistortion techniques are focused on suppressing the IMD3 and IMD5, but not the in-band nonlinearity or memory effects.

The schematic of an analog broadband RF pre-distortion circuit using reflective antiparallel diodes is shown in Figure 2-25 [30]. A power splitter splits the input signal into two paths, where a pair of antiparallel diodes are connected. The  $\lambda/4$  impedance transformers are used as broadband matching networks. When this circuit is added before the EAM, IMD3 is suppressed by more than 7 dB and SFDR is improved by 11 dB over the frequency range of 3.1 GHz - 4.8 GHz.

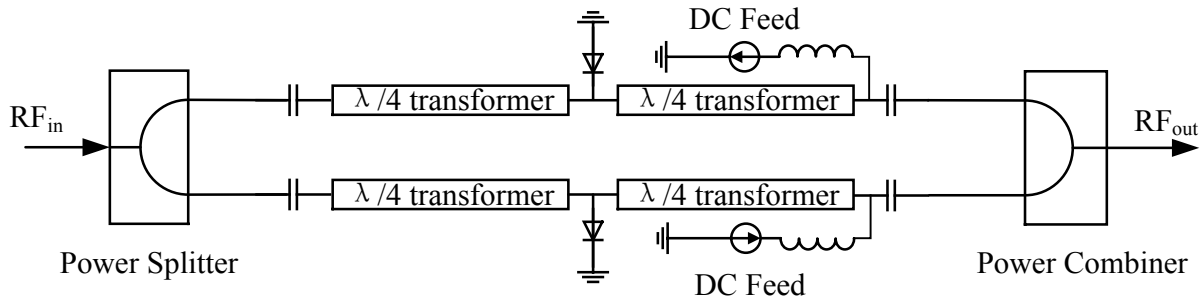


Figure 2-25 Schematic of analog predistortion circuit reported in [30]

In order to increase the bandwidth of the analog predistortion circuit and reduce the size and parasitic, a new analog circuit was proposed where two zero bias GaAs beam lead detector diodes were used [31], [32], as shown in Figure 2-26. Because of the high series resistance of the zero bias diodes, the broadband matching network is no longer needed. Therefore, the size of the circuit can be reduced. Power consumption is also reduced because the diodes can be biased at below 3 mA. It was experimentally verified that SFDRs were improved by 10 dB from 7 GHz to 14 GHz and 6 dB from 15 GHz to 18 GHz.

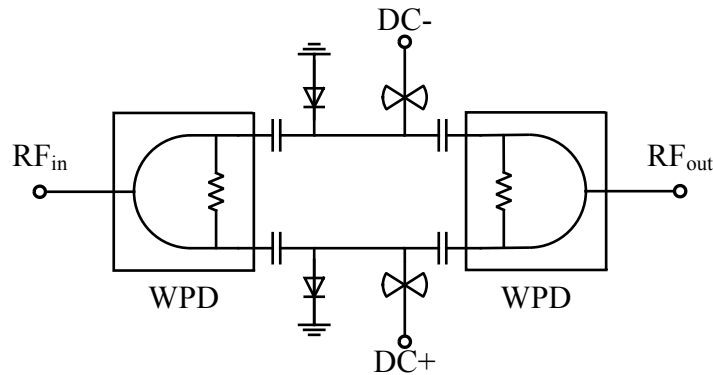


Figure 2-26 Schematic of analog predistortion circuit reported in [31]

The size of the circuit in [31] was further reduced by removing the Wilkinson power

dividers [33], as shown in Figure 2-27. Since the power dividers are removed, a dual Schottky diode is used to suppress the IMD3. The circuit can work from 10 MHz up to 40 GHz. In the two-tone test, SFDR was improved by more than 5 dB from 1 GHz to 30 GHz.

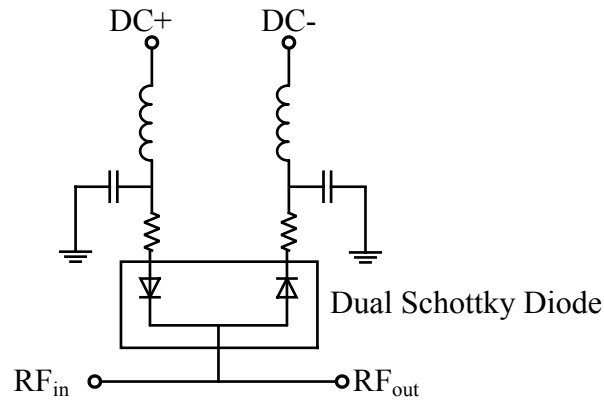


Figure 2-27 Schematic of analog predistortion circuit reported in [33]

### 2.3.3 Digital Predistortion

Digital predistortion (DPD) has been studied for decades and has been widely applied in satellite communications and ground wireless communications. DPD is good at improving the in-band linearity and capable of dealing with the memory effects. However, the performance of DPD is limited by the sampling rate of ADC. Therefore, they usually ignore the out-of-band distortion and leave it to analog filters. Most of the DPD techniques can be directly applied into the RoF transmission system, since the DPD techniques do not care about the intermediate transmission process.

A typical block diagram of a baseband DPD is shown in Figure 2-28. The DPD module pre-distorts the digital baseband signal, which is then converted into an RF signal by DAC and up-conversion modules. In the current communication systems, the RF signal is amplified by the PA and then sent out through the antenna. While in the RoF systems, the RF signal passes through the RoF link before it is amplified. The output RF signal is captured and down-converted into a baseband signal, which is used for DPD training. Finally the coefficients are updated in the DPD module.

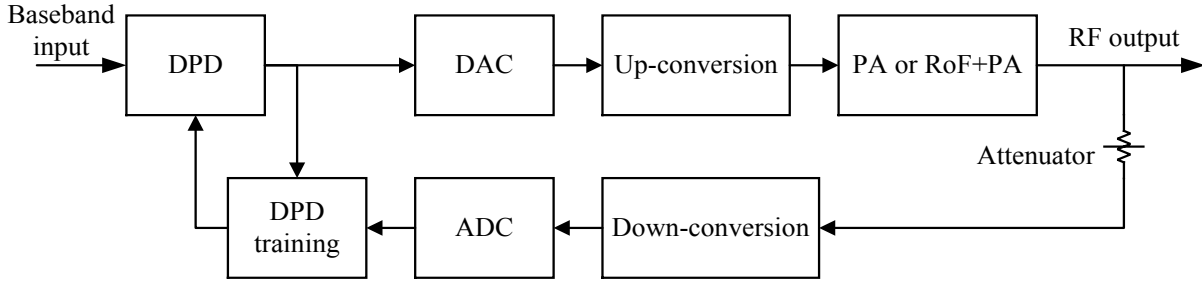


Figure 2-28 Block diagram of DPD

The DPD can also work with the digital RF signal, as an RF DPD. In this case, the block diagram of the RF DPD is shown in Figure 2-29.

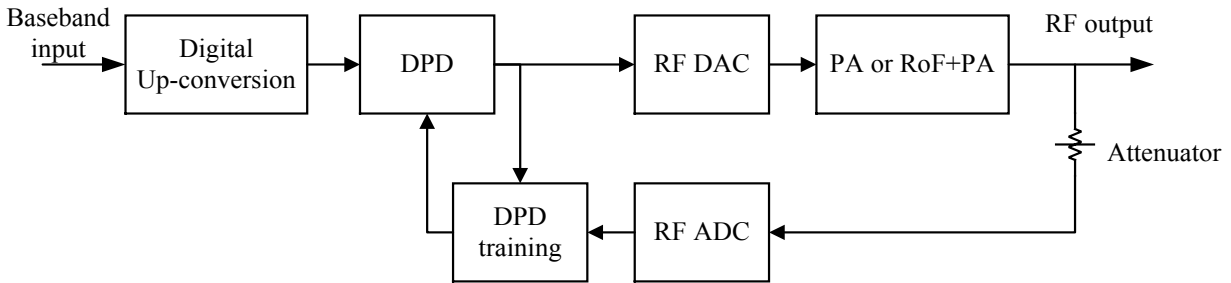


Figure 2-29 Block diagram of RF DPD

For a nonlinear system without memory effect, or where the memory effect is negligible, the nonlinearity of the system can be expressed with a nonlinear instantaneous model [12], as shown in (2.1).

$$y(t) = a_0 + \sum_{n=1}^N a_n u^n(t) \quad (2.1)$$

where  $y(t)$  is the output,  $u(t)$  is the input,  $N$  is the polynomial degree, and  $a_0, \dots, a_N$  are the polynomial coefficients.

As the bandwidth of the signal increases, the memory effect becomes stronger and stronger. Therefore, a nonlinear dynamical model has to be used, such as the Volterra series or one of its evolved forms, for the behavior modeling of an RF power amplifier or an RoF system. The classical discrete-time expression for Volterra series is shown in (2.2) [12].

$$\begin{aligned}
y(t) &= \sum_{m_1=0}^M h_1(m_1)u(t - m_1) \\
&+ \sum_{m_1=0}^M \sum_{m_2=0}^M h_2(m_1, m_2)u(t - m_1)u(t - m_2) \\
&+ \sum_{m_1=0}^M \dots \sum_{m_n=0}^M h_n(m_1, \dots, m_n)u(t - m_1) \dots u(t - m_n) \\
&= \sum_{n=1}^N \sum_{m_1=0}^M \dots \sum_{m_n=0}^M h_n(m_1, \dots, m_n) \prod_{j=1}^n u(t - m_j) \tag{2.2}
\end{aligned}$$

where  $y(t)$  is the output,  $u(t)$  is the input,  $N$  is the polynomial degree,  $M$  is the memory depth,  $h_n(m_1, \dots, m_n)$  are the polynomial coefficients.

However, this Volterra series model has an obvious drawback. As can be seen, the number of the polynomial coefficients increases exponentially as the polynomial degree and the memory depth increase. Therefore, a lot of effort has been made to simplify the Volterra series. Some of the most important simplified polynomials are memory polynomial [34], generalized memory polynomial [35], dynamic deviation reduction [36] and 2D-DPD [37].

Memory polynomial (MP) has been widely used because it is simple while robust, which can be described by (2.3) [34].

$$y(t) = \sum_{n=1}^N \sum_{m=0}^M a_{nm}x(t - m)|x(t - m)|^{n-1} \tag{2.3}$$

where  $a_{nm}$  are the coefficients of the DPD model.

As can be seen, the memory polynomial is much simpler than the full Volterra series by only keeping the diagonal terms and it is still very effective in many cases.

Generalized memory polynomial (GMP) is more effective than MP by adding more cross terms adjacent to the diagonal terms. The expression is given in (2.4) [35].

$$\begin{aligned}
y(n) = & \sum_{k=0}^{K_a-1} \sum_{l=0}^{L_a-1} a_{kl} x(n-l) |x(n-l)|^k \\
& + \sum_{k=1}^{K_b} \sum_{l=0}^{L_b-1} \sum_{m=1}^{M_b} b_{klm} x(n-l) |x(n-l-m)|^k \\
& + \sum_{k=1}^{K_c} \sum_{l=0}^{L_c-1} \sum_{m=1}^{M_c} c_{klm} x(n-l) |x(n-l+m)|^k
\end{aligned} \tag{2.4}$$

where  $K_a L_a$  is the number of coefficients of diagonal terms,  $K_b L_b M_b$  is the number of coefficients of cross terms between the signal and the lagging envelope, and  $K_c L_c M_c$  is the number of coefficients of cross terms between the signal and the leading envelope.

Experiment in [35] shows the GMP is better than MP at eliminating the power leakage in adjacent channels and a 60 dB of dynamic range is achieved.

Dynamic deviation reduction (DDR) rewrites the Volterra series by mathematical reforms. After a series of reforms, the Volterra series is rewritten in the form of (2.5) [36].

$$\begin{aligned}
y(n) = & \sum_{p=1}^P h_{p,0}(0, \dots, 0) x^p(n) \\
& + \sum_{p=1}^P \left\{ \sum_{r=1}^p \left[ x^{p-r}(n) \sum_{i_1}^M \dots \sum_{i_r=i_{r-1}}^M h_{p,r}(0, \dots, 0, i_1, \dots, i_r) \prod_{j=1}^r x(n-i_j) \right] \right\}
\end{aligned} \tag{2.5}$$

where  $r$  represents the order of the dynamics involved in the model.

By choosing the value of  $r$ , the number of cross terms is changed by including only the most important cross terms. Experiment in [36] shows that when  $r=3$  the best performance can be achieved if the memory depth is set to 5 for that specific experiment setup.

The 2-D DPD technique is proposed especially for the two-band application. This model takes into account not only the individual distortion in each band, but also the effect of cross-modulation between the two bands. Even if the two bands are separated in frequency by 100MHz,

the sampling rate is very low because there are only two baseband samplings. The model is expressed in (2.6) [37].

$$\begin{aligned}
 y_1(n) &= \sum_{m=0}^{M-1} \sum_{k=0}^N \sum_{j=0}^k c_{k,j,m}^{(1)} x_1(n-m) * |x_1(n-m)|^{k-j} |x_2(n-m)|^j \\
 y_2(n) &= \sum_{m=0}^{M-1} \sum_{k=0}^N \sum_{j=0}^k c_{k,j,m}^{(2)} x_2(n-m) * |x_1(n-m)|^{k-j} |x_2(n-m)|^j
 \end{aligned} \tag{2.6}$$

where  $y_1(n), y_2(n)$  are the complex envelope of the output signals,  $x_1(n), x_2(n)$  are the complex envelope of the input signals,  $c_{k,j,m}^{(1)}, c_{k,j,m}^{(2)}$  are the coefficients of this model.

The 2-D DPD is very good at improving the in-band linearity in the two-band scenario. Experiment results show an adjacent channel power ratio of less than -50 dBc and a normalized mean square error of less than -40 dB [37].

# Chapter 3. Theoretical Analysis of Envelope-Assisted RF DPD

In this chapter, we will explain how the nonlinearities and memory effects of an RoF system are suppressed or minimized by DPD. The limitation of the traditional baseband DPD is discussed, and a new DPD model is proposed to address that limitation. Finally the DPD structure and the extraction of the DPD coefficients are discussed.

## 3.1 Modeling Nonlinearities and Memory Effects of RoF Systems

As it is stated in Chapter 2, if the memory effect is negligible in a nonlinear system, the nonlinearity of the system can be modeled and diminished by a nonlinear instantaneous model, as given in (2.1). If the memory effect is strong, the Volterra series or one of its evolved forms has to be employed, as given in (2.2) – (2.6), or many other forms proposed in literature.

DPD works in a way that it creates the reverse nonlinearities and memory effects to what are induced by the RoF systems. Figure 3-1 shows how the nonlinearity is corrected by the DPD. The output of RoF system with RF power amplifier tends to be very nonlinear near the saturation region. After inserting the DPD module, the final output becomes linear in the whole region below the saturation level.

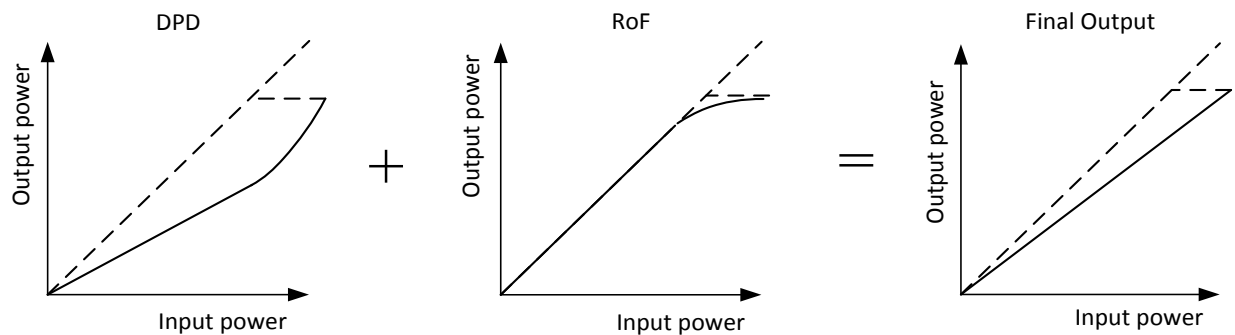


Figure 3-1 Correction of nonlinearity

Figure 3-2 shows how the memory effect is eliminated by the DPD. Because of the existence of the matching network, temperature-dependent influence, etc., the output wave of the

RoF system usually shows a phase distortion. With the help of a dynamic DPD, the phase distortion of the final output could be eliminated.

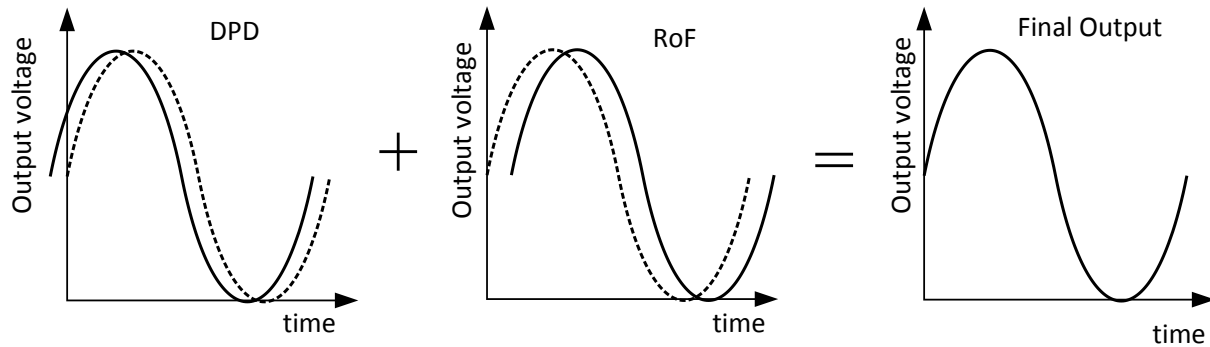


Figure 3-2 Correction of memory effect

### 3.2 Envelope-Assisted RF DPD

Among the numerous DPD models, memory polynomial is one of the simplest forms which can correct both the nonlinearities and the memory effects. It works very well with the 2G or 3G applications. However, as the bandwidth becomes higher and higher in 4G and 5G, the DPD is forced to work at a much higher frequency. For example, in LTE-A, if the carrier aggregation is enabled, the signal bandwidth can reach 100 MHz, which means that the baseband sampling rate of the ADC need to be 500 MHz. For the upcoming 5G technology, this baseband sampling rate could be even higher. Such a high sampling rate could be a challenge for the ADC.

The good news is that lots of effort has been focused on the research and development of RF sampling ADC, such as the 13b 4GS/s pipelined-SAR ADC [38] and 12b 10GS/s interleaved pipeline ADC [39]. With the availability of RF sampling ADC, now the DPD could work with the RF signals. With the increased sampling rate, the DPD can even correct the IMD3 and IMD5.

However, if the memory polynomial works at such a high sampling rate, the memory depth of the DPD might be too long, and there might be too many coefficients in the polynomial if there is a strong long-term memory effect in the system. In order to simultaneously correct the short-term and long-term memory effect, and eliminate the in-band and out-of-band nonlinearities in the RoF systems with a reasonable number of coefficients, the envelope-assisted

RF DPD is proposed in this thesis. The mathematical expression of this new model is given in (3.1).

$$z(n) = \sum_{j=1}^J \sum_{p=0}^P a_{jp} x(n-p) |x(n-p)|^{j-1} + \sum_{k=1}^K \sum_{q=1}^Q b_{kq} x(n) |w(n-q)|^{k-1} \quad (3.1)$$

where  $z(n)$  is the output of the proposed DPD model,  $x(n)$  is the real value of the RF signal in time domain,  $w(n)$  is the sum of the absolute values of the baseband envelopes of each modulating signal,  $J$  is the highest nonlinear order of the RF signal,  $P$  is the memory depth in RF domain,  $K$  is the highest nonlinear order of the baseband signals,  $Q$  is the memory depth in baseband domain,  $a_{jp}$  and  $b_{kq}$  are the coefficients of the DPD model.

As can be seen, the proposed model is composed of two memory polynomials. The first part of (3.1) is aimed to eliminate the out-of-band nonlinearity, in-band nonlinearity and short-term memory effect, because the samples of  $x(n)$  are sampled at a very high radio frequency. The second part of (3.1) is aimed to eliminate the in-band nonlinearity and long-term memory effect because the samples of  $w(n)$  are sampled at a much lower frequency.

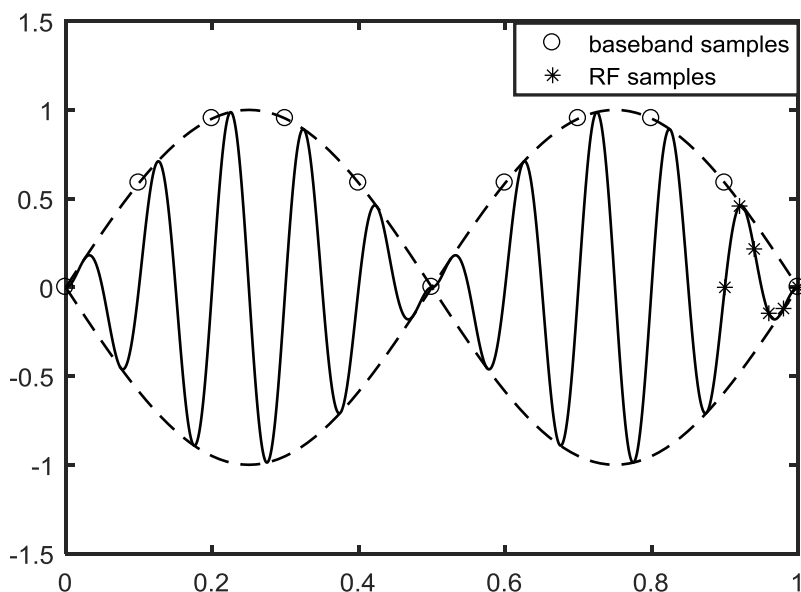


Figure 3-3 Baseband samples and RF samples

Figure 3-3 shows an example of the combination of baseband samples and RF samples. The baseband samples cover a long time span, as in a traditional baseband DPD, so they can be

used to suppress the long-term memory effect. The RF samples cover a short time span, distributed closely on the RF signal. Therefore, they can be used to eliminate the short-term memory effect, as well as the out-of-band nonlinearities such as IMD3 and IMD5, that a baseband DPD cannot deal with because of the limited sampling bandwidth.

### 3.3 Indirect Learning DPD Structure

The indirect learning architecture was first proposed to train a multilayered neural network by Demetri Psaltis, Athanasios Sideris, and Alan A. Yamamura in 1988 [40]. It was applied to DPD by Changsoo Eun and Edward J. Powers in 1997 [41], where the Volterra series was used in the DPD. It was combined with memory polynomial by L. Ding et al. [42].

The indirect learning structure for DPD is shown in Figure 3-4. The RF signal  $x(n)$  and baseband envelope  $w(n)$  pass through the predistortion module and the predistorted output signal  $z(n)$  is fed into the nonlinear device such as the RoF link or power amplifier. The output signal  $y(n)$  of the nonlinear device is monitored and attenuated by  $G$ , which represents the gain of the nonlinear device. After attenuation, the RF signal  $x_b(n)$  and baseband envelope  $w_b(n)$  pass through the training predistortion module (A) in the feedback loop, which is identical to the predistortion module in the forward loop. The output signal  $z_b(n)$  is used to compare with the predistorted signal  $z(n)$  and the error  $e(n)$  between  $z(n)$  and  $z_b(n)$  is used to train the predistortion module.

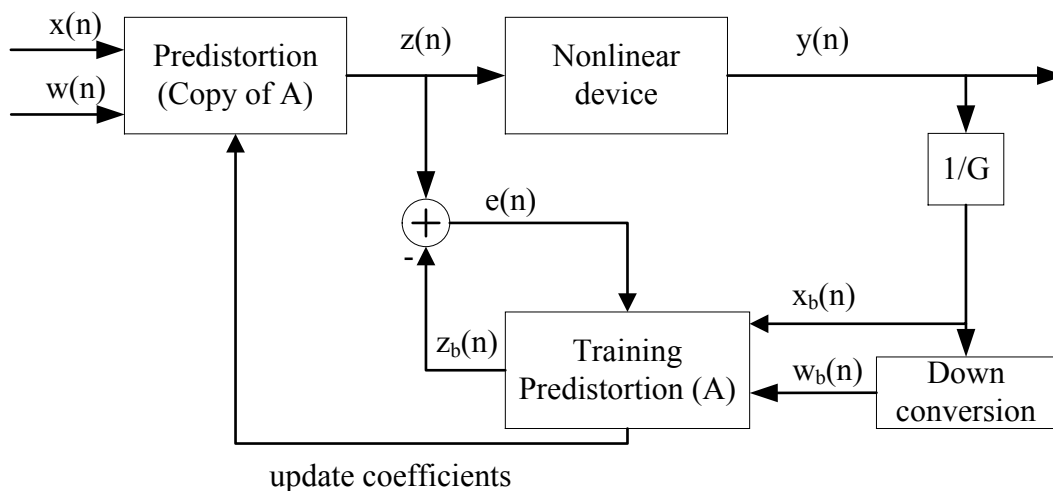


Figure 3-4 Indirect learning structure for DPD

In the ideal situation, the attenuated output signal  $x_b(n)$  should be equal to the input signal  $x(n)$ , which means the output signals  $z(n)$  and  $z_b(n)$  of these two DPDs are also equal to each other. In reality, there is always a difference between  $x(n)$  and  $x_b(n)$ , so as between  $z(n)$  and  $z_b(n)$ . The training process is a process to find the solution for the DPD coefficients when the error  $e(n)$  is minimized. If the training process of DPD is converged, it means the error  $e(n)$  is minimized, the solution for the DPD coefficients is found, the DPD acts inversely to the nonlinear device, and the nonlinearities and memory effects have been minimized. If the training process is not converged, it means the solution for such a DPD could not be found.

### 3.4 Extraction of Model Coefficients

Several techniques are available for the extraction of DPD coefficients in the indirect learning architecture, such as least squares algorithm (LS), least mean squares (LMS), recursive least squares (RLS). The least squares algorithm is most straightforward one, compared with the other two. Therefore, the least square algorithm is used to calculate the coefficients in this thesis.

As shown in Section 3.3, there are two DPDs in the indirect learning architecture, which are identical to each other. Therefore, we can calculate the coefficients of the DPD in backward loop, instead of calculating those of the DPD in the forward loop.

For the forward DPD, the relation between output signal and input signal can be expressed with (3.1). If we define

$$u_{jp}(n) = x(n-p)|x(n-p)|^{j-1} \quad (3.2)$$

and

$$v_{kq}(n) = x(n)|x(n-q)|^{k-1} \quad (3.3)$$

then we can rewrite (3.1) as

$$z(n) = \sum_{j=1}^J \sum_{p=0}^P a_{jp} u_{jp}(n) + \sum_{k=1}^K \sum_{q=1}^Q b_{kq} v_{kq}(n) \quad (3.4)$$

or in the form of vectors as

$$z(n) = [u_{10}(n), \dots, u_{1P}(n), \dots, u_{J0}(n), \dots, u_{JP}(n), v_{11}(n), \dots, v_{1Q}(n), \dots, v_{K1}(n), \dots, v_{KQ}(n)]\alpha \quad (3.5)$$

where  $\alpha = [a_{10}, \dots, a_{1P}, \dots, a_{J0}, \dots, a_{JP}, b_{11}, \dots, b_{1Q}, \dots, b_{KQ}]^T$ .

Usually thousands of samples are used in the least squares algorithm to find the best solution, so we can build a matrix as

$$\begin{bmatrix} z(1) \\ z(2) \\ \vdots \\ z(N) \end{bmatrix} = \begin{bmatrix} u_{10}(1) & \cdots & u_{JP}(1) & v_{11}(1) & \cdots & v_{KQ}(1) \\ u_{10}(2) & \cdots & u_{JP}(2) & v_{11}(2) & \cdots & v_{KQ}(2) \\ \vdots & \ddots & \vdots & \vdots & \ddots & \vdots \\ u_{10}(N) & \cdots & u_{JP}(N) & v_{11}(N) & \cdots & v_{KQ}(N) \end{bmatrix} \alpha \quad (3.6)$$

or in the simplified form:

$$Z = U\alpha \quad (3.7)$$

For the backward DPD, the input is the attenuated output signal  $x_b(n)$  and the output signal is  $z_b(n)$ . We can derive a similar expression between  $x_b(n)$  and  $z_b(n)$ :

$$Z_b = U_b\alpha \quad (3.8)$$

where matrix  $U_b$  has the similar form as matrix  $U$  except it is built with  $x_b(n)$ .

A typical measure of the difference between  $z_b(n)$  and  $z(n)$  can be expressed in the form of mean squared error (MSE):

$$MSE = \frac{1}{N} \sum_1^N (z(n) - z_b(n))^2 \quad (3.9)$$

This MSE can be minimized by taking the derivative of (3.9) and equating to zero. In this way, we can get:

$$Z = U_b\alpha \quad (3.10)$$

Since matrix  $U_b$  is not square, we cannot simply inverse it. Instead, the normal equation has to be used to estimate the coefficients:

$$\hat{a} = (U_b^H U_b)^{-1} U_b^H Z \quad (3.11)$$

where  $U_b^H$  represents the Hermitian (complex) transpose of  $U_b$ .

Before the first time of calculation, the coefficients in the forward DPD need to be initialized in the way that the input RF signal  $x(n)$  passes through the DPD unchanged, which means  $z(n)$  equals to  $x(n)$  before the coefficients are updated for the first time. After that,  $z(n)$  can be calculated using the updated coefficients and the coefficients can be updated recursively.

## Chapter 4. Simulation with Envelope-Assisted RF DPD

Simulation has been run with Matlab to verify the validity of the proposed envelope-assisted RF DPD, which can be used to suppress the nonlinearities and memory effects of an RoF system. Optimal memory depths in RF and baseband domain have been found. Two-band and three-band tests have been taken, where each band carries a 20 MHz LTE signal. Performance of the proposed model is compared with traditional baseband DPD. In this chapter, the simulation system is introduced and then the simulation results are reported.

### 4.1 Overview of the Simulation System

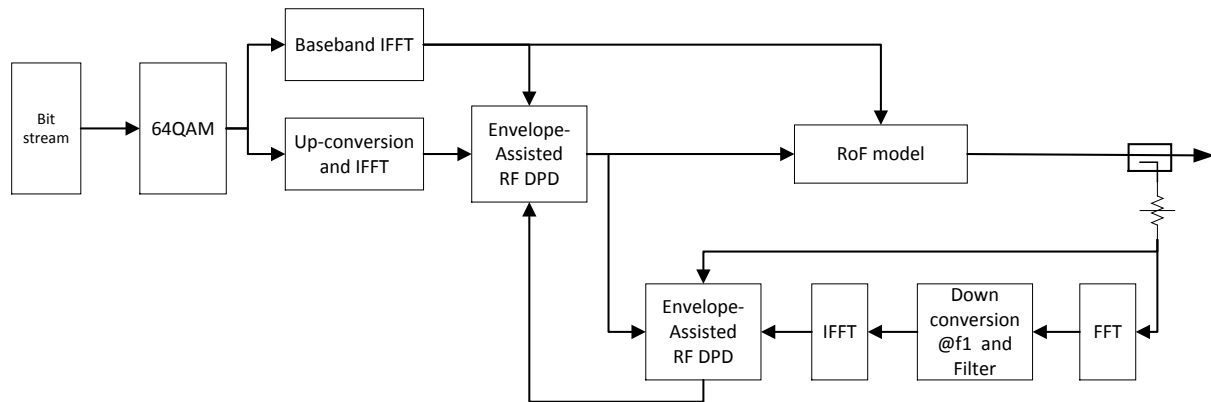


Figure 4-1 Indirect learning DPD structure of the proposed DPD in LTE communication

The indirect learning DPD structure of the proposed DPD in LTE communication is shown in Figure 4-1. This is an architecture for one band test. The bit stream is mapped into the digital symbols with digital modulation techniques such as QPSK, 16QAM, or 64QAM. In LTE or LTE-A, each symbol represents the complex value of a subcarrier which has a bandwidth of 15 kHz. Therefore, these digital symbols are allocated onto the subcarriers in frequency domain. One inverse fast Fourier transform (iFFT) converts the signal in frequency domain into a baseband signal in time domain. For a 20 MHz LTE signal, there are 100 resource blocks allocated for transmitting control signals and data. Each resource block contains 12 subcarrier occupying a bandwidth of 180 KHz. Therefore, 1200 subcarriers are used to transfer a 20 MHz LTE signal. The iFFT size is 2048, corresponding to a baseband sampling frequency of 30.72

MHz. A copy of the signal in frequency domain is up-converted to RF and transformed to a discrete RF signal in time domain by the other iFFT. The size of this RF iFFT is 262144, corresponding to a RF sampling frequency of 3.93216 GHz. Cyclic prefix has been added to the baseband and RF signals in time domain. The length of the cyclic prefix is 4.7  $\mu$ s for each OFDM symbol, as defined in the LTE standard, corresponding to 143 samples of the baseband signal and 18304 samples of the RF signal. A series of zeros has been added before the cyclic prefix to separate the repeated OFDM symbols. The length of the zeros is equal to the length of the cyclic prefix. The RF signal and the baseband envelope are then fed into the DPD module, which generates the predistorted RF signal and sends it to the RoF model or RoF link. The output signal of the RoF model or RoF link is attenuated and sent to the DPD in backward loop. A copy of the attenuated RF signal is down-converted into a baseband envelope by a fast Fourier transform (FFT), bandpass filter and iFFT. The DPD in the backward loop uses the RF signal and baseband envelope to calculate the coefficients which are then updated into the DPD in the forward loop. Coefficients in the forward DPD is initialized to pass the RF signal unchanged.

The architecture is adjusted to run the two-band test, as shown in Figure 4-2. In the two-band test, the summation of two baseband envelopes is used instead of a single-band envelope.

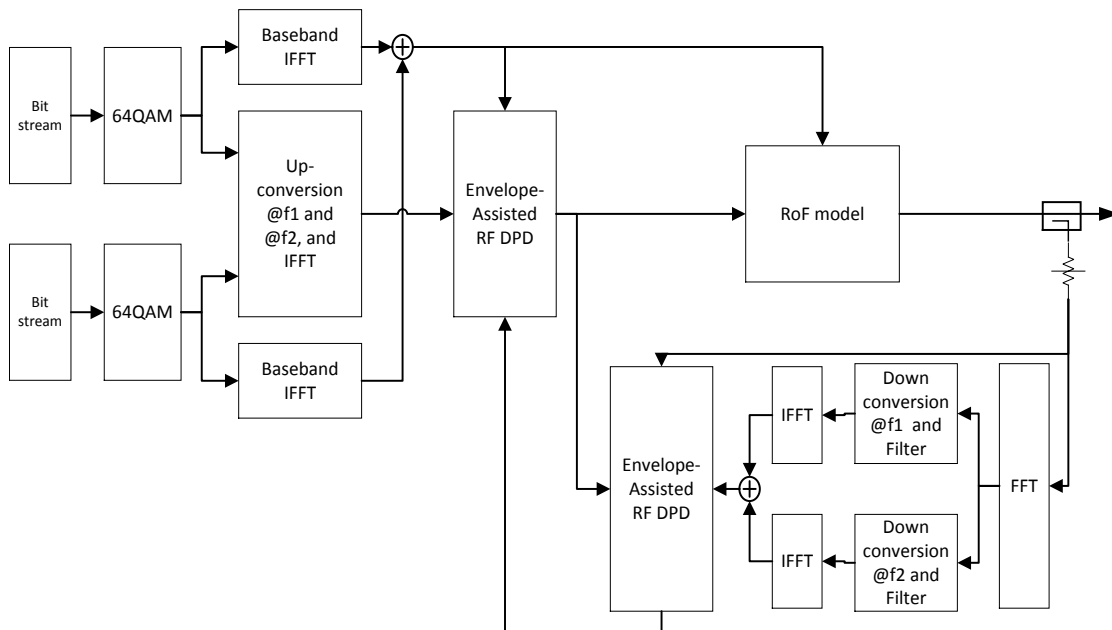


Figure 4-2 Indirect learning DPD structure of the proposed DPD for two-band test

A similar adjustment can be made to run the three-band test, which is not shown here. The difference is just that the summation of three baseband envelopes is used for the predistortion.

## 4.2 RoF Model

In simulation, an RoF model mimics a real RoF link. However, the RoF model is not extracted from the RoF link in our lab. Instead, it is specially designed to incorporate the in-band and out-of-band nonlinearities, the short-term and long-term memory effects. With such a model, the proposed DPD technique can be proved being capable of eliminating the in-band and out-of-band nonlinearities, the short-term and long-term memory effects simultaneously.

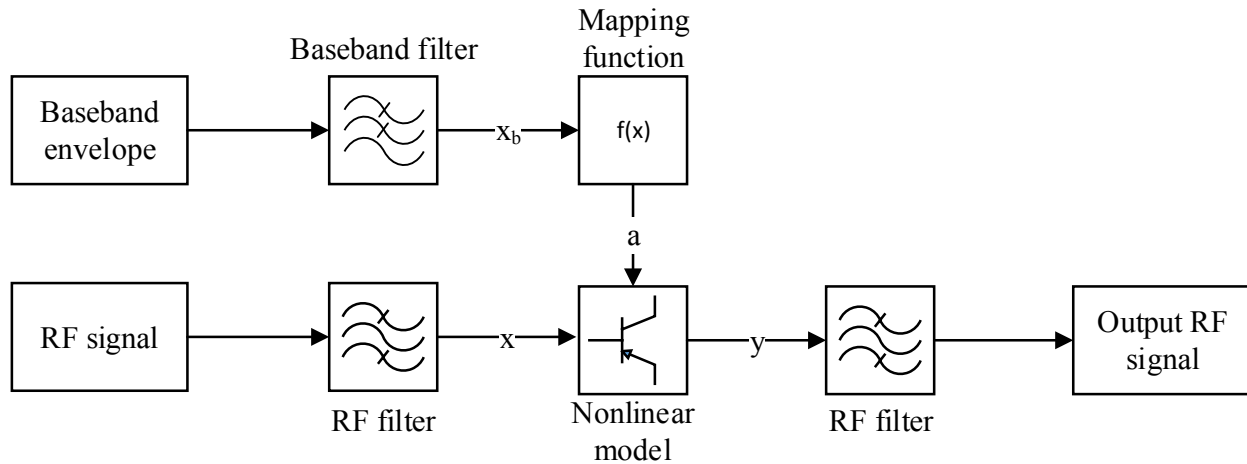


Figure 4-3 RoF model for simulation

The structure of the RoF model is shown in Figure 4-3. The RF signal passes through the RF filter before it is fed into the nonlinear model. The RF filter works as an input matching network and introduces short-term memory effect. The baseband envelope of the signal passes through the baseband filter, which produces long-term memory effect. The output of the baseband filter is mapped into a control signal ‘a’, which is used to adjust the characteristic of the nonlinear model. In such a way, the long-term memory effect is merged into the RF signal. The output signal of the nonlinear model passes through another RF filter which mimics the output matching network and adds short-term memory effect onto the output RF signal. The transfer functions of the baseband filter and the RF filter are given in (4.1) and (4.2) respectively.

$$H(z) = \frac{1 - 0.5z^{-1} + 0.25z^{-2}}{0.5 - 0.32z^{-2}} \quad (4.1)$$

$$H(z) = 0.1 + 0.4z^{-1} + 0.25z^{-2} + 0.15z^{-3} + 0.1z^{-4} \quad (4.2)$$

The nonlinear model is built with an exponential function, which is expressed in (4.3)

$$y = b * (1 - \exp(-x/a)) \quad (4.3)$$

where 'a' is the control signal, 'b' is a constant which can be used to adjust the maximum of the output signal.

The relation between 'x' and 'y' is shown in Figure 4-4. When the 'x' is small, 'y' increases linearly as 'x'. When 'x' is large enough, 'y' will be saturated toward the maximum of 10. This saturation creates both in-band nonlinearity and out-of-band nonlinearity. When 'a' changes between 8 and 10, the curve changes between the solid line and the dotted line. Since 'a' changes at the modulation rate, the corresponding change of the curve will induce long-term memory effect.

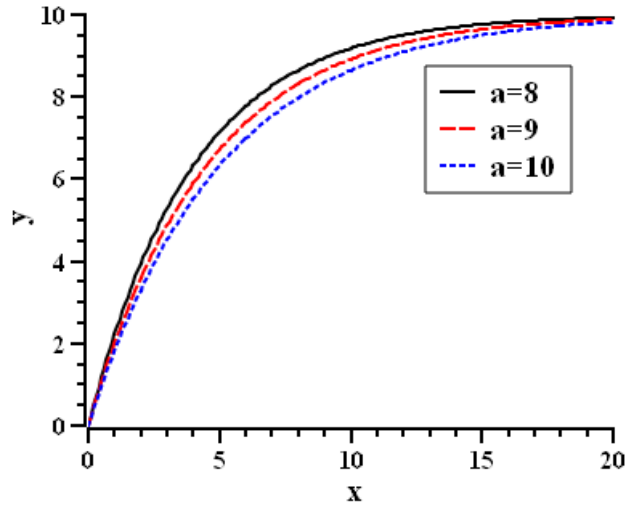


Figure 4-4 Input-output curve of the nonlinear model

A mapping function is used to map the baseband envelope into a value between 8 and 10, as given in (4.4).

$$a = 10 - 2 * \exp(-x_b/c) \quad (4.4)$$

where 'c' is a constant which changes the shape of the curve.

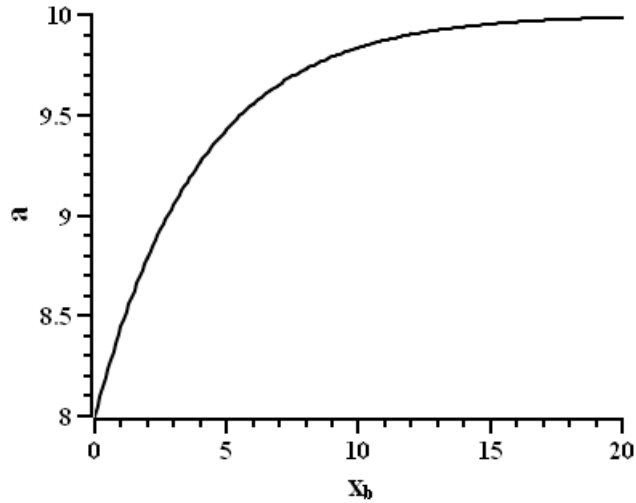


Figure 4-5 Mapping function between  $x_b$  and  $a$

The curve of the mapping function is shown in Figure 4-5. As can be seen, when the baseband signal changes, the output signal changes between 8 and 10.

Two RF filters are built with infinite impulse response filter (IIR) and the baseband filter is built with finite impulse response filter (FIR).

### 4.3 Optimal Memory Depth of the RF Polynomial

Memory depth is a characteristic of a specific transmission link. Different link has different memory depth. Therefore, before checking the performance of the proposed DPD, the RF and baseband memory depth should be tested first. Error vector magnitude (EVM) is one of the most important measure for in-band distortion. Therefore, the memory depth will be checked in terms of EVM improvement.

Two-band simulation has been run to find the optimal RF and baseband memory depth, with which the EVM is minimized and number of coefficients of the DPD model is as small as possible. The LTE signal contains two 20 MHz LTE bands located at 800 MHz and 900 MHz. Figure 4-6 shows the relationship between EVM and RF memory depth on two LTE bands respectively. As can be seen, the improvement of EVM is saturated after RF memory depth of 7 on the first band and 6 on the other band. Based on this simulation result, we choose an RF

memory depth of 8 for simulation with the RoF model which is introduced in section 4.2. With this value of RF memory depth, the EVM of each band is expected to be below 37 dB and the EVM improvement on each band is expected to be over 11 dB.

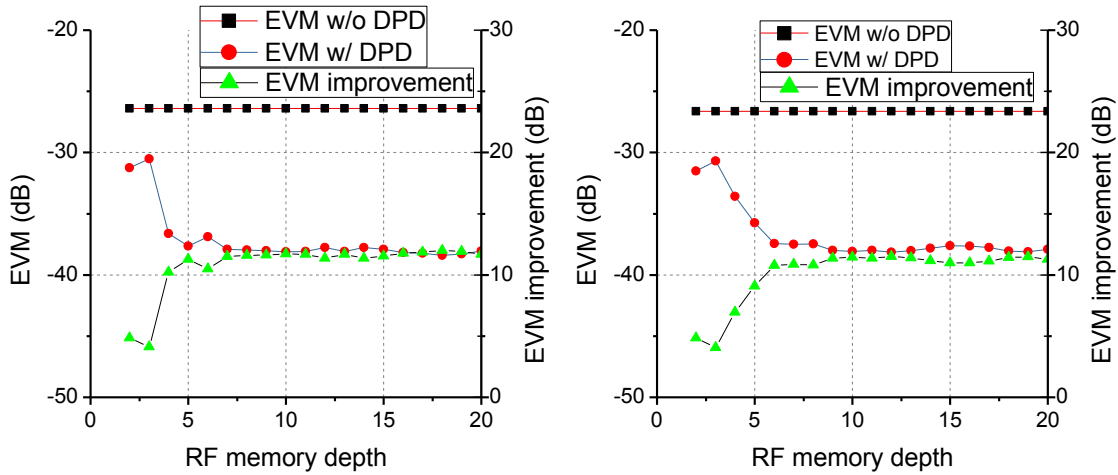


Figure 4-6 EVM vs RF memory depth (Left: lower band. Right: upper band.)

#### 4.4 Optimal Memory Depth of the Baseband Polynomial

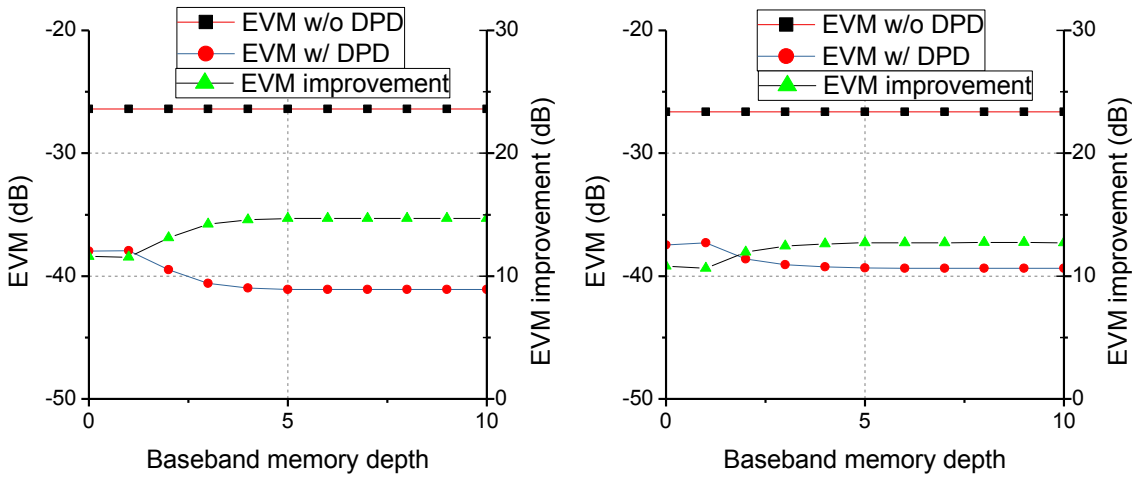


Figure 4-7 EVM vs baseband memory depth (Left: lower band. Right: upper band.)

Figure 4-7 shows how the EVM changes as the baseband memory depth increases. Simulation is run with an RF memory depth of 8 and the baseband memory depth changes from 0 to 10. The same signals are used as in section 4.3. As mentioned in section 4.3, the EVM

improvement is saturated when the RF memory depth is over 7. However, Figure 4-7 shows that the EVM can be further improved by 3 dB and 2 dB on lower band and upper band respectively when the baseband memory depth is 5. The EVM improvement is saturated again when the memory depth is more than 5. Therefore we set the baseband memory depth to 5 for the following simulation.

From the simulation results aforementioned, it can be seen that short-term memory effect has been minimized by the RF memory polynomial and long-term memory effect has been minimized by the baseband memory polynomial.

## 4.5 Comparison with Baseband DPD Techniques

In this section, the performance of the proposed DPD is evaluated and the comparison with a baseband DPD is made. The baseband DPD used for comparison is the 2D DPD, which is introduced in section 2.3.3. The mathematical expression of the 2D DPD is given in (2.6).

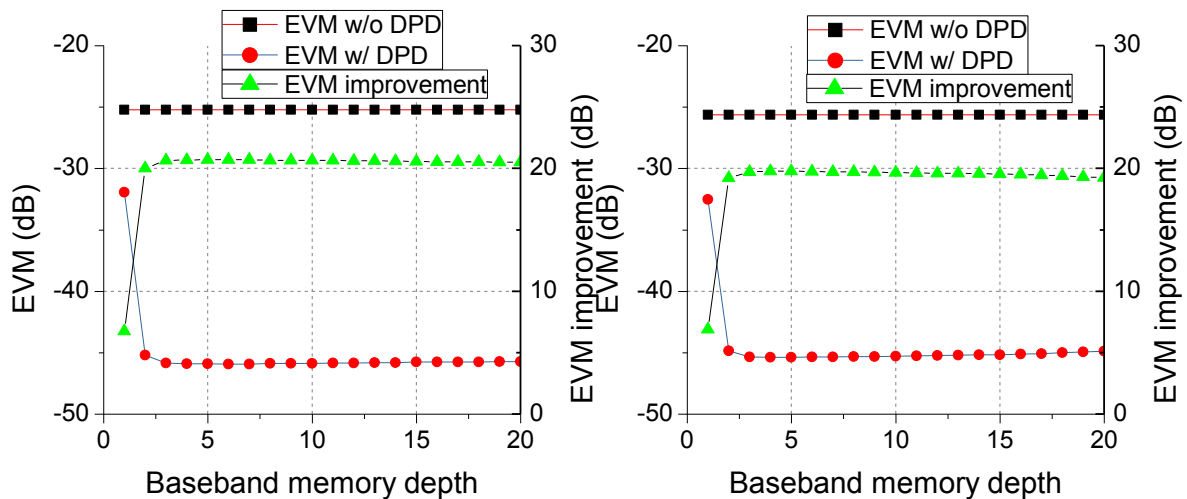


Figure 4-8 EVM vs memory depth of the 2D DPD

To build the 2D DPD model, the memory depth needs to be tested. The same signals are used as in section 4.3 to find the memory depth. As shown in Figure 4-8, when the memory depth is larger than 3, the EVM improvement is saturated. Therefore, the 2D DPD model for the simulation is built with a memory depth of 4.

#### 4.5.1 Case 1: Band 1 @800MHz and Band 2 @900MHz

In this simulation case, two LTE bands are located at 800 MHz and 900 MHz and each band has a bandwidth of 20 MHz. Performance of the proposed DPD and a baseband DPD has been evaluated. Simulation results are shown below.

Figure 4-9 shows the output spectrum of the RoF model, as well as the spectrum of the input signal. The red line represents the input signal, which is generated in Matlab. The blue line represents the output spectrum without DPD. The yellow line and pink line represent the output spectrum with the proposed DPD and the baseband DPD respectively.

As can be seen, the out-of-band nonlinearities, such as IMD3, IMD5 and power leakage in adjacent channels, have been greatly suppressed by the proposed DPD. IMD3 is improved by 19.2 dB at 700 MHz and 11.8 dB at 1000 MHz. The baseband DPD can suppress the power leakage in adjacent channels, but cannot suppress the IMD3 and IMD5.

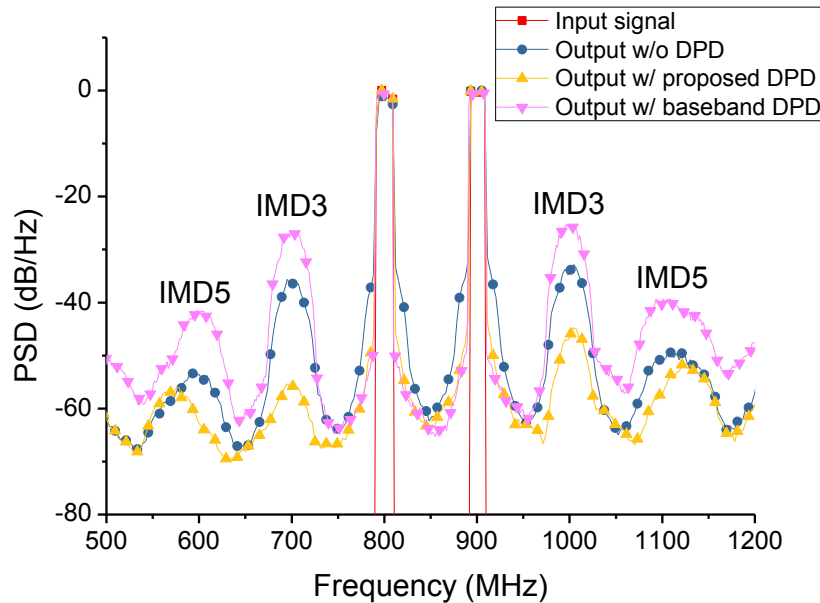


Figure 4-9 Output spectrum from 500 MHz to 1200 MHz in simulation (case 1)

Figure 4-10 and Figure 4-11 are the enlarged spectra around the two bands. Adjacent channel power ratio (ACPR) is the measure of out-of-band distortion in adjacent channels. ACPR is improved by 13.5 dB with the proposed DPD, and it is improved by 19.5 dB with the baseband DPD.

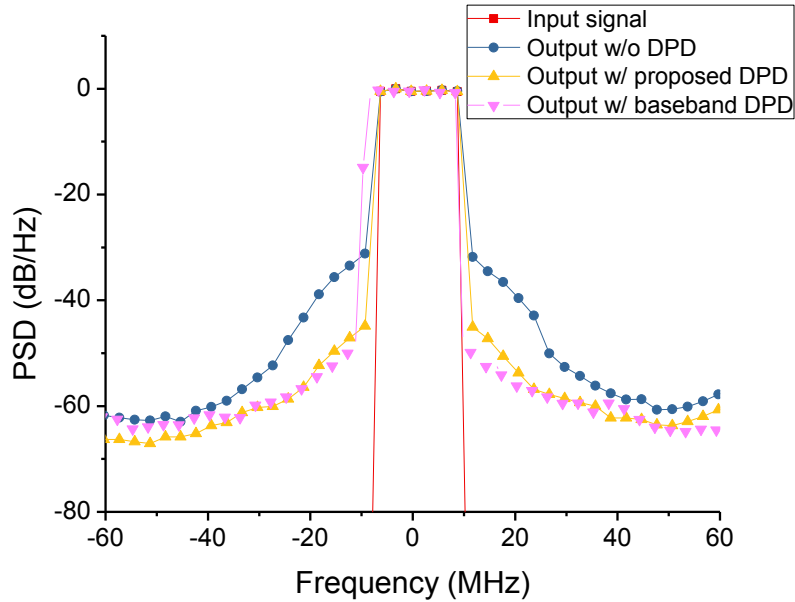


Figure 4-10 Spectrum around the lower band in simulation (case 1)

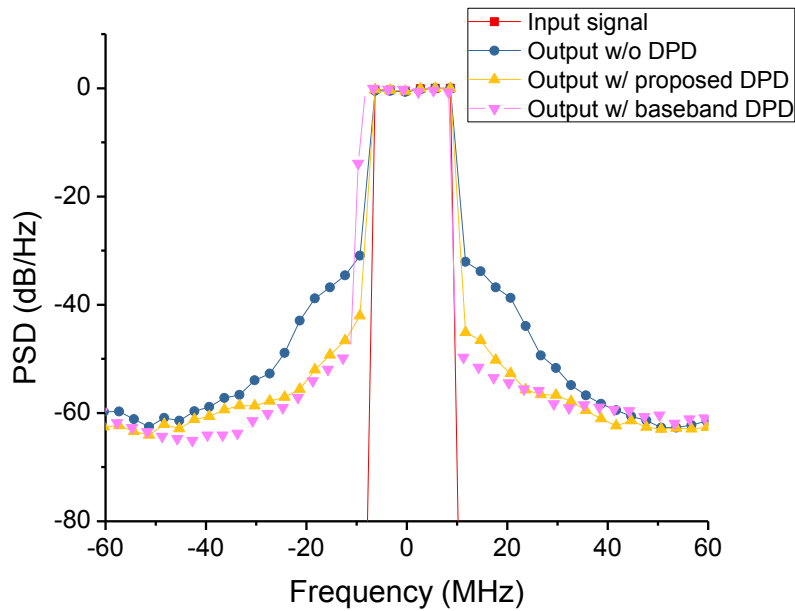


Figure 4-11 Spectrum around the upper band in simulation (case 1)

So far, it can be seen that the proposed DPD is good at improving all out-of-band nonlinearities, while the baseband DPD is especially good at improving power leakage in adjacent channels.

Figure 4-12, Figure 4-13 and Figure 4-14 are the constellations of the lower band signal without DPD, with the proposed DPD and with baseband DPD respectively. The EVMs of the

simulation result are -26.4 dB, -41 dB and -46 dB correspondingly.

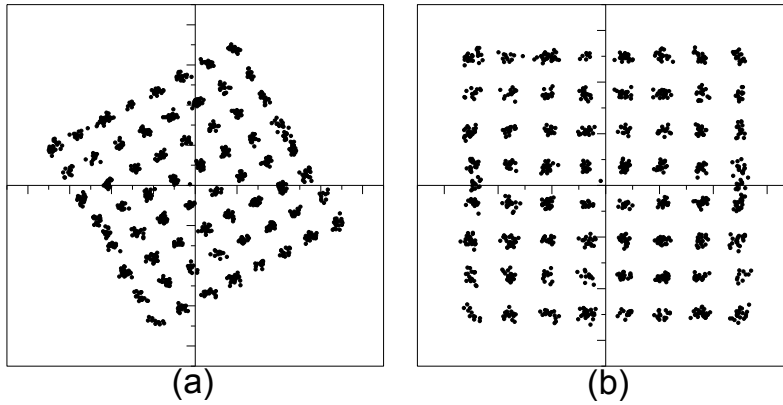


Figure 4-12 Constellation of signal in lower band without DPD (a) before phase adjustment and (b) after phase adjustment

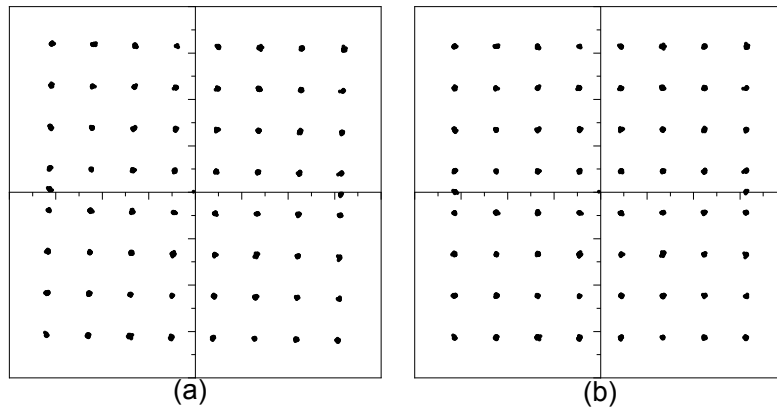


Figure 4-13 Constellation of signal in lower band with the proposed DPD (a) before phase adjustment and (b) after phase adjustment

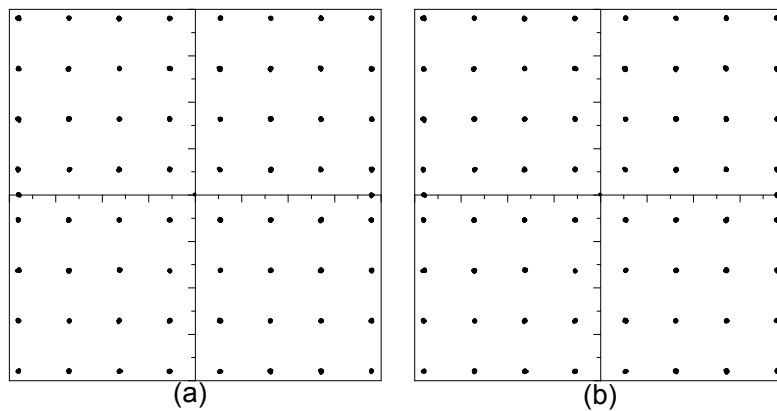


Figure 4-14 Constellation of signal in lower band with 2D DPD (a) before phase adjustment and (b) after phase adjustment

Figure 4-15, Figure 4-16 and Figure 4-17 are the constellations of the upper band signal without DPD, with the proposed DPD and with the baseband DPD respectively. The EVMs of the simulation result are -26.6 dB, -39.3 dB and -45.4 dB correspondingly.

Based on these constellations, it can be seen that the baseband DPD is better than the proposed DPD at improving the EVM. However, the proposed DPD is also very good at this job.

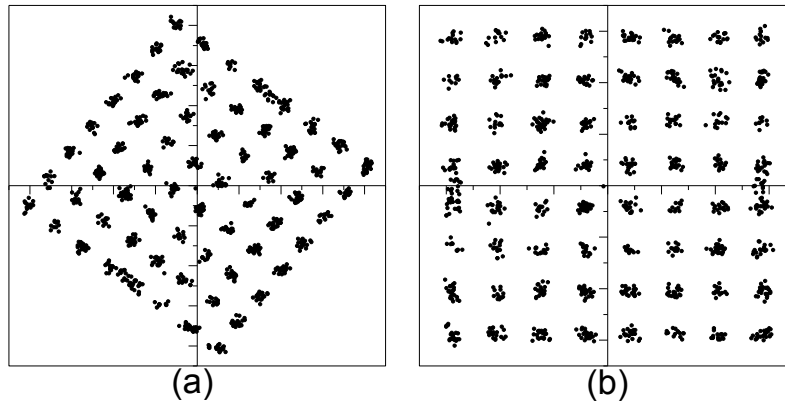


Figure 4-15 Constellation of signal in upper band without DPD (a) before phase adjustment and (b) after phase adjustment

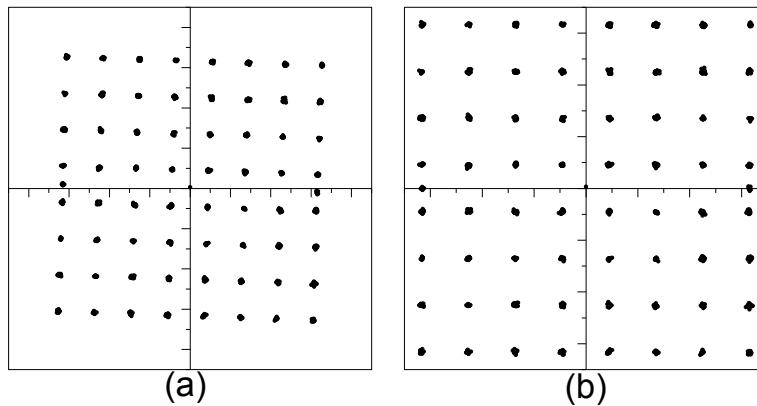


Figure 4-16 Constellation of signal in upper band with the proposed DPD (a) before phase adjustment and (b) after phase adjustment

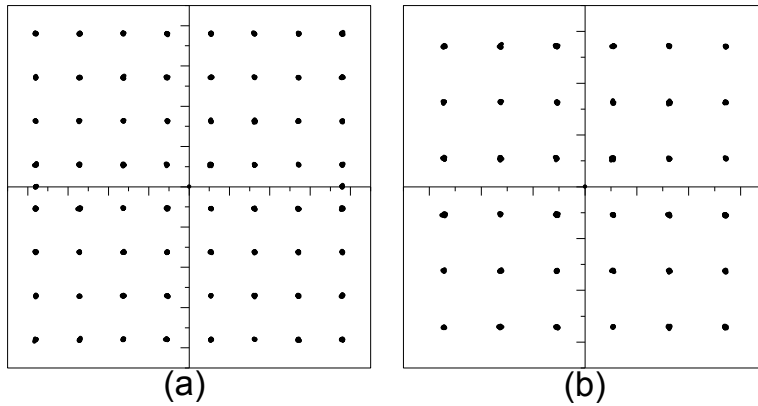


Figure 4-17 Constellation of signal in upper band with 2D DPD (a) before phase adjustment and (b) after phase adjustment

Figure 4-18 and Figure 4-19 show the AM-AM and AM-PM distortions and how these distortions are improved by the proposed DPD on the two bands. Figure 4-20 and Figure 4-21 are the simulation results with the baseband DPD.

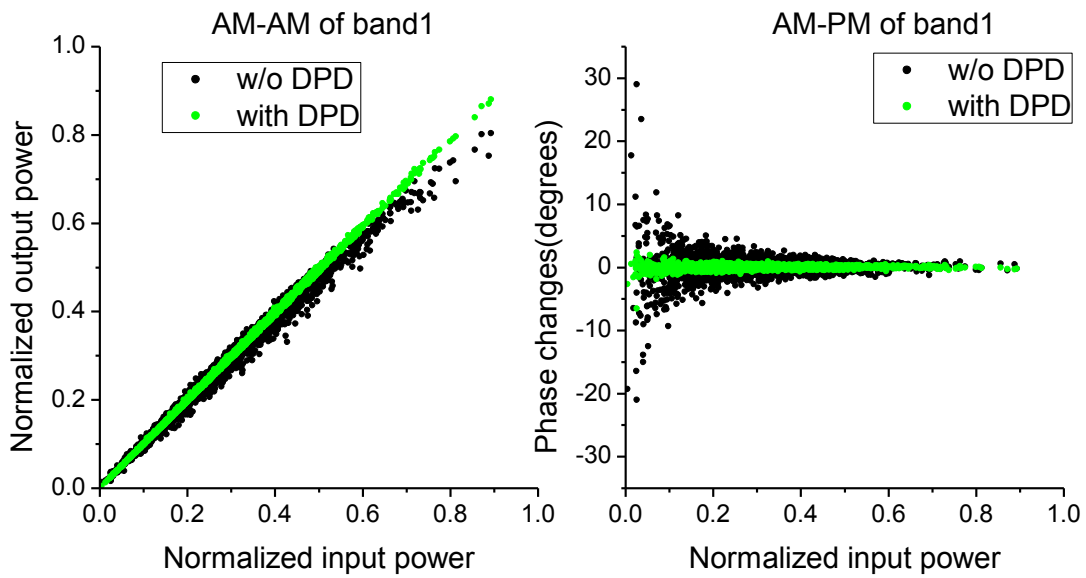


Figure 4-18 AM-AM and AM-PM distortion on lower-band signal with and without proposed DPD

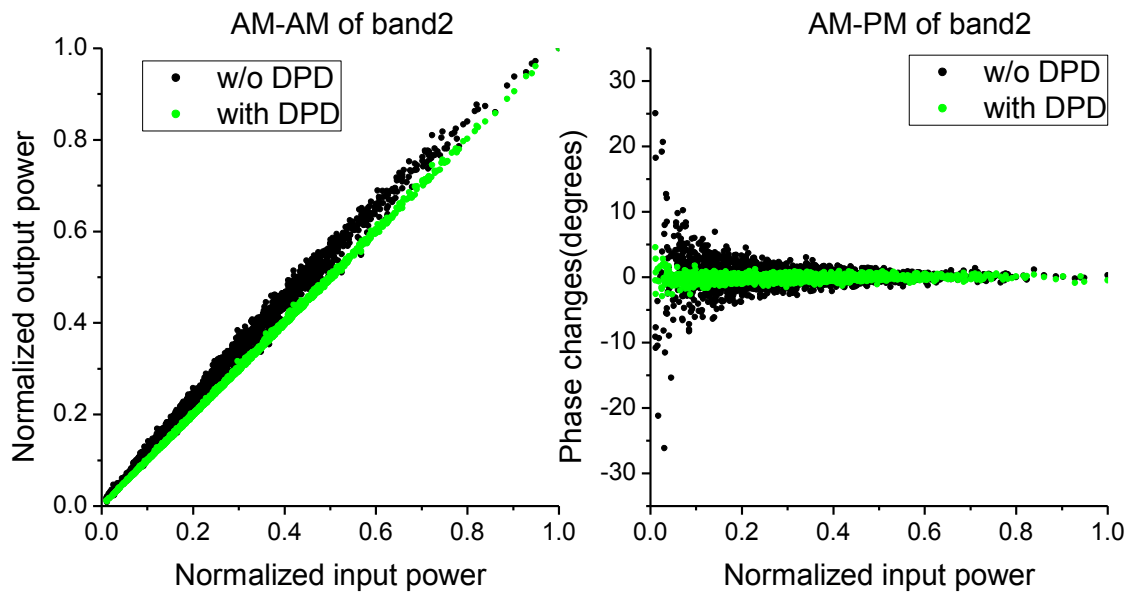


Figure 4-19 AM-AM and AM-PM distortion on upper-band signal with and without proposed DPD

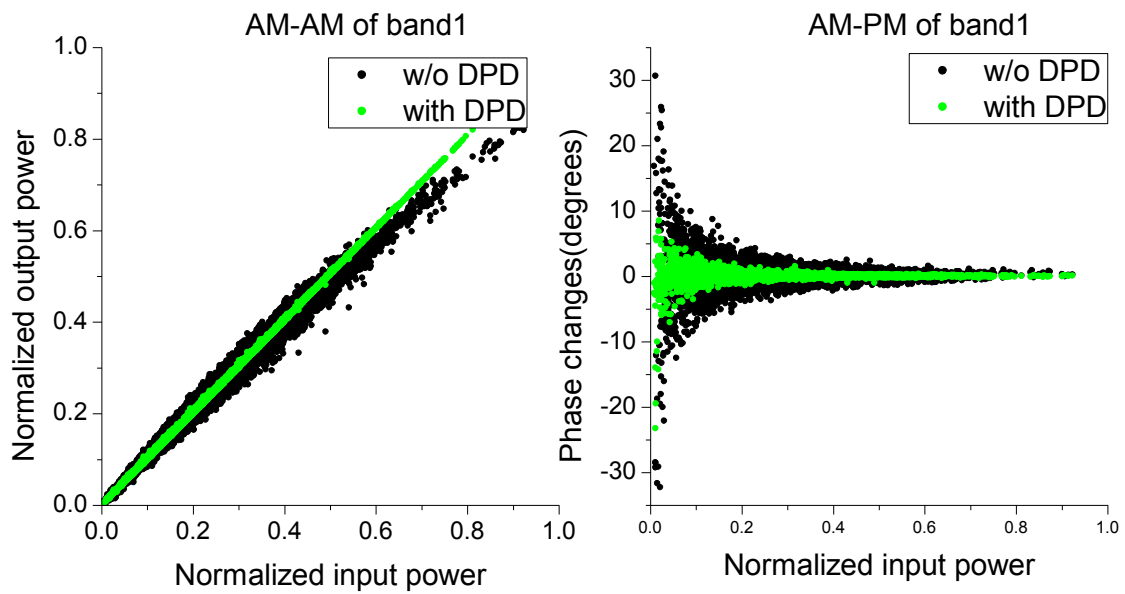


Figure 4-20 AM-AM and AM-PM distortion on lower-band signal with and without baseband DPD

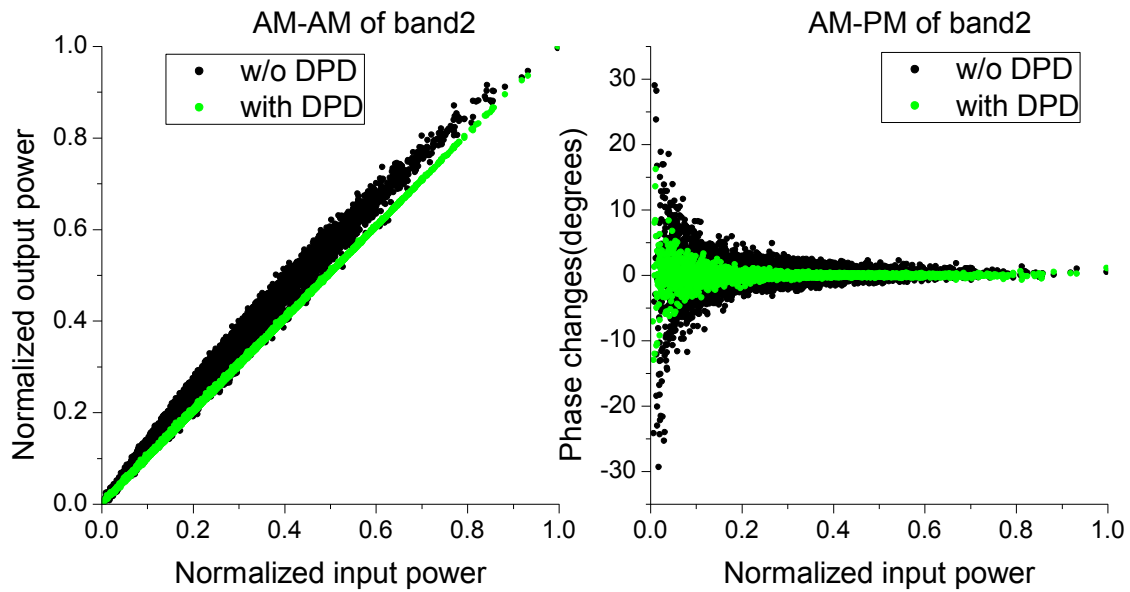


Figure 4-21 AM-AM and AM-PM distortion on upper-band signal with and without baseband DPD

#### 4.5.2 Case 2: Band 1 @800MHz and Band 2 @840MHz

This case is aimed to evaluate the performance of the proposed DPD when the two bands are located closely with each other, at 800 MHz and 840 MHz. The spectrum from 500 MHz to 1100 MHz is shown in Figure 4-22. It can be seen that the proposed DPD performs very well in eliminating the out-of-band distortions. IMD3 is improved by 27.5 dB at 760 MHz and 24 dB at 880 MHz. The baseband DPD cannot suppress the IMD3 or IMD5. Even the power leakage in adjacent channels becomes worse.

The enlarged spectra around two bands are shown in Figure 4-23 and Figure 4-24. ACPR is suppressed by 15.5 dB with the proposed DPD while the baseband DPD cannot decrease the ACPR in this case.

The constellations of the signals are shown in Figure 4-25 to Figure 4-30. EVM of the lower band is decreased from -26.6 dB to -43 dB and -37.6 dB by the proposed DPD and the baseband DPD respectively.

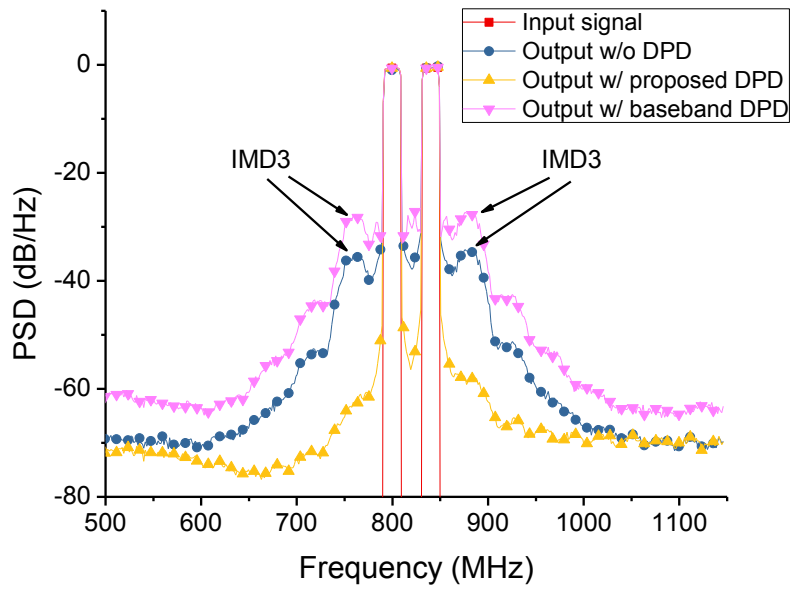


Figure 4-22 Output spectrum from 500 MHz to 1100 MHz in simulation case 1

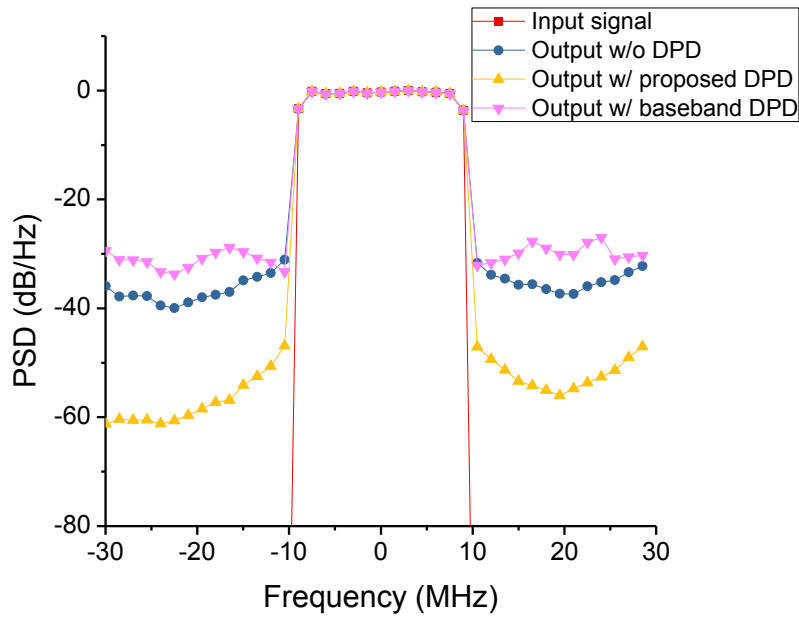


Figure 4-23 Spectrum around the lower band in simulation case 2

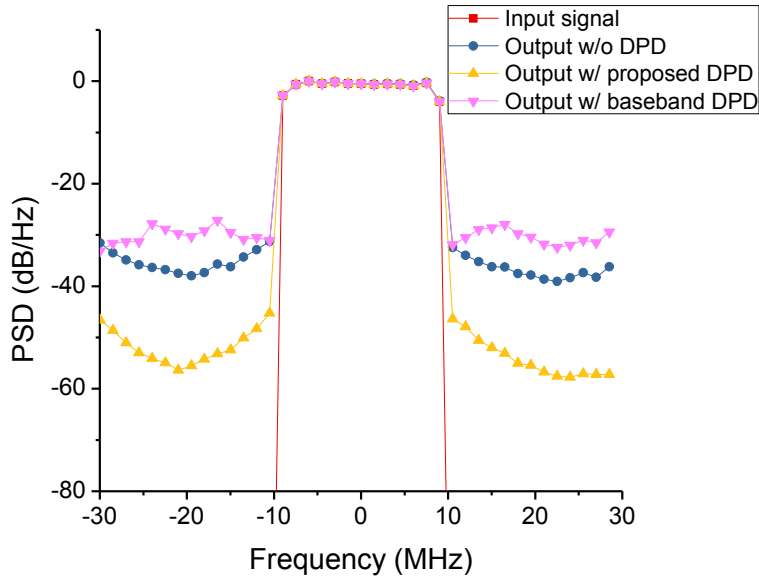


Figure 4-24 Spectrum around the upper band in simulation case 2

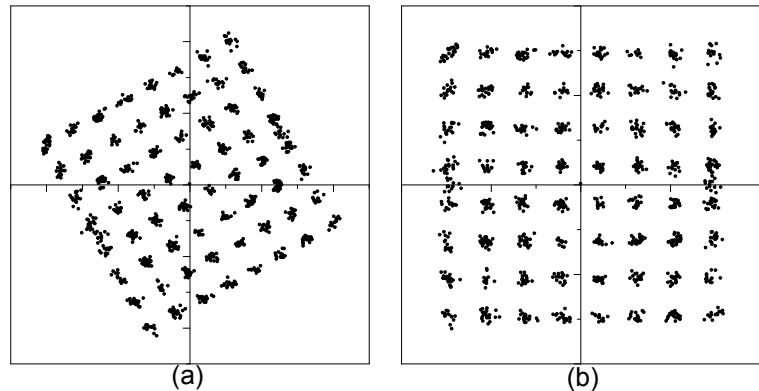


Figure 4-25 Constellation of signal in lower band without DPD (a) before phase adjustment and (b) after phase adjustment

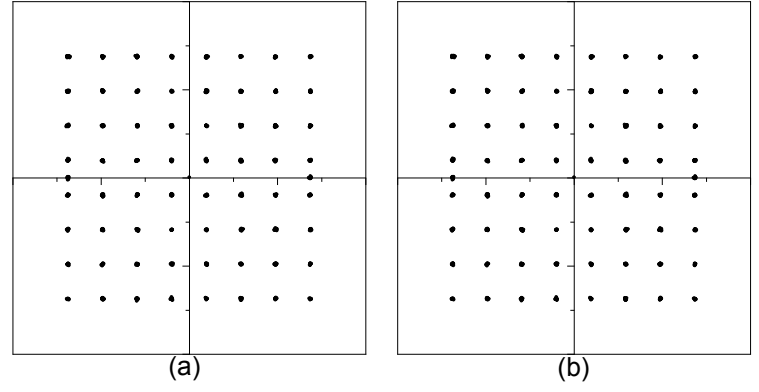


Figure 4-26 Constellation of signal in lower band with proposed DPD (a) before phase adjustment and (b) after phase adjustment

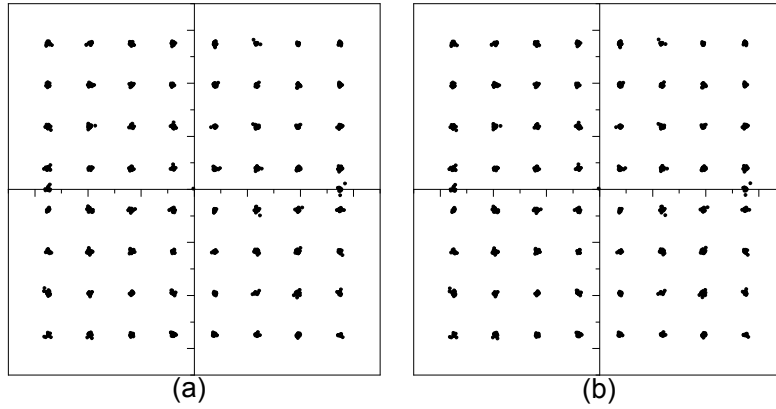


Figure 4-27 Constellation of signal in lower band with 2D DPD (a) before phase adjustment and (b) after phase adjustment

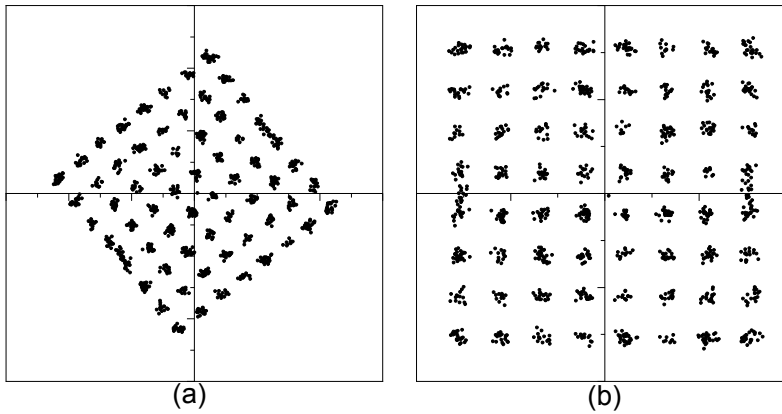


Figure 4-28 Constellation of signal in upper band without DPD (a) before phase adjustment and (b) after phase adjustment

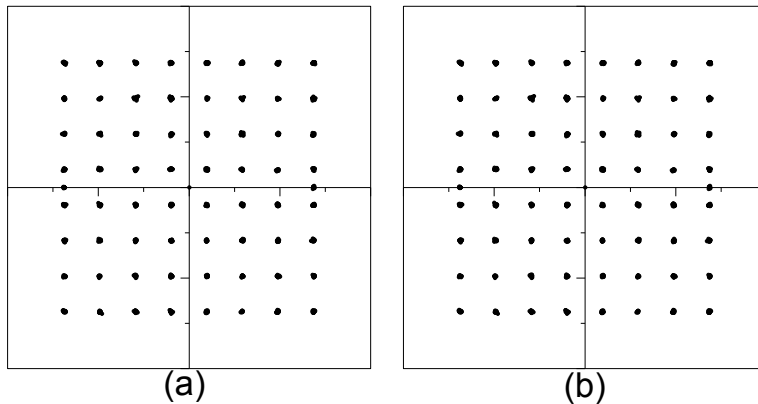


Figure 4-29 Constellation of signal in upper band with proposed DPD (a) before phase adjustment and (b) after phase adjustment

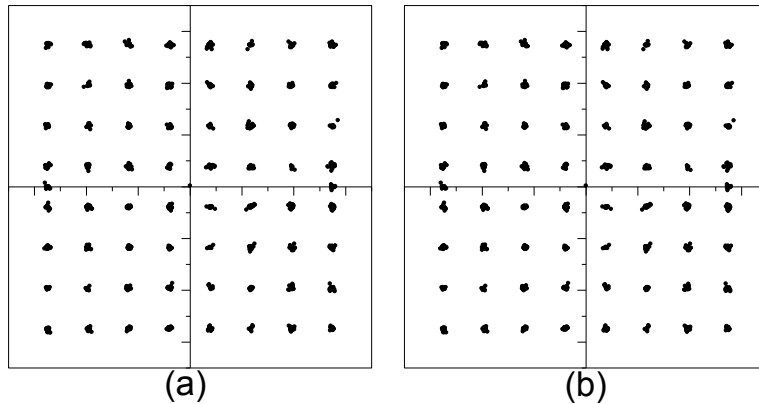


Figure 4-30 Constellation of signal in upper band with 2D DPD (a) before phase adjustment and (b) after phase adjustment

#### 4.5.3 Case 3: Band 1 @800MHz, Band 2 @850MHz and Band 3 @900MHz

The three-band test has been run to check the performance of the proposed DPD in the scenarios of multi-band transmission. The output spectrum is shown in Figure 4-31, where the out-of-band distortions are obviously depressed. IMD3 is decreased by 17.9 dB at 700 MHz, 19 dB at 750 MHz, 12 dB at 950 MHz, and 7.5 dB at 1000 MHz.

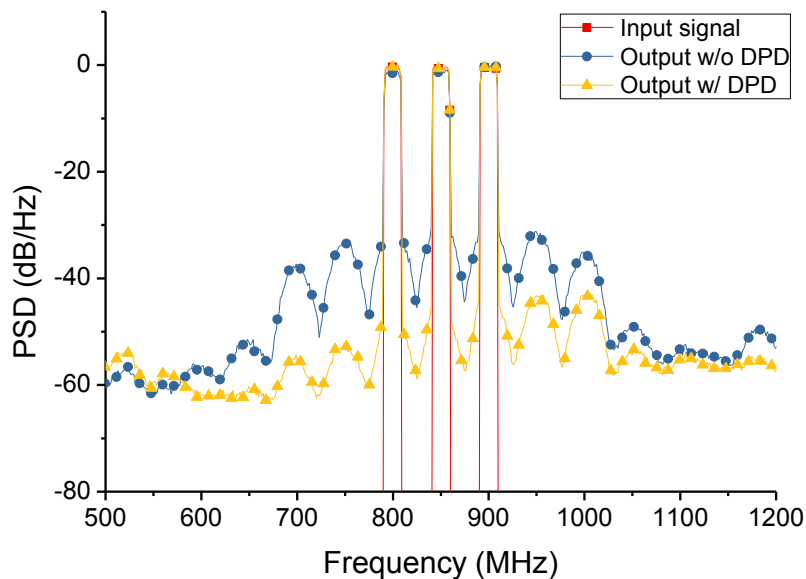


Figure 4-31 Output spectrum from 500 MHz to 1200 MHz in simulation case 3

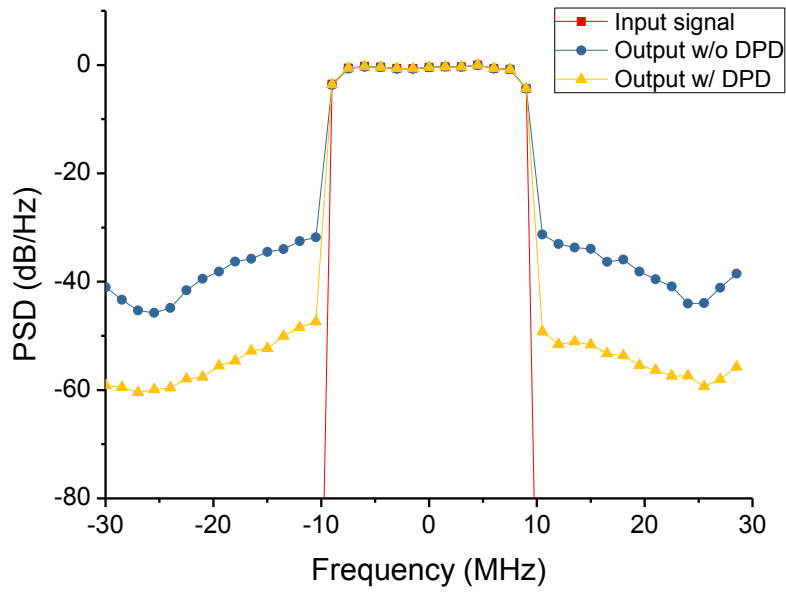


Figure 4-32 Spectrum around the lower band in simulation case 3

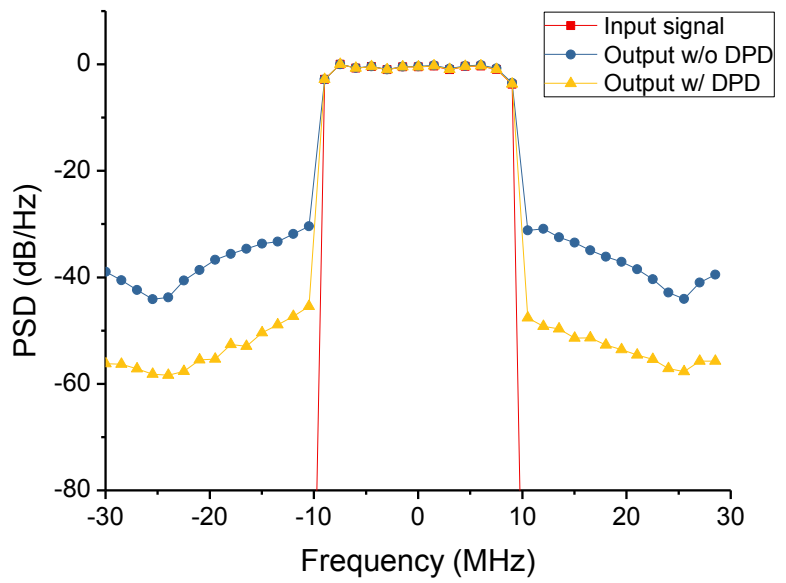


Figure 4-33 Spectrum around the middle band in simulation case 3

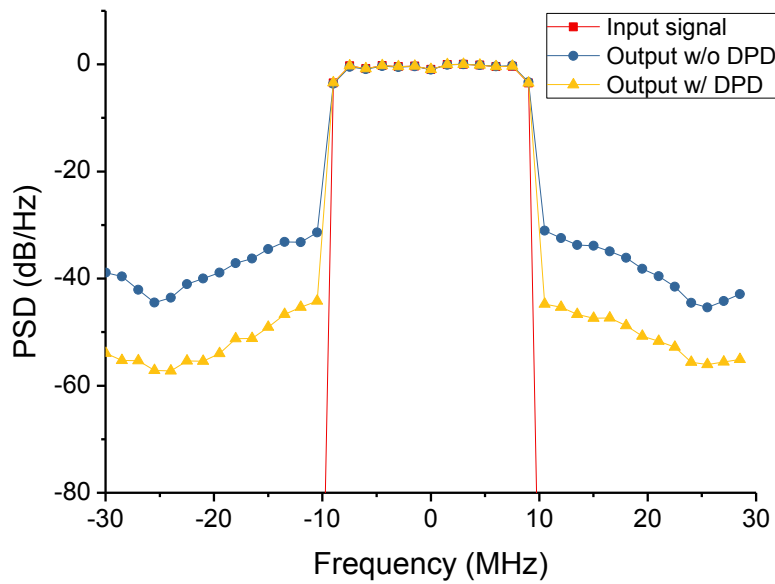


Figure 4-34 Spectrum around the upper band in simulation case 3

The enlarged spectra around each band are shown in Figure 4-32, Figure 4-33, and Figure 4-34. ACPR of each band is suppressed by 16.8 dB 15.7 dB and 13.2 dB correspondingly.

Figure 4-35 to Figure 4-40 are the constellations of each band. EVM of each band is improved by 17.4 dB, 15.9 dB, and 13.8 dB correspondingly.

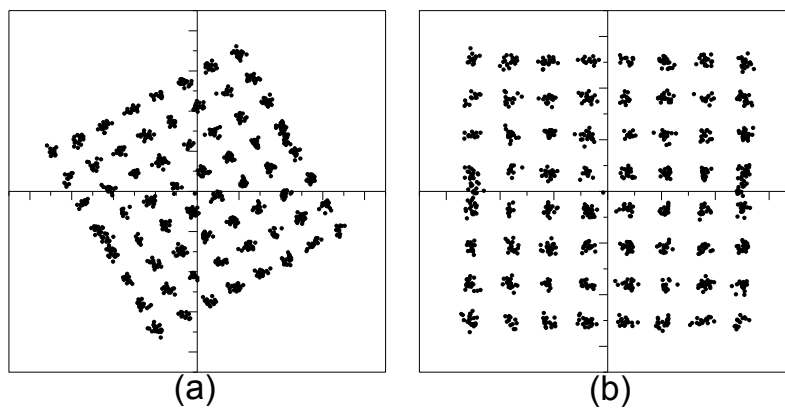


Figure 4-35 Constellation of signal in lower band without DPD (a) before phase adjustment and (b) after phase adjustment

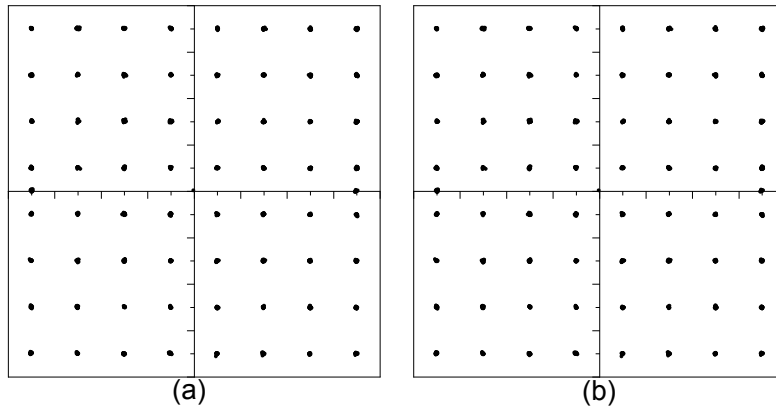


Figure 4-36 Constellation of signal in lower band with the proposed DPD (a) before phase adjustment and (b) after phase adjustment

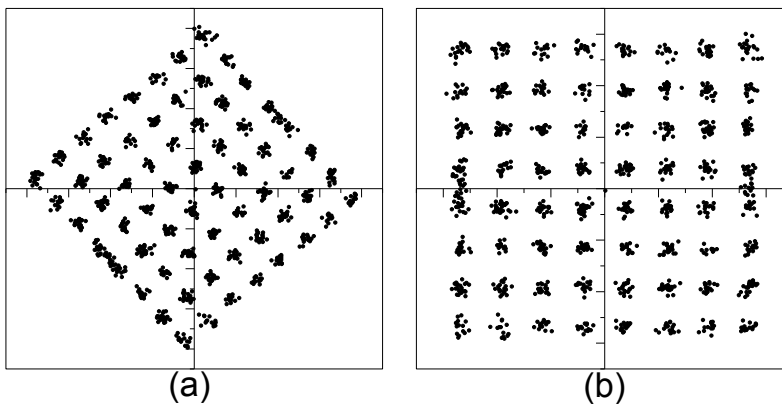


Figure 4-37 Constellation of signal in middle band without DPD (a) before phase adjustment and (b) after phase adjustment

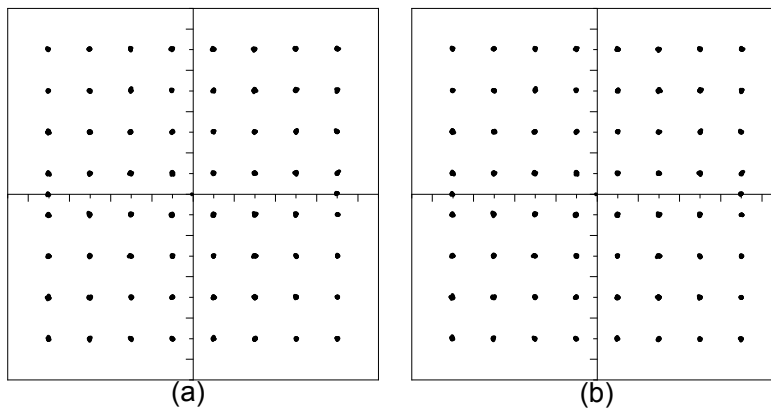


Figure 4-38 Constellation of signal in middle band with the proposed DPD (a) before phase adjustment and (b) after phase adjustment

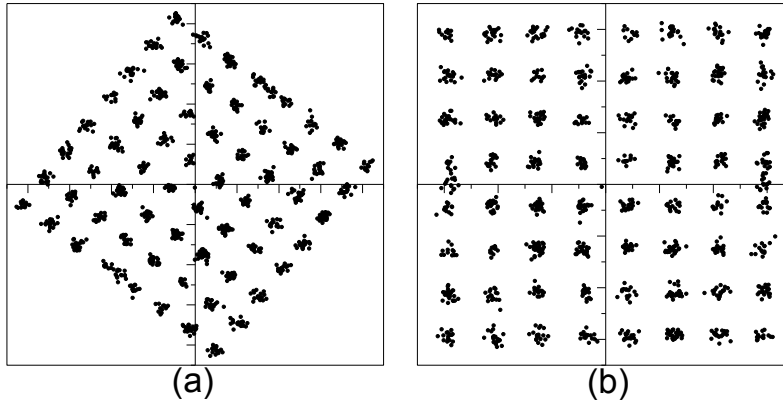


Figure 4-39 Constellation of signal in upper band without DPD (a) before phase adjustment and (b) after phase adjustment

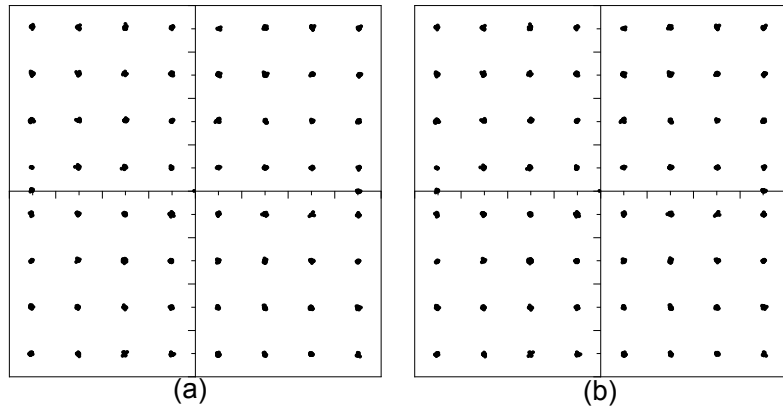


Figure 4-40 Constellation of signal in upper band with the proposed DPD (a) before phase adjustment and (b) after phase adjustment

#### 4.5.4 Complexity Consideration

One important thing that must to be taken into account is the complexity of the DPD model. For most of the DPD models, the structures and extraction of coefficients are usually quite similar. The main difference is the number of coefficients. Suppose the same nonlinearity degree of 5 is used in all DPD models, the numbers of coefficients with different memory depth is listed in Table 4-1.

We can also compare the number of coefficients by fixing the memory depth to 5, for instance. The number of coefficients increases as the nonlinearity degree increases, as listed in Table 4-2.

Table 4-1 Number of coefficients vs memory depth

<b>memory depth*</b>	<b>1</b>	<b>2</b>	<b>3</b>	<b>4</b>	<b>5</b>	<b>6</b>	<b>7</b>	<b>8</b>
<b>proposed DPD**</b>	14	23	32	41	50	59	68	77
<b>2D DPD</b>	30	45	60	75	90	105	120	135

\* Suppose nonlinearity degree is 5.

\*\* Suppose lengths of RF memory effect and baseband memory effect are equal.

Table 4-2 Number of coefficients vs nonlinearity degree

<b>nonlinearity degree*</b>	<b>1</b>	<b>2</b>	<b>3</b>	<b>4</b>	<b>5</b>	<b>6</b>	<b>7</b>	<b>8</b>
<b>proposed DPD**</b>	6	17	28	39	50	61	72	83
<b>2D DPD</b>	6	18	36	60	90	126	168	216

\* Suppose memory depth is 5.

\*\* Suppose lengths of RF memory depth and baseband memory depth are equal.

As can be seen, the proposed DPD model employs much less coefficients than the 2D DPD model does as the memory depth or nonlinearity degree increases.

In the aforementioned simulation, the proposed DPD has an RF memory depth of 8 and a baseband memory depth of 5. The total number of coefficients is 65. The baseband DPD has a memory depth of 4 and the number of coefficients is 75.

## 4.6 Simulation Summary

The performance of the proposed DPD is summarized in Table 4-3, Table 4-4, and Table 4-5, as well as the performance of the 2D DPD for comparison.

As can be seen, the performance of the proposed DPD is quite good in all three cases, while the 2D DPD can only work better than the proposed DPD in case 1 in terms of EVM and ACPR improvement. Because of the limited sampling bandwidth, baseband DPD usually cannot suppress the IMD3 or IMD5. Besides, the 2D DPD cannot work in transmission systems where there are 3 or more bands.

Table 4-3 Comparison of EVM improvement in simulation

<b>EVM improvement (dB)</b>	<b>Proposed DPD</b>	<b>2D DPD</b>
<b>Case 1 (two-band)</b>	14.6	20.7
<b>Case 2 (two-band)</b>	16.3	10
<b>Case 3 (three-band)</b>	15.7	NA

Table 4-4 Comparison of ACPR improvement in simulation

<b>ACPR improvement (dB)</b>	<b>Proposed DPD</b>	<b>2D DPD</b>
<b>Case 1 (two-band)</b>	13.5	29.5
<b>Case 2 (two-band)</b>	15.5	0
<b>Case 3 (three-band)</b>	15.2	NA

Table 4-5 Comparison of IMD3 improvement in simulation

<b>IMD3 improvement (dB)</b>	<b>Proposed DPD</b>	<b>2D DPD</b>
<b>Case 1 (two-band)</b>	19.5	NA
<b>Case 2 (two-band)</b>	27.5	NA
<b>Case 3 (three-band)</b>	14.1	NA

According to the simulation result, it can be expected that the proposed DPD can be used in various application scenarios, especially in the broadband and multi-band transmission. It is also worth mentioning that the number of coefficients is at a moderate level compared to some complex baseband DPD.

## Chapter 5. Experiments with Envelope-Assisted RF DPD

After verifying the validity of the proposed DPD with simulation, experiment has been conducted to evaluate the performance of the proposed DPD in a real application. An RoF transmission link has been set up and the similar tests have been done on the RoF transmission link.

### 5.1 Experiment Setup Overview

The experiment setup is shown in Figure 5-1. The 64QAM OFDM LTE signal is generated in Matlab and then loaded into a Tektronix AWG7122B arbitrary waveform generator (AWG). The AWG sends the signals to the optical transmitter at a sampling rate of 10.32192 Giga samples per second (GS/s) with an output power level of -19.2 dBm. A MITEQ SCM fiber optic link is used to transmit and receive the optical signal. The optical transmitter is a direct modulator, which uses the RF signal to modulate the optical signal. After passing through an 8-kilometer standard single mode optical fiber, the optical signal is detected by the optical receiver of the MITEQ SCM fiber optical link and demodulated back into an RF signal. An SHF810 broadband amplifier is connected after the optical receiver to enhance the power level of the RF signal from -15.4 dBm to 13.4 dBm, corresponding to a gain of 28 dB. An Agilent DSO81204B oscilloscope samples the amplified RF signal at a sampling rate of 10.32192 GS/s and saves the data into a file, which can be processed by Matlab.

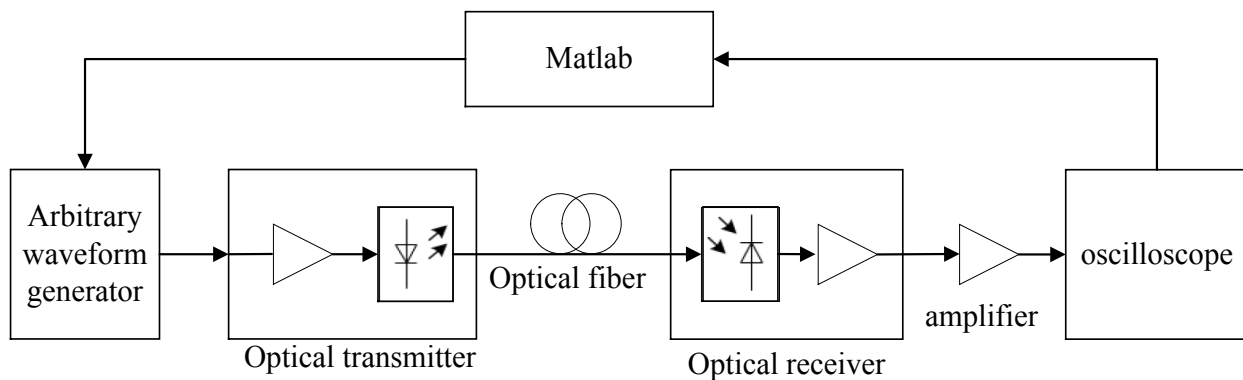


Figure 5-1 Experiment setup of the RoF transmission link

## 5.2 RoF Model

In the training process, an RoF model is built to mimic the RoF link so as to speed up the training process. The RoF model is built with the envelope-assisted RF DPD model. After obtaining a set of input and output data of the RoF link, the coefficients of the RoF model can be extracted easily with the least square method. The first loop of the training process is conducted on the RoF link and the following loops can be conducted with the RoF model.

## 5.3 Optimal Memory Depth of the RF Polynomial

In the same way as in the simulation, experiment starts with finding the optimal memory depth. Two-band test has been conducted with two 20 MHz LTE bands located at 800 MHz and 900 MHz. The result is shown in Figure 5-2. As can be seen, RF memory depth of 8 is a good choice to minimize the EVM while keeping the number of coefficients as small as possible.

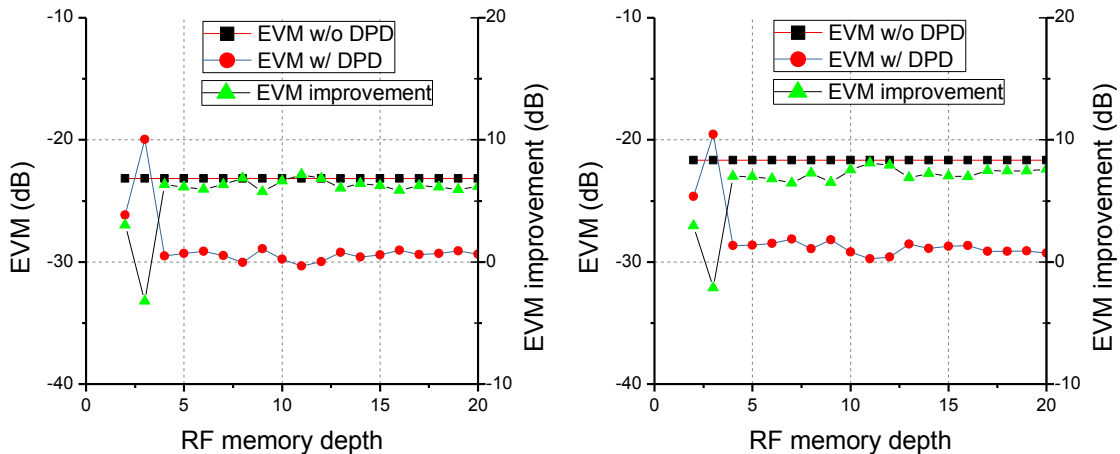


Figure 5-2 EVM vs RF memory depth (Left: lower band. Right: upper band.)

## 5.4 Optimal memory Depth of the Baseband Polynomial

Baseband memory depth test has been done to find the optimal value. The same signals are used as in section 5.3. However, the experiment result shows that EVM changes very slightly as the baseband memory depth increases, which means that the RoF link only has detectable short-term memory effect but the long-term memory effect is very weak. However, the baseband

memory polynomial still can be used to eliminate the potential, although very weak, long-term memory effect. In the following experiment, the baseband memory depth has been set to 1.

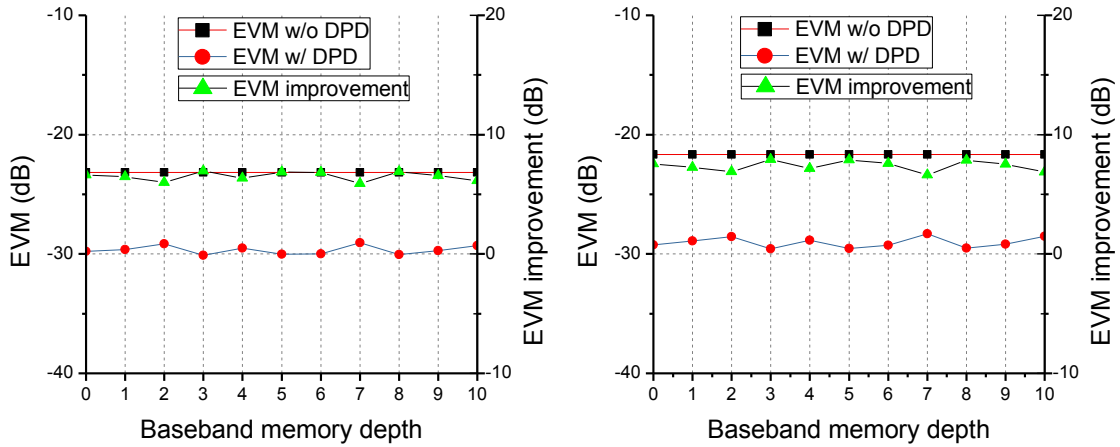


Figure 5-3 EVM vs baseband memory depth (Left: lower band. Right: upper band.)

## 5.5 Comparison with Baseband DPD Techniques

To compare with the baseband DPD, the memory depth of the baseband DPD is optimized by experiment with the same signals as in section 5.3., as shown in Figure 5-4. Since the EVM degrades as the memory depth increases, the memory depth of the baseband DPD is set to 1.

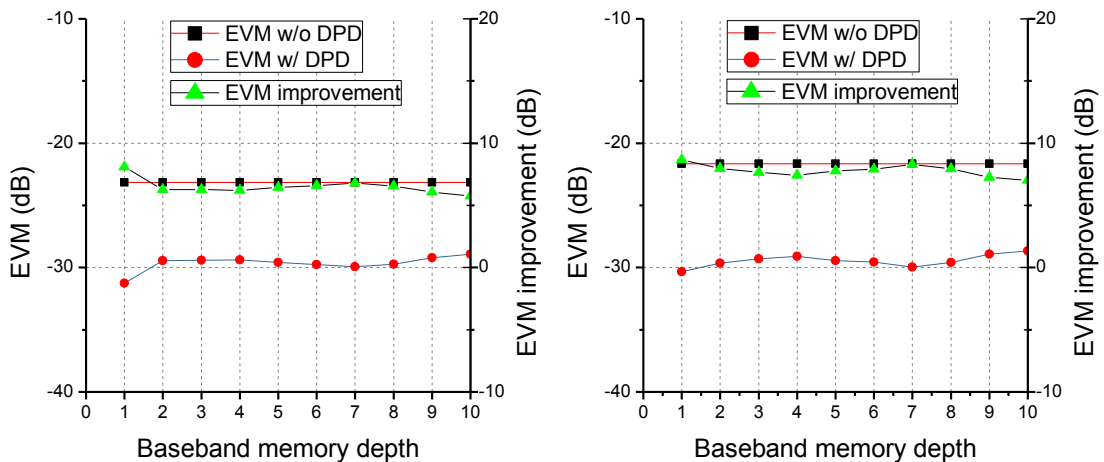


Figure 5-4 EVM vs memory depth of the 2D DPD

### 5.5.1 Case 1: Band 1 @800MHz and Band 2 @900MHz

Figure 5-5 shows the output spectrum from 500 MHz to 1200 MHz. IMD3 is decreased by 14.3 dB at 700 MHz and 10.1 dB at 1000 MHz.

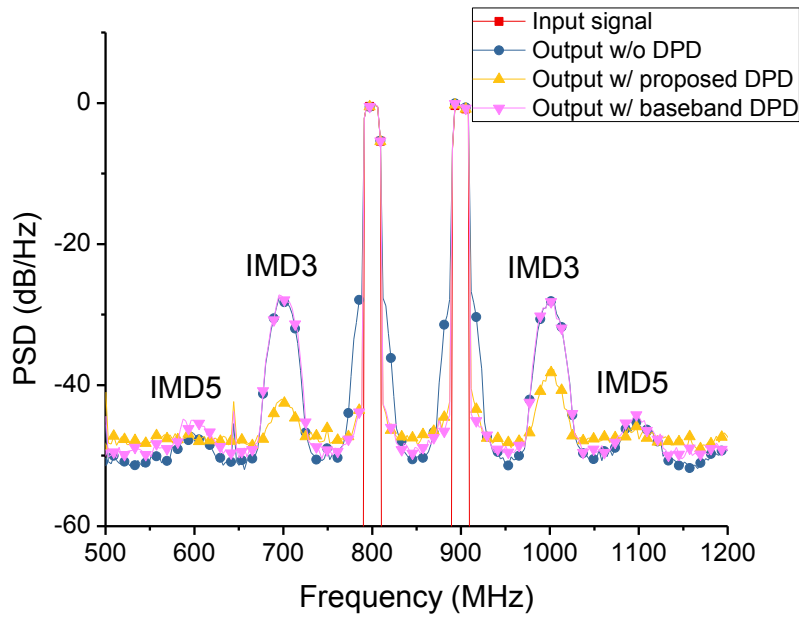


Figure 5-5 Output spectrum from 500 MHz to 1200 MHz in experiment case 1

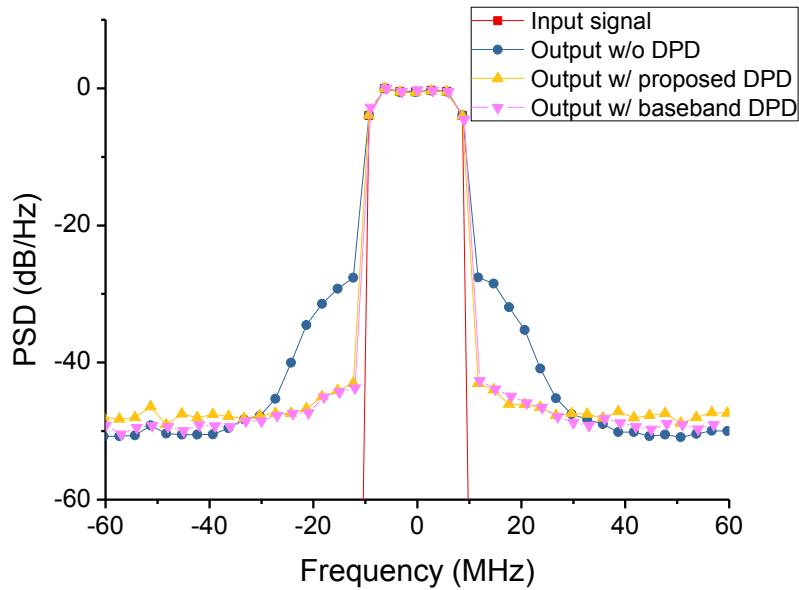


Figure 5-6 Spectrum around the lower band in experiment case 1

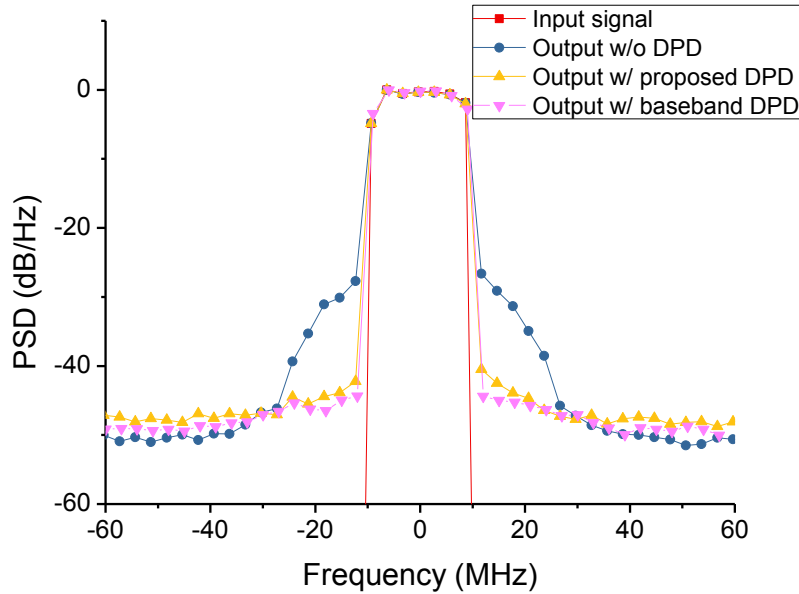


Figure 5-7 Spectrum around the upper band in experiment case 1

Figure 5-6 and Figure 5-7 give a detailed view around the two bands. ACPR is improved by both DPD models. The proposed DPD provides an improvement of 14.8 dB while the baseband DPD achieved an improvement of 16.4 dB.

The constellations of the signals are given in Figure 5-8 to Figure 5-13. The EVM of the lower-band and higher-band signals is improved by 6.5 dB and 7.2 dB respectively with the proposed DPD. It is decreased by 8.1 dB and 8.7 dB with the baseband DPD.

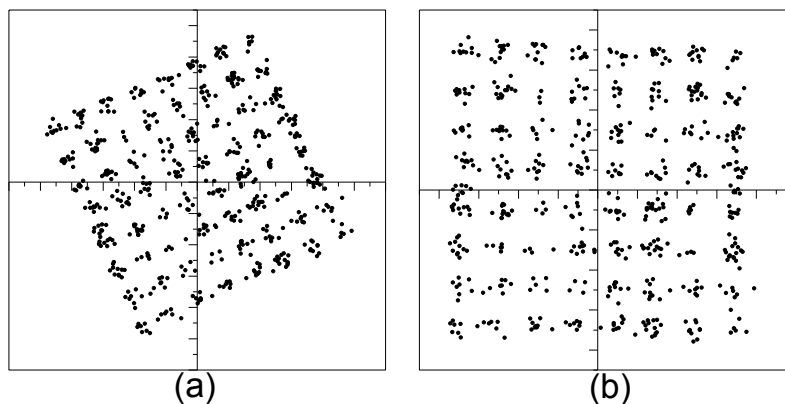


Figure 5-8 Constellation of signal in lower band without DPD (a) before phase adjustment and (b) after phase adjustment

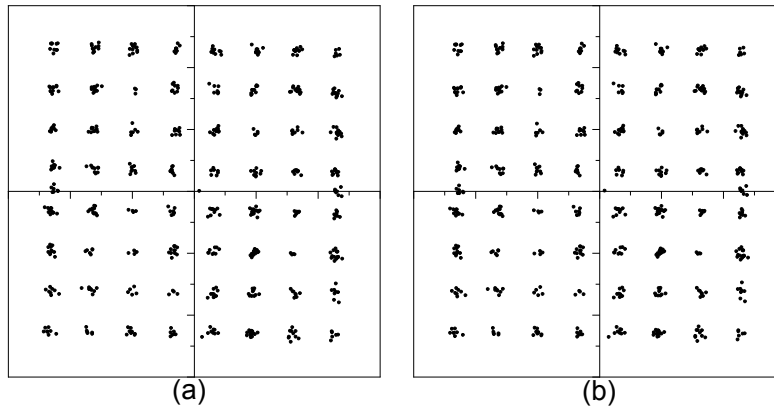


Figure 5-9 Constellation of signal in lower band with the proposed DPD (a) before phase adjustment and (b) after phase adjustment

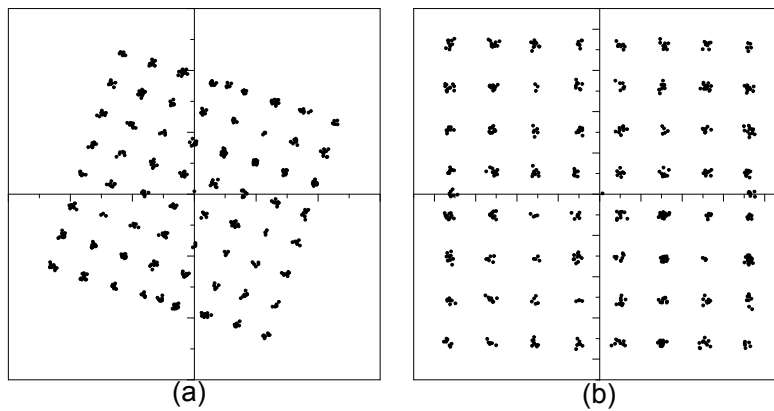


Figure 5-10 Constellation of signal in lower band with 2D DPD (a) before phase adjustment and (b) after phase adjustment

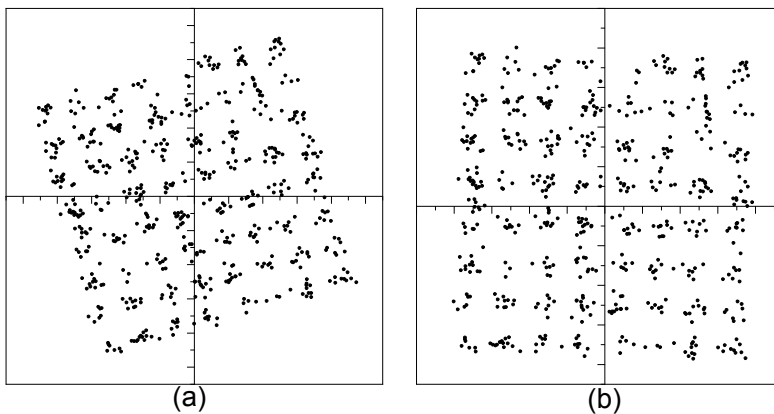


Figure 5-11 Constellation of signal in upper band without DPD (a) before phase adjustment and (b) after phase adjustment

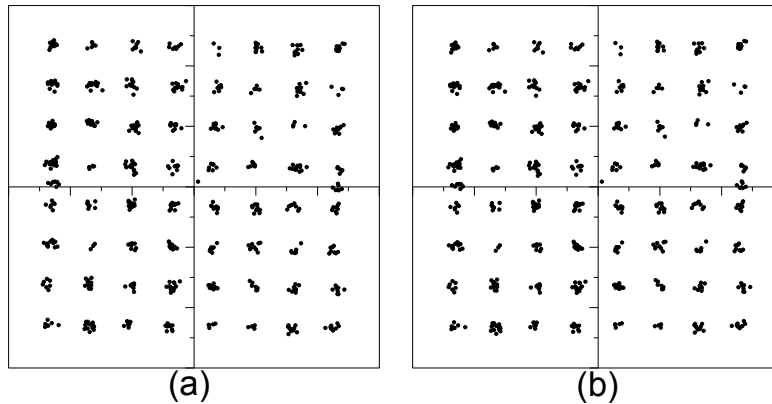


Figure 5-12 Constellation of signal in upper band with the proposed DPD (a) before phase adjustment and (b) after phase adjustment

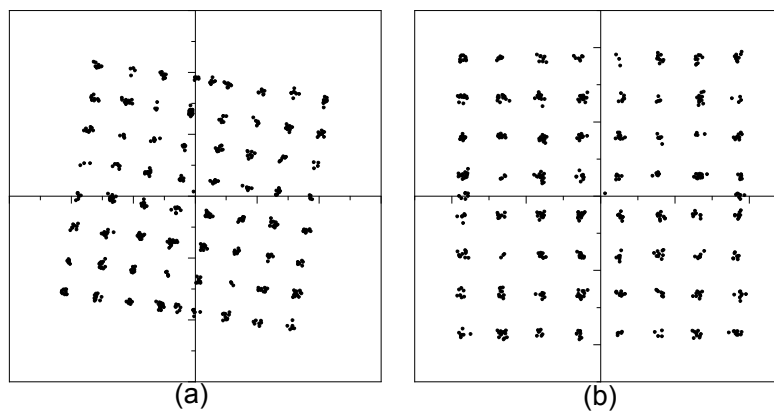


Figure 5-13 Constellation of signal in upper band with 2D DPD (a) before phase adjustment and (b) after phase adjustment

### 5.5.2 Case 2: Band 1 @800MHz and Band 2 @840MHz

In this test case, two bands are closely located at 800 MHz and 840 MHz. Output spectrum from 500 MHz to 1100 MHz is shown in Figure 5-14. IMD3 is suppressed by 11 dB at 760 MHz and 8 dB at 880 MHz by the proposed DPD.

The enlarged views around the two bands indicate that the ACPR is improved by 9.2 dB and 7.9 dB on the lower band and higher band respectively with the proposed DPD, as shown in Figure 5-15 and Figure 5-16. There is nearly no change on the ACPR with the baseband DPD, because the sampling bandwidth of the baseband DPD is limited in this case.

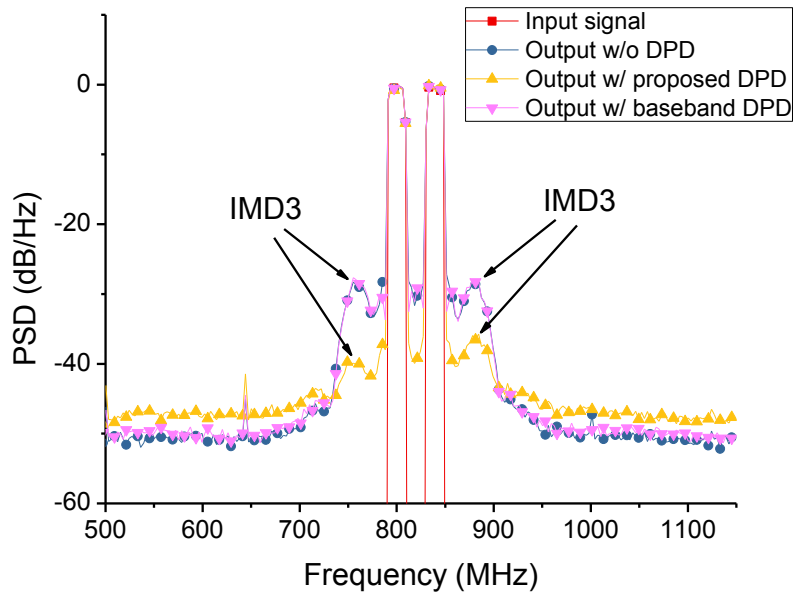


Figure 5-14 Output spectrum from 500 MHz to 1100 MHz in experiment case 2

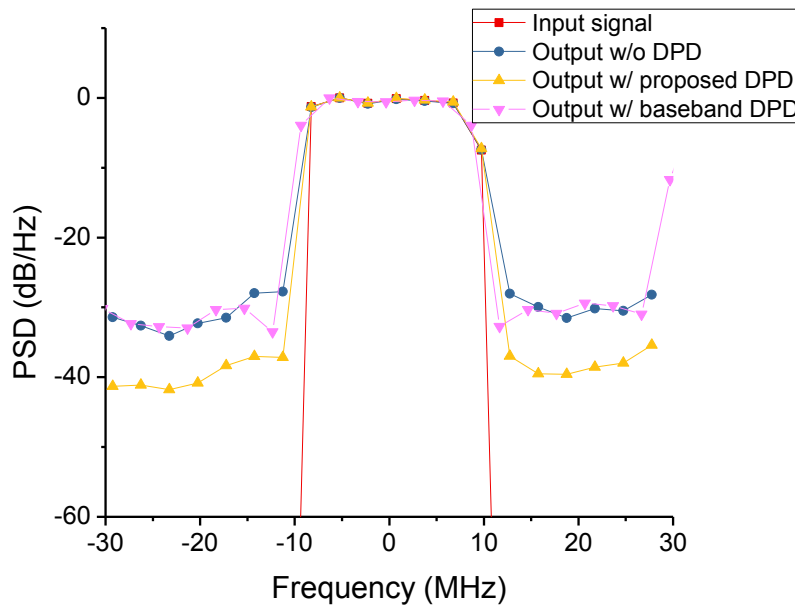


Figure 5-15 Spectrum around the lower band in experiment case 2

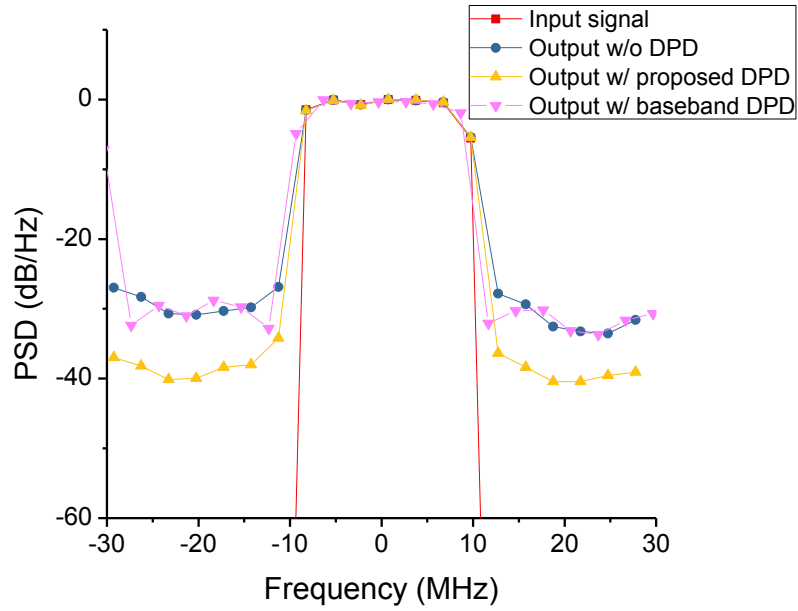


Figure 5-16 Spectrum around the upper band in experiment case 2

Figure 5-17 to Figure 5-22 are the constellations of the output signals. Calculated EVM shows improvement of 4.7 dB and 4.9 dB on the lower band and higher band respectively with the proposed DPD. The improvement is 6.6 dB and 7.1 dB with the baseband DPD.

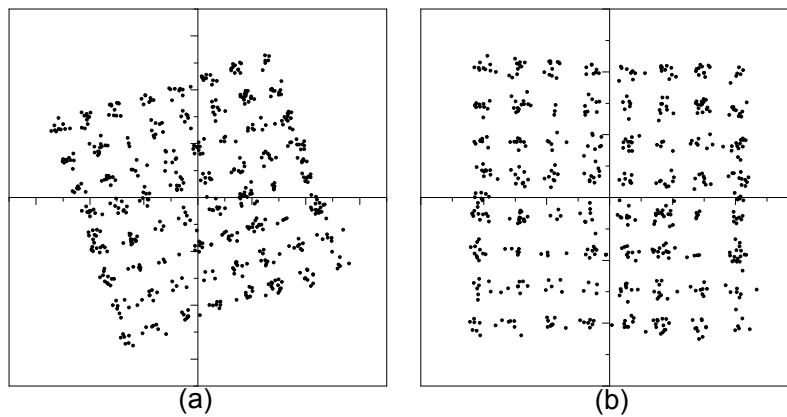


Figure 5-17 Constellation of signal in lower band without DPD (a) before phase adjustment and (b) after phase adjustment

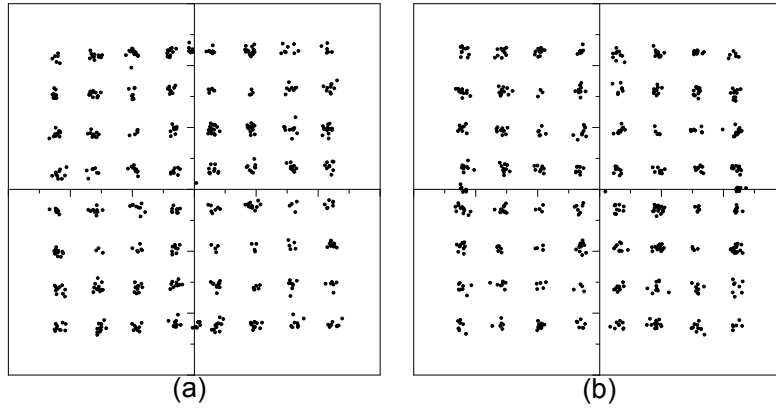


Figure 5-18 Constellation of signal in lower band with the proposed DPD (a) before phase adjustment and (b) after phase adjustment

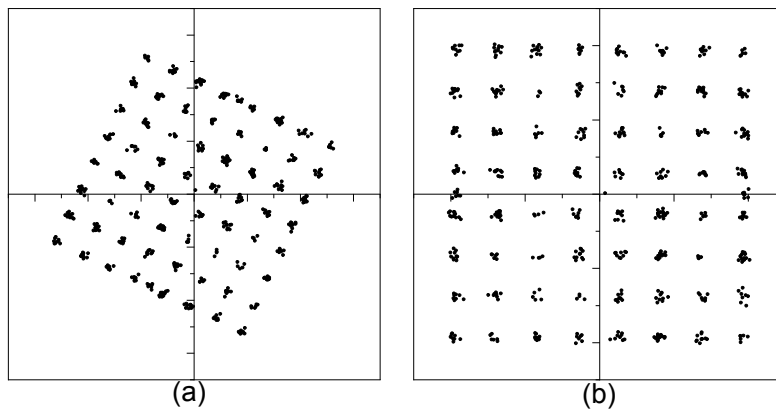


Figure 5-19 Constellation of signal in lower band with 2D DPD (a) before phase adjustment and (b) after phase adjustment

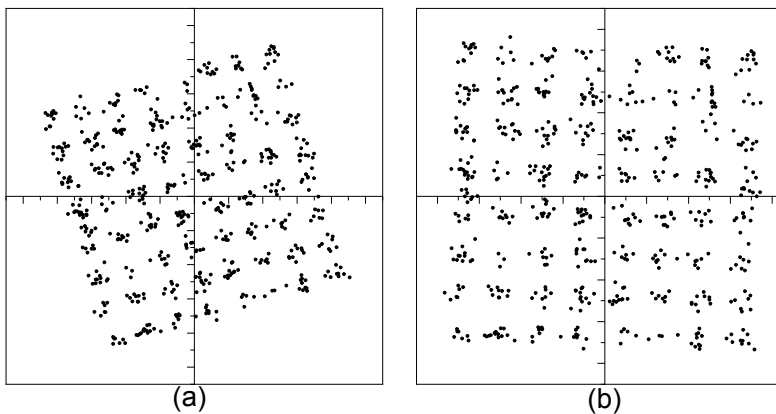


Figure 5-20 Constellation of signal in upper band without DPD (a) before phase adjustment and (b) after phase adjustment

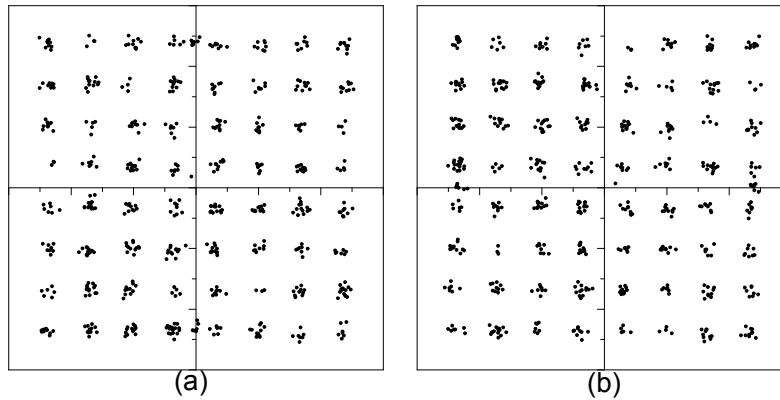


Figure 5-21 Constellation of signal in upper band with the proposed DPD (a) before phase adjustment and (b) after phase adjustment

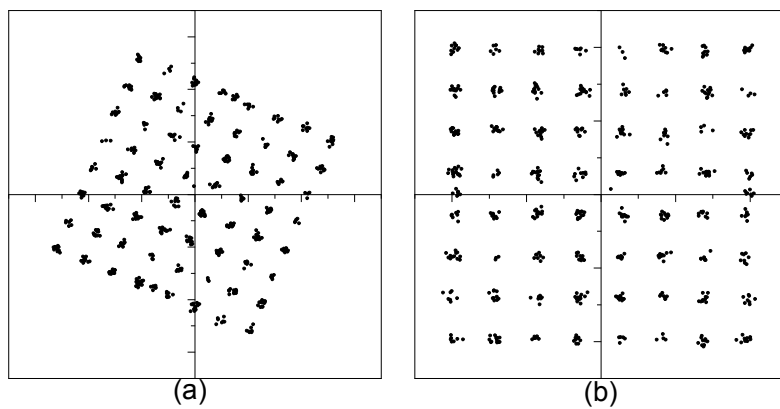


Figure 5-22 Constellation of signal in upper band with 2D DPD (a) before phase adjustment and (b) after phase adjustment

### 5.5.3 Case 3: Band 1 @800MHz, Band 2 @850MHz and Band 3 @900MHz

Experiment of three-band test has been done to evaluate the performance of the proposed DPD. The output spectrum is shown in Figure 5-23. IMD3 is suppressed by 13.2 dB at 700 MHz, 17 dB at 750 MHz, 13.5 dB at 950 MHz, and 10.6 dB at 1000 MHz with the proposed DPD.

Figure 5-24, Figure 5-25, and Figure 5-26 show that ACPR is decreased by 16.6 dB, 17 dB and 14.4 dB on three bands respectively.

EVM is calculated based on the constellation data in Figure 5-27 to Figure 5-32 and the result shows that it is improved by 9 dB, 9.7 dB and 8.1 dB on three bands.

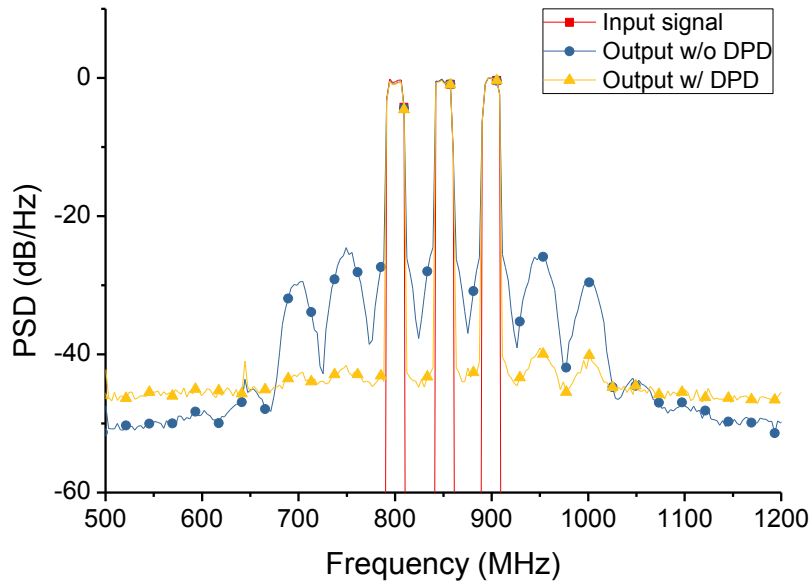


Figure 5-23 Output spectrum from 500 MHz to 1200 MHz in experiment case 3

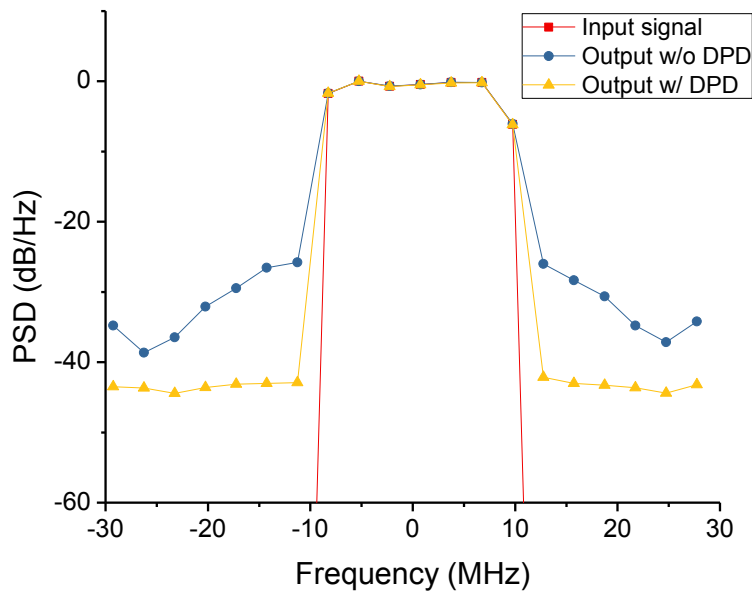


Figure 5-24 Spectrum around the lower band in experiment case 3

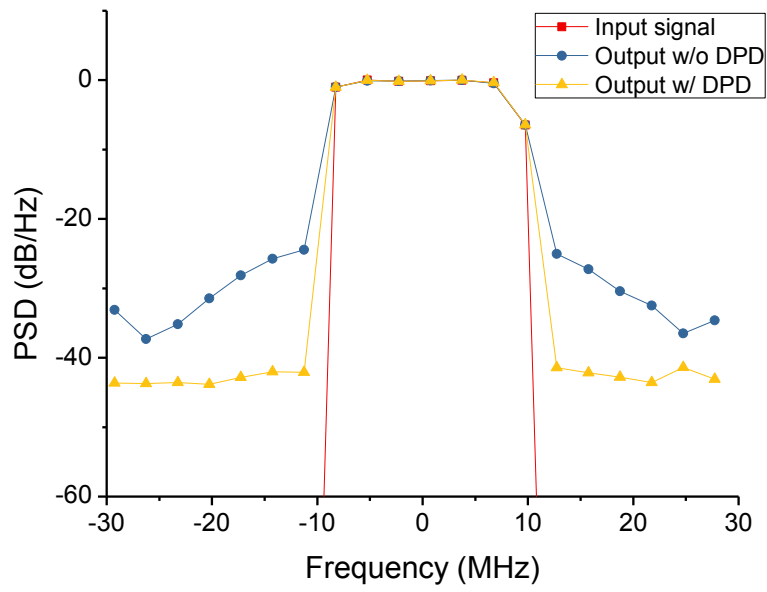


Figure 5-25 Spectrum around the middle band in experiment case 3

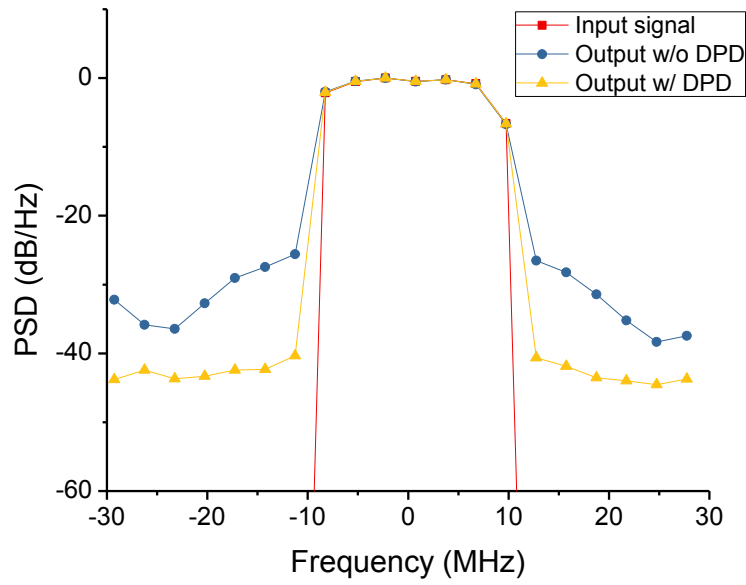


Figure 5-26 Spectrum around the upper band in experiment case 3

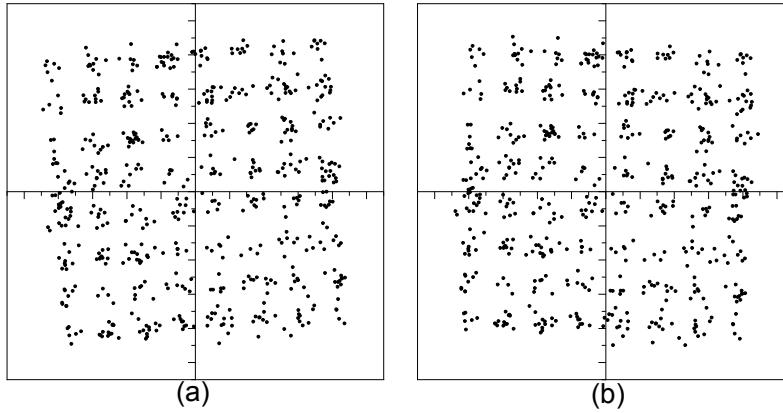


Figure 5-27 Constellation of signal in lower band without DPD (a) before phase adjustment and (b) after phase adjustment

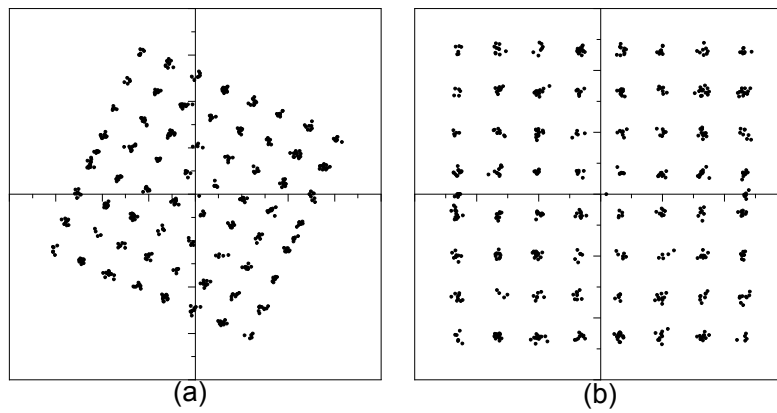


Figure 5-28 Constellation of signal in lower band with the proposed DPD (a) before phase adjustment and (b) after phase adjustment

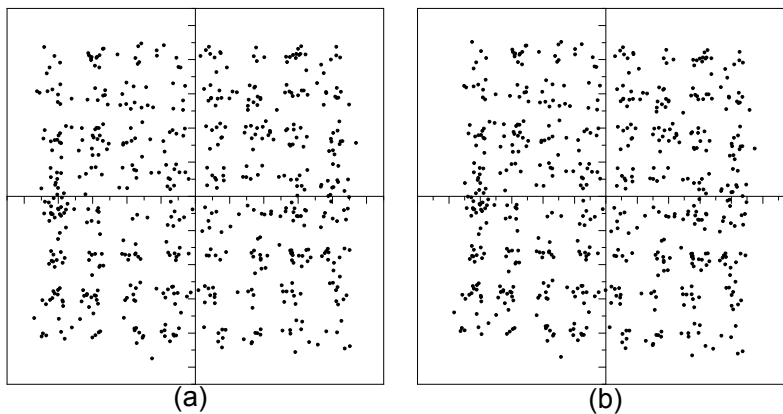


Figure 5-29 Constellation of signal in middle band without DPD (a) before phase adjustment and (b) after phase adjustment

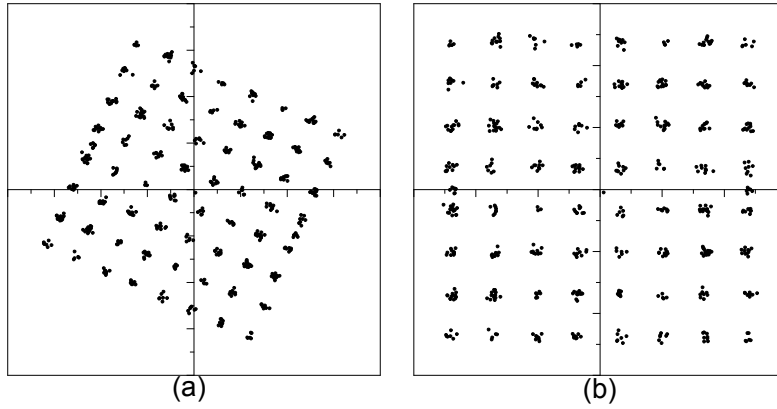


Figure 5-30 Constellation of signal in middle band with the proposed DPD (a) before phase adjustment and (b) after phase adjustment

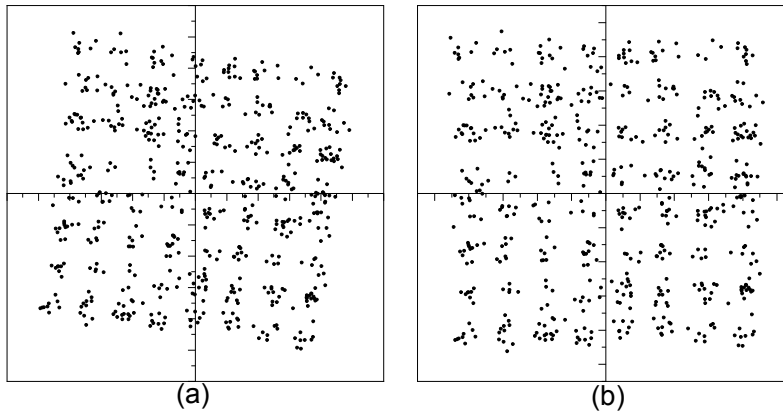


Figure 5-31 Constellation of signal in upper band without DPD (a) before phase adjustment and (b) after phase adjustment

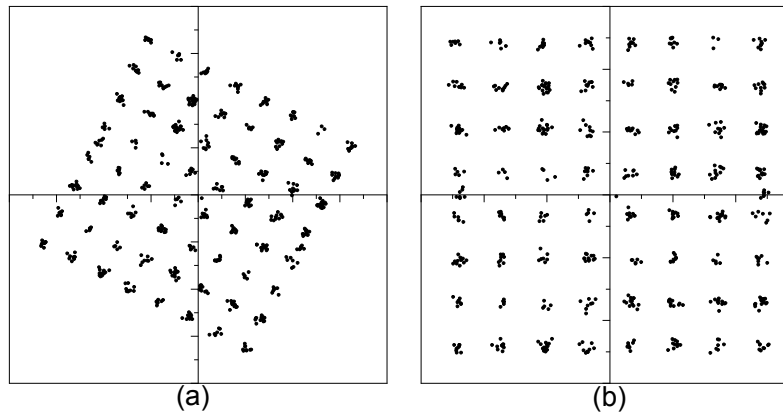


Figure 5-32 Constellation of signal in upper band with the proposed DPD (a) before phase adjustment and (b) after phase adjustment

## 5.6 Influence of Input RF Power on EVM

Experimentation has been conducted to study the influence of the input power of the RF signal on EVM of the output signal of the RoF link. The experiment result is shown in Figure 5-33. As can be seen, the EVM increases as the input RF power increases when there is no DPD adopted in the RoF link. If DPD is applied in the RoF link, the EVM decreases from -29 dB to -30 dB as the input power increases from -19.2 dBm to -17.2 dBm. When the input power further increases from -17.2 dBm to -14.7 dBm, the EVM increases back to around -29 dB.

This phenomenon can be explained as follows. When the input RF power level is very low, the power levels of the signal and the noise (or distortion) are very low. When the input RF power is increased at this stage, the power level of the signal is increased faster than that of the noise. Therefore, the EVM is decreased as the input power is increased.

However, beyond some specific point, the power level of noise and distortion is enhanced faster than that of the signal. Most of the increased input power is transformed into distortion. Even the distortion can be partly eliminated by the DPD technique, the EVM cannot be optimized further. On the contrary, if the distortion is too strong, the EVM will degrade. That is reason why the EVM climbs back when the input power level is increased beyond -17.2 dB in Figure 5-33.

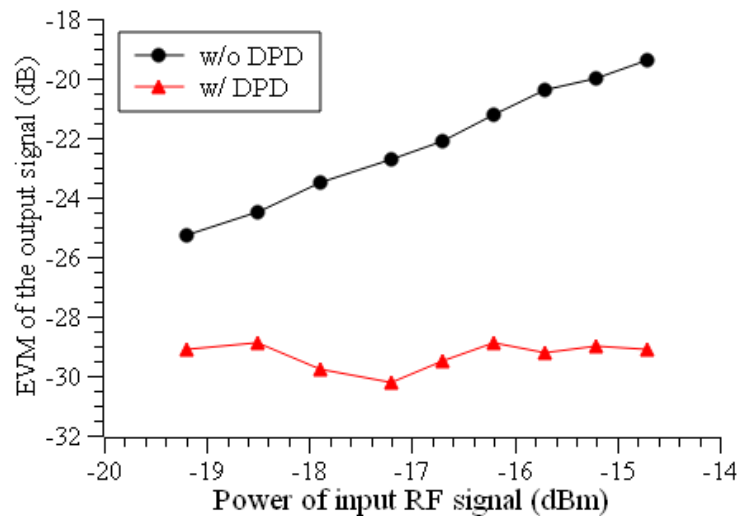


Figure 5-33 Influence of input RF power on EVM

## 5.7 Improvement on Sampling Bandwidth

Until now, the proposed DPD looks perfect. However, the sampling bandwidth is an important issue. In the aforementioned experiments, the signal is sampled in the RF domain without down conversion. To decrease the phase difference between the input RF signal and the output RF signal sampled by the oscilloscope, the sampling bandwidth has been set at a very high value, 10.32192 GHz. Although the 10GS/s ADC has been developed in industry [39], it can be expected that ADCs with such a high sampling bandwidth would be very expensive. Therefore, decreasing the sampling bandwidth of the proposed DPD is urgently preferred taking into consideration the cost.

To decrease the sampling bandwidth, the RF signal is down-converted first to an intermediate frequency signal, which contains all the bands in frequency domain. Then the down-converted signal can be sampled with a much lower sampling rate. The experiment result shows that even with a sampling rate of 150 MHz, the EVM can reach a very close level as in the previous experiment. To suppress the IMD3, a sampling bandwidth of 400 MHz, from 650 MHz to 1050 MHz, is sufficient. To suppress the IMD3 and IMD5 simultaneously, a sampling bandwidth of 600 MHz, from 550 MHz to 1150, is sufficient.

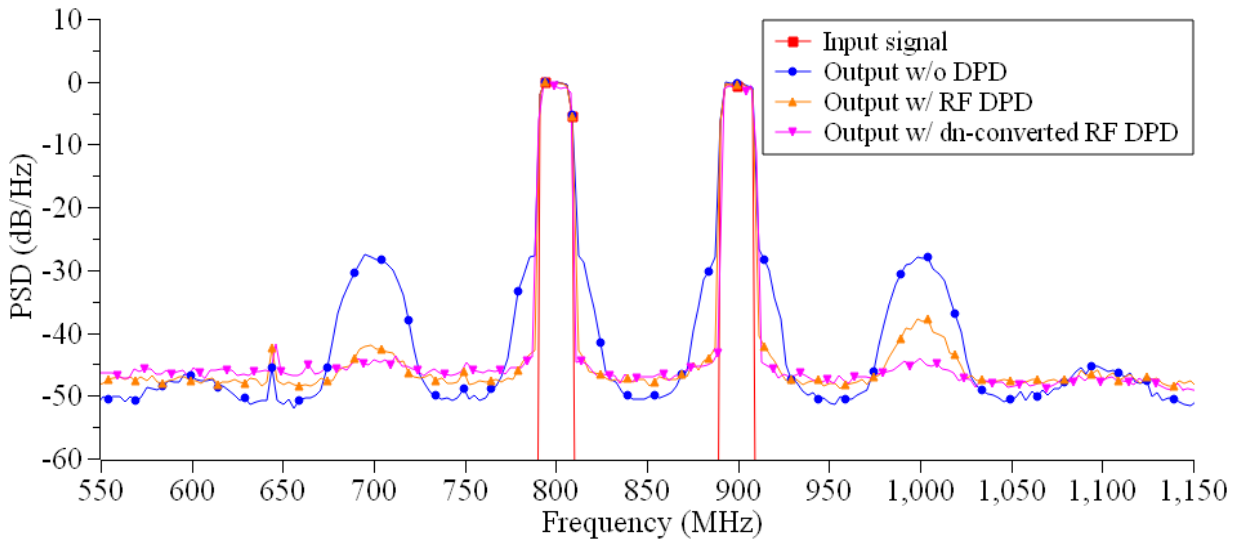


Figure 5-34 Output spectrum from 550 MHz to 1150 MHz

Figure 5-34 shows the output spectrum when the proposed DPD is implemented with down conversion and a sampling bandwidth of 600 MHz, from 550 MHz to 1150 MHz. The

result is compared to without down conversion. Improvement on IMD3 at 700 MHz is slightly better than the case of without down conversion, and improvement on IMD3 at 1000 MHz is significantly better than that of without down conversion.

Figure 5-34 also shows an important phenomenon of unbalanced IMD3. This phenomenon was explained in [43] with a two-layer structure of a transistor. If each layer amplifiers the signal ( $f_1$ ,  $f_2$ ) and induces IMD2 ( $f_2-f_1$ ,  $f_1+f_2$ ) and IMD3 ( $2f_2-f_1$ ,  $2f_1-f_2$ ), there will be three sources of the IMD3 of the final output signal. The first source is the IMD3 induced by the first layer and amplified by the second layer. The second source is the IMD3 induced by the second layer between the fundamentals amplified by the first layer. The third source is the IMD2 ( $F_1+F_2$ ) induce by the second layer between the fundamentals ( $f_1$ ,  $f_2$ ) and IMD2 ( $f_2-f_1$ ) induced by the first layer. The second-layer IMD2 between  $f_1$  and ( $f_2-f_1$ ) is  $f_2$ , and this explains why the EVM of the upper band is higher than that of the lower band. The second-layer IMD2 between  $f_2$  and ( $f_2-f_1$ ) is  $2f_2-f_1$ , and this source contributes to the upper IMD3 and finally causes the unbalanced IMD3.

Improvement on ACPR is quite close to the previous experiment results, as shown in Figure 5-35 and Figure 5-36.

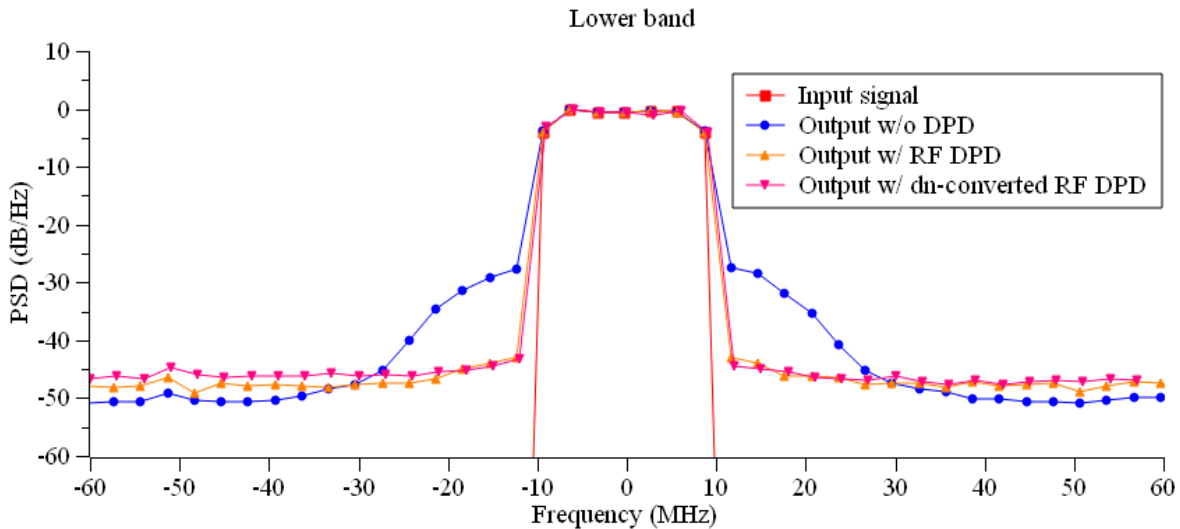


Figure 5-35 Spectrum around lower band

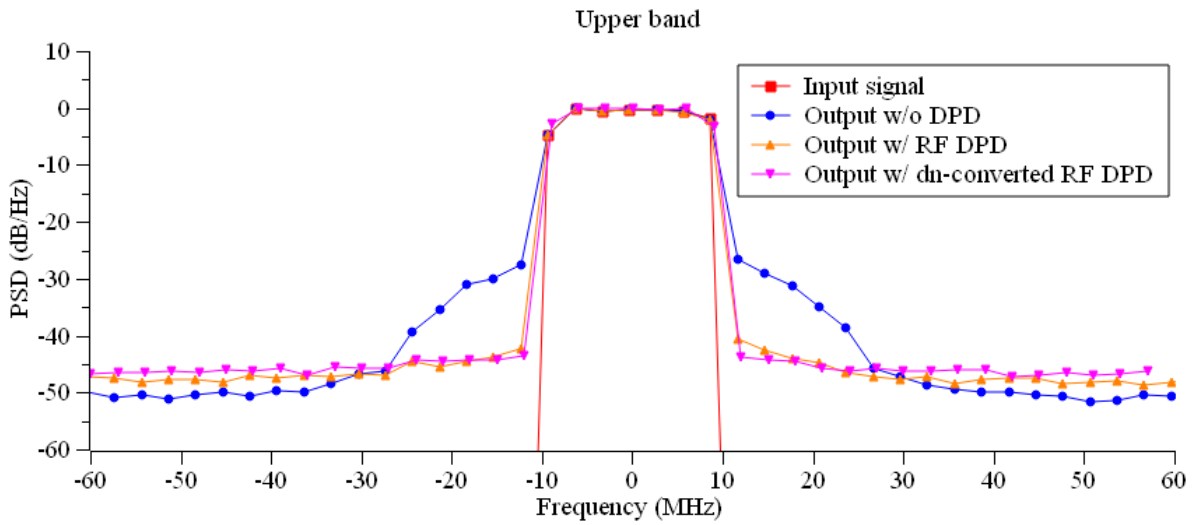


Figure 5-36 Spectrum around upper band

Constellations have been shown in Figure 5-37 and Figure 5-38, with the EVM improvement of 8.4 dB and 7.4 dB on lower and upper bands respectively. This improvement is better than the previous experiment results.

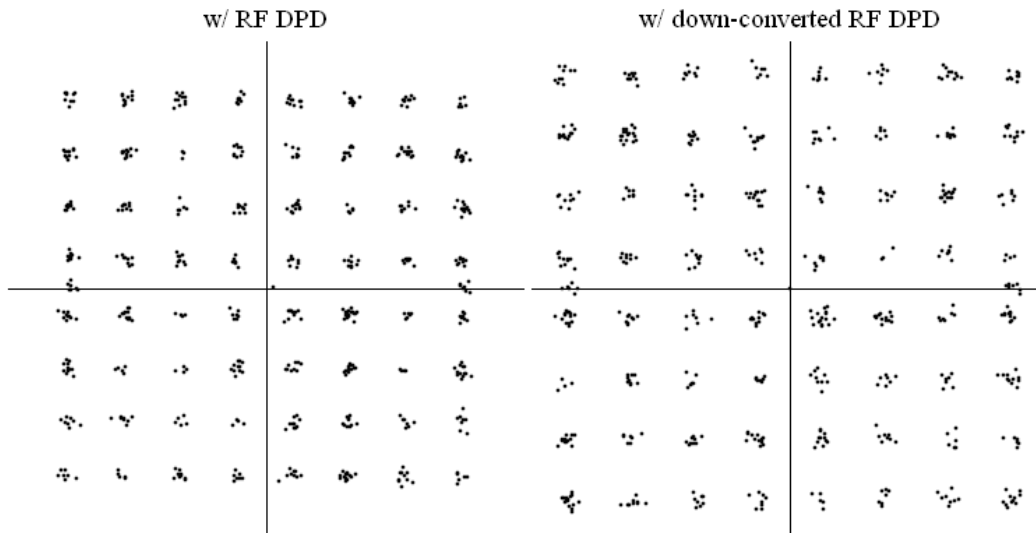


Figure 5-37 Constellation of lower band

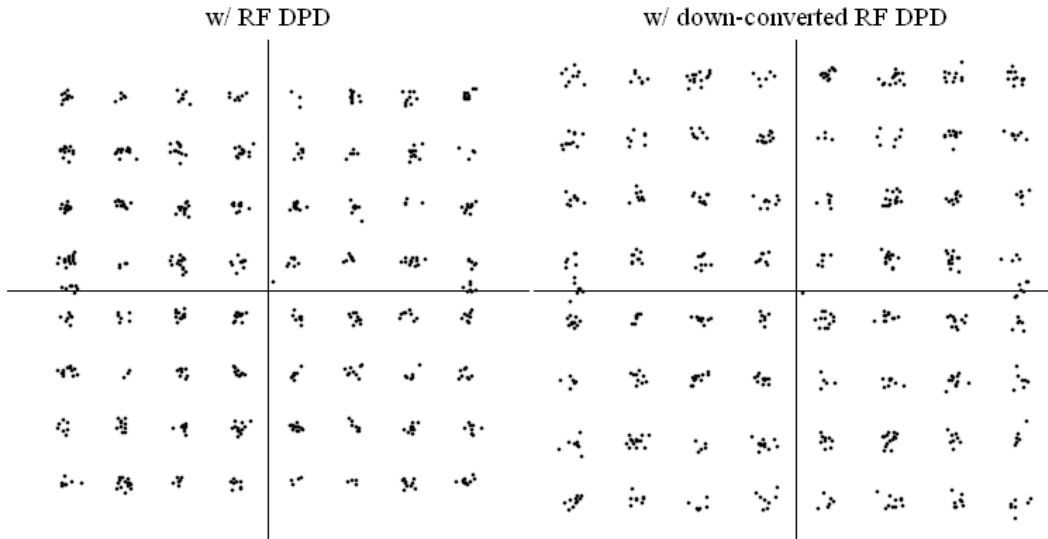


Figure 5-38 Constellation of upper band

## 5.8 Influence of Sampling Bandwidth on EVM

Experiment has been done to study the influence of the sampling bandwidth on the EVM. As can be seen in Figure 5-39 and Figure 5-40, even with a sampling bandwidth of 150 MHz, the EVM can reach as low as -28 dB. As the sampling bandwidth goes higher, the EVM is decreased. However, the change of EVM improvement is not very significant.

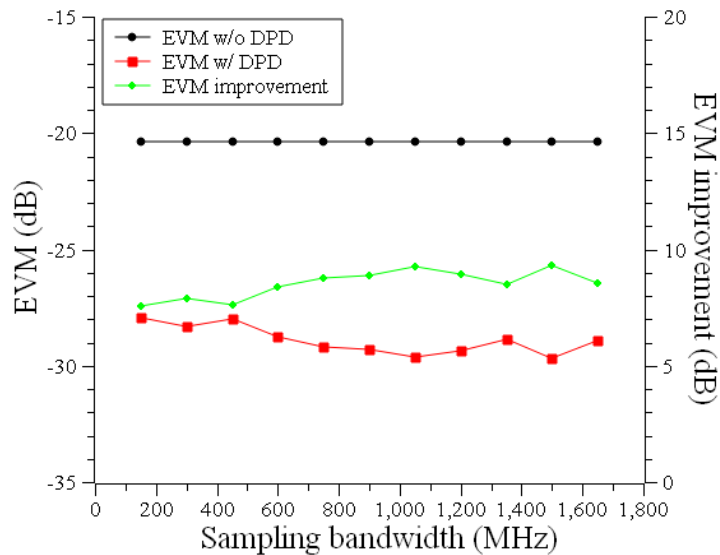


Figure 5-39 EVM vs sampling bandwidth on lower band

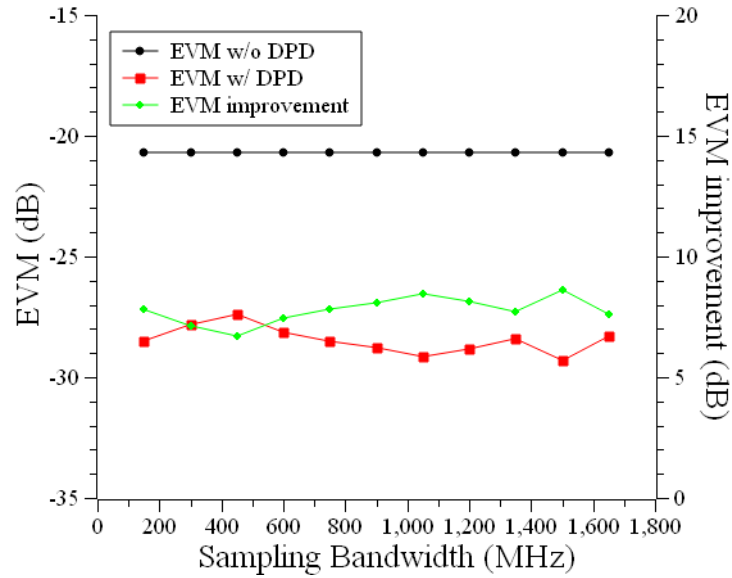


Figure 5-40 EVM vs sampling bandwidth on upper band

## 5.9 Experiment Summary

Experiment result has been summarized in Table 5-1, Table 5-2 and Table 5-3. The experiment result agrees with the simulation result, which indicates that the proposed DPD can not only improve the EVM and ACPR, but also suppressing the IMD3 and IMD5. Furthermore, the proposed DPD can work well in all test cases. This makes it well positioned for broadband and multi-band applications.

Table 5-1 Comparison of EVM improvement in experiment

EVM improvement (dB)	Proposed DPD	Proposed DPD w/ down conversion	2D DPD
<b>Case 1 (two-band)</b>	6.9	7.9	8.4
<b>Case 2 (two-band)</b>	4.8	not tested	6.9
<b>Case 3 (three-band)</b>	8.9	not tested	NA

Table 5-2 Comparison of ACPR improvement in experiment

ACPR improvement (dB)	Proposed DPD	Proposed DPD w/ down conversion	2D DPD
<b>Case 1 (two-band)</b>	14.8	18.3	16.4
<b>Case 2 (two-band)</b>	8.6	not tested	0
<b>Case 3 (three-band)</b>	16	not tested	NA

Table 5-3 Comparison of IMD3 improvement in experiment

<b>IMD3 improvement (dB)</b>	<b>Proposed DPD</b>	<b>Proposed DPD w/ down conversion</b>	<b>2D DPD</b>
<b>Case 1 (two-band)</b>	12.2	17.5	NA
<b>Case 2 (two-band)</b>	9.5	not tested	NA
<b>Case 3 (three-band)</b>	13.6	not tested	NA

The influence of the input power on the EVM has been studied and the result shows that the EVM could be minimized with specific input power level.

The issue of sampling bandwidth is resolved by adopting down conversion before sampling. This can greatly reduce the cost of the back loop of RoF transmission system, and the experiment result is even better than that of without down conversion. The influence of sampling bandwidth on the EVM has also been studied in experiments, although the influence is not so significant.

## Chapter 6. Conclusion

### 6.1 Thesis Conclusion

RoF transmission systems can provide ultra-high bandwidth and greatly reduce the cost of the infrastructure, especially the fronthaul section. However, they suffer from signal distortion potentially caused by various components in the RoF link, especially the optical modulator and RF power amplifier. To eliminate the in-band and out-of-band nonlinearities, short-term and long-term memory effects simultaneously, the envelope-assisted RF digital predistortion technique has been proposed in this thesis. This DPD model is evolved from the memory polynomial, and composed of an RF memory polynomial and a baseband memory polynomial. Therefore, this model takes both the RF signal and the baseband envelope as inputs to realize the digital predistortion. Short-term memory effect is expected to be suppressed by the RF polynomial and long-term memory effect is expected to be weakened by the baseband polynomial. The indirect learning architecture is adopted and the least squares method is used to calculate the coefficients of the model.

Simulation work has been done with Matlab to evaluate the performance of the proposed DPD. An RoF model is built which can produce in-band and out-of-band nonlinearities, and short-term and long-term memory effects simultaneously. Optimal RF and baseband memory depths have been found by running simulation with different memory depths. This indicates that the short-term memory effect is diminished by the RF memory polynomial and the long-term memory effect is lessened by the baseband memory polynomial. Three test cases have been run. The first test is a normal two-band test, while the second test is a two-band test with the two bands closely located. The third test is a three-band test. EVM, ACPR and IMD3 have been improved by 14.6 dB, 13.5 dB and 19.5 dB respectively in the first test. The improvements are 16.3 dB, 15.5 dB and 27.5 dB in the second test, and 15.7 dB, 15.2 dB and 14.1 dB in the third test. These simulation results prove that the proposed DPD works very well in the two-band transmission, three-band transmission, and even when two bands are closely located. Comparison with a baseband DPD has been made showing that the baseband DPD is only better at eliminating the in-band nonlinearity in the first test and the proposed DPD is better at

suppressing the out-of-band nonlinearity. Besides, the proposed DPD works very well in the second and third tests as in the first test. Therefore, the proposed DPD can be used in broadband and multi-band applications, which makes it well-positioned for the ultra-wideband transmission in the 4G and 5G architecture.

Experiments have been done on an RoF link in the lab. Optimal RF and baseband memory depths have been found. The optimal baseband memory depth is 1, which means the memory effect of the RoF link used in the experiment is dominated by short-term memory effect. Similar tests have been done on the RoF link as in the simulation work and the experiment results agree with the simulation results proving the validity of the proposed DPD in the real RoF transmission. EVM is improved by 6.9 dB, 4.8 dB and 8.9 dB in three tests. ACPR is suppressed by 14.8 dB, 8.6 dB and 16 dB in these three scenarios. IMD3 is lessened by 12.2 dB, 9.5 dB and 13.6 dB in all three cases. Performance of the 2D DPD has been evaluated to make comparison with the proposed DPD as well. As it has been proved by the simulation results, the 2D DPD is only good at improving the EVM and ACPR in the first test, while the proposed DPD can adapt itself very well in all three scenarios. Influence of the input power on the EVM improvement has been studied and the experiment results show that the EVM can be optimized at specific input power level, when the signal power level is not too low and the noise level is not too high. Sampling bandwidth has been reduced by down-converting the RF signal and sampling it at an intermediate frequency. Lower sampling bandwidth avoids the extremely expensive RF ADCs. Influence of the sampling bandwidth on the EVM has been tested. However, the experiment result shows that higher sampling bandwidth does not lead to significant EVM improvement.

Based on the simulation and experiment results, it can be concluded that the proposed DPD is capable of dealing with in-band and out-of-band nonlinearities, short-term and long-term memory effects of the RoF transmission system simultaneously. Because it is not limited by the number of bands, it can be used in broadband and multi-band scenarios as defined in the 4G standard and is well-positioned for the upcoming 5G technology.

## 6.2 Future Work

Although the proposed DPD works very well in various scenarios, it is not perfect. One of the imperfections is that it is not as good at improving the EVM as the baseband DPD. How to further optimize the EVM may be of interest.

Another potential problem is that as the bandwidth increases, the digital circuit to implement the DPD will meet some challenges. Either it will be too complicated to realize the DPD, or it will be too expensive to do so. Therefore, effort may be done to combine the analog predistortion techniques with the digital ones.

Experiment with high power amplifier or power amplifier with bandpass filters can be done to further prove the validity of the proposed DPD. If the long-term memory effect of power amplifier is stronger, the advantage of the proposed DPD will be more obvious.

## Reference

- [1] M. R. Bhalla, A. V. Bhalla, “Generations of mobile wireless technology: a survey”, *Int. J. of Comput. Applicat.*, vol. 5, no. 4, Aug. 2010.
- [2] A. Checko, “Cloud radio access network architecture. Towards 5G mobile networks”, Ph.D. thesis, Dept. Photonics Eng., Denmark Technical Univ., Lyngby, Denmark, 2016.
- [3] A. Ng’oma, “Radio-over-fiber technology for broadband wireless communication systems”, Ph.D. thesis, Dept. Elect. Eng., Eindhoven Technology Univ., Eindhoven, Netherlands, 2005.
- [4] S. Kumar and M. J. Deen, *Fiber Optic Communications: Fundamentals and Applications*, 1st ed. Chichester, United Kingdom: John Wiley & Sons, Ltd, 2014.
- [5] X. Zhang, D. Shen, T. Liu, “Review of linearization techniques for fiber-wireless systems”, *IEEE International Wireless Symposium*, Xi’an, China, 2014.
- [6] C. K. Kao and G. A. Hockham, “Dielectric fiber surface waveguides for optical frequencies,” *Proc. IEE*, vol. 113, no. 7, pp. 1151-1151, Jul. 1966.
- [7] P. Sillard, M. Bigot-Astruc, and D. Molin, “Few-mode fibers for mode-division-multiplexed systems,” *J. Lightw. Technol.*, vol. 32, no. 16, pp. 2824–2829, Aug. 2014.
- [8] K. Saitoh, and S. Matsuo, “Multicore fiber technology,” *J. Lightw. Technol.*, vol. 34, no. 1, pp. 55–66, Jan. 2016.
- [9] B. Zhu, T. F. Taunay, M. Fishteyn, X. Liu, S. Chandrasekhar, M. F. Yan, J. M. Fini, E. M. Monberg, and F. V. Dimarcello, “112-Tb/s space-division multiplexed DWDM transmission with 14-b/s/Hz aggregate spectral efficiency over a 76.8-km seven-core fiber,” *Opt. Exp.*, vol. 19, no. 17, pp. 16665–16671, Aug. 2011.
- [10] I. Tomkos, D. Chowdhury, J. Conradi, D. Culverhouse, K. Ennser, C. Giroux, B. Hallock, T. Kennedy, A. Kruse, S. Kumar, N. Lascar, I. Roudas, M. Sharma, R. Vodhanel, and R. C.

- Wang, "Demonstration of negative dispersion fibers for DWDM metropolitan area networks," *IEEE J. Sel. Top. Quantum Electron.*, vol. 7, pp. 439–460, 2001.
- [11] Fairchild SS8050 Datasheet, Fairchild Semiconductor Corporation [Online]. Available: <https://www.fairchildsemi.com/datasheets/SS/SS8050.pdf>
- [12] J. Wood, *Behavioral Modeling and Linearization of RF Power Amplifiers*, 1st ed., Norwood, MA: Artech House, 2014.
- [13] W.H. Doherty, "A new high efficiency power amplifier for modulated waves," *Proc. IRE*, Vol. 24, No. 9, pp. 1163-1182, 1936.
- [14] H. He, T. Ge, and J. Chang, "A review on supply modulators for envelope-tracking power amplifiers," *Int. Symp. Integr. Circuits (ISIC)*, Singapore, 2016.
- [15] J. Domokos, "A power amplifier system," Patent WO2004019486, 2004.
- [16] M. P. Wilson, "High efficiency amplification," Patent WO2005057769, 2005.
- [17] S. Akihisa, and K. Kuniyuki, "Power amplifier for radio transmitter," Patent JP9064757, 1997.
- [18] R. Daniele, and A. Abbaiti, "Linear microwave power amplifier with supply power controlled by modulation envelope," Patent WO9534128, 1995.
- [19] I. Bar-David, "Method and apparatus for improving the efficiency of power amplifiers operating under a large peak-to-average ratio," Patent US20006437641 (Paragon), 2001.
- [20] A. Festoe, and K. Onarheim, "Efficient power supply for rapidly changing power requirements," Patent WO2005041404, 2005.
- [21] S.C. Cripps, *RF Power Amplifiers for Wireless Communications*, 2nd ed., Norwood, MA: Artech House, 2006.

- [22] B. Masella, B. Hraimel, and X. Zhang, "Enhanced spurious-free dynamic range using mixed polarization in optical single sideband Mach-Zehnder modulator," *J. Lightw. Technol.*, vol. 27, no. 15, pp. 3034–3041, 2009.
- [23] B. Hraimel, X. Zhang, W. Jiang, K. Wu, T. Liu, T. Xu, Q. Nie, and K. Xu, "Experimental demonstration of mixed polarization to linearize electro-absorption modulators in radio-over-fiber links," *IEEE Photon. Technol. Lett.*, vol. 23, no. 4, pp. 230–232, 2011.
- [24] B. Hraimel, and X. Zhang, "Performance improvement of radio-over fiber links using mixed polarization electro-absorption modulators," *IEEE Trans. Microw. Theory Techn.*, vol. 59, no. 12, pp. 3239 - 3248, 2011.
- [25] B. Hraimel, X. Zhang, T. Liu, T. Xu, Q. Nie, and D. Shen, "Performance enhancement of an OFDM ultra-wideband transmission-over-fiber link using a linearized mixed-polarization single-drive x-cut Mach-Zehnder modulator," *IEEE Trans. Microw. Theory Techn.*, vol. 60, issue 10, pp. 3328-3338, Oct. 2012.
- [26] B. Hraimel, and X. Zhang, "Suppression of radio over fiber system nonlinearity using a semiconductor optical amplifier and mixed polarization," *Opt. Fiber Commun. Conf. Expo. Nat. Fiber Opt. Eng. Conf. (OFC/NFOEC)*, OTHR2, Mar. 2013.
- [27] K. K. Loi, J. H. Hodiak, X. B. Mei, C. W. Tu, and W. S. C. Chang, "Linearization of 1.3- $\mu\text{m}$  MQW electroabsorption modulators using an all-optical frequency-insensitive technique," *IEEE Photon. Technol. Lett.*, vol. 10, no. 7, pp. 964-966, Jul. 1998.
- [28] Z. Wu, K. Xu, J. Niu, Q. Lv, Y. Dai, and J. Lin, "Third-order intermodulation distortion improvement radio-over-fiber link using dual-wavelength intensity modulation," *High Speed Intell. Commun. Forum*, May 2012.
- [29] R. Zhu and X. Zhang, "Linearization of radio-over-fiber systems by using two lasers with different wavelengths," *IEEE MTT-S Int. Microw. Symp.*, Jun. 2014.
- [30] Y. Shen, B. Hraimel, X. Zhang, G. E. R. Cowan, K. Wu, and T. Liu, "A novel analog broadband RF predistortion circuit to linearize electro-absorption modulators in multiband

- OFDM radio-over-fiber systems,” *IEEE Trans. Microw. Theory Techn.*, vol. 58, no. 11, pp. 3327-3335, Sept. 2010.
- [31] R. Zhu, X. Zhang, B. Hraimel, D. Shen, and T. Liu, “Broadband predistortion circuit using zero bias diodes for radio over fiber systems,” *IEEE Photon. Technol. Lett.*, vol. 25, no. 21, pp. 2101-2104, Nov. 2013.
- [32] R. Zhu and X. Zhang, “Broadband predistortion circuit design for electro-absorption modulator in radio over fiber system,” *Opt. Fiber Commun. Conf. Expo.*, Mar. 2014.
- [33] R. Zhu, Z. Xuan, and X. Zhang, “Novel broadband analog predistortion circuit for radio-over-fiber systems,” *IEEE MTT-S Int. Microw. Symp.*, May 2015.
- [34] J. Kim and K. Konstantinou, “Digital predistortion of wideband signals based on power amplifier models with memory,” *Electron. Lett.*, vol. 37, pp. 1417–1418, Nov. 2001.
- [35] D. R. Morgan, Z. Ma, J. Kim, M. G. Zierdt, and J. Pastalan, “A generalized memory polynomial model for digital pre distortion of RF power amplifiers,” *IEEE Trans. Signal Process.*, vol. 54, no. 10, pp. 3852–3860, Oct. 2006.
- [36] A. Zhu, J. C. Pedro, and T. J. Brazil, “Dynamic deviation reduction-based Volterra behavioral modeling of RF power amplifiers,” *IEEE Trans. Microwave Theory Tech.*, vol. 54, no. 12, pp. 4323–4332, Dec. 2006.
- [37] S. A. Bassam, M. Helaoui, and F. M. Ghannouchi, “2-D digital predistortion (2-D-DPD) architecture for concurrent dual-band transmitters,” *IEEE Trans. Microw. Theory Tech.*, vol. 59, no. 10, pp. 2547–2553, Oct. 2011.
- [38] B. Vaz *et al.*, “A 13b 4GS/s digitally assisted dynamic 3-stage asynchronous pipelined-SAR ADC,” presented at 2017 IEEE International Solid-State Circuits Conference (ISSCC). 2017 © IEEE. DOI: 10.1109/ISSCC.2017.7870368.
- [39] S. Devarajan *et al.*, “A 12b 10GS/s interleaved pipeline ADC in 28nm CMOS technology,” presented at 2017 IEEE International Solid-State Circuits Conference (ISSCC). 2017 © IEEE. DOI: 10.1109/ISSCC.2017.7870374.

- [40] D. Psaltis, A. Sideris, and A.A. Yamamura, "A multilayered neural network controller," *IEEE Contr. Syst. Mag.*, vol. 8, no. 2, pp. 17-21, 1988.
- [41] C. Eun and E. J. Powers, "A new Volterra predistorter based on the indirect learning architecture," *IEEE Trans. on Signal Processing*, Jan. 1997.
- [42] L. Ding *et al.*, "Memory polynomial predistorter based on the indirect learning architecture," in *Proc. IEEE Global Telecommunicat. Conf. GLOBECOM*, Taipei, Taiwan, Nov. 2002, vol. 1, pp. 967–971.
- [43] J. Vuolevi and T. Rahkonen, "The effects of source impedance on the linearity of BJT common-emitter amplifiers," in *Proc. ISCAS 2000*, vol. VI, May 2000, pp. 197–200.